For Reference

NOT TO BE TAKEN FROM THIS ROOM

For Reference

NOT TO BE TAKEN FROM THIS ROOM

Ex LIBRIS
UNIVERSITATIS
ALBERTAENSIS

Digitized by the Internet Archive
in 2020 with funding from
University of Alberta Libraries

https://archive.org/details/Sunku1969

THE UNIVERSITY OF ALBERTA

BENDING OF A CLASS OF DOUBLY CONNECTED PLATES AND REGULAR POLYGONAL PLATES ON ELASTIC FOUNDATION

by

© BADRINARAYANA SUNKU

A THESIS

SUBMITTED TO THE FACULTY OF GRADUATE STUDIES

IN PARTIAL FULFILMENT OF THE REQUIREMENTS FOR THE DEGREE

OF MASTER OF SCIENCE

DEPARTMENT OF MECHANICAL ENGINEERING

EDMONTON, ALBERTA

FALL, 1969

Thesis
1968 (F)
236

THE UNIVERSITY OF ALBERTA

FACULTY OF GRADUATE STUDIES

The undersigned certify that they have read, and recommend to the Faculty of Graduate Studies for acceptance, a thesis entitled "BENDING OF A CLASS OF DOUBLY CONNECTED PLATES AND REGULAR POLYGONAL PLATES ON ELASTIC FOUNDATION" submitted by BADRINARAYANA SUNKU in partial fulfilment of the requirements for the degree of Master of Science.

ABSTRACT

The method of point matching is used to solve a class of uniformly loaded clamped doubly connected plates having a circular hole. The general solution of the plate equation in polar coordinates satisfying the clamped boundary conditions exactly at the inner circular edge is used to solve the following problems:

1. Uniformly loaded clamped eccentric annular plates.
2. Uniformly loaded clamped regular polygonal plates having a concentric circular hole.
3. Uniformly loaded clamped elliptic plates having a concentric circular hole.

Numerical results for the maximum deflection and maximum moments at the inner and outer edges are presented for various ratios of the radius of the hole to the size of the plate for the case of Poisson's ratio $\nu = 0.3$. Graphical results for deflection, slope and moment curves are also presented for the typical cases.

The method of point matching is also applied to the bending of uniformly loaded clamped regular polygonal plates on elastic foundation and the numerical and typical graphical results are also presented for this case.

ACKNOWLEDGEMENTS

The author wishes to extend his thanks and appreciation to

- Dr. K.C. Cheng for his supervision of this thesis,
- the members of the Computing Science Department for their advice and cooperation in computer programming,
- Dr. J.R. Colbourne for pointing out numerical and typing errors in the original manuscript,
- Mr. A. Semeniuk who carefully read and corrected the manuscript and Mr. V. Srinivasan for the useful discussions,
- Miss June Talpash for her careful typing of this thesis with patience,
- The Department of Mechanical Engineering for the financial support in the form of a fellowship,
- Miss Linda Benesch for her assistance in the preparation of the manuscript.

TABLE OF CONTENTS

Page

CHAPTER I: INTRODUCTION 1

CHAPTER II: THEORETICAL ANALYSIS

2.1 Analysis of Uniformly Loaded Clamped Doubly Connected Plates with a Circular Internal Boundary and Arbitrary External Boundary 6

CHAPTER III: APPLICATIONS AND NUMERICAL RESULTS

3.1 Uniformly Loaded Clamped Eccentric Annular Plate 13

3.2 Uniformly Loaded Clamped Regular Polygonal Plate Having a Concentric Circular Hole 36

3.3 Uniformly Loaded Clamped Elliptic Plate Having a Concentric Circule Hole 51

CHAPTER IV: REGULAR POLYGONAL PLATES ON ELASTIC FOUNDATION

4.1 Governing Equation and Its General Solution 68

4.2 Uniformly Loaded Clamped Regular Plates on Elastic Foundation 69

CHAPTER V: CONCLUDING REMARKS 80

REFERENCES 84

APPENDIX A

Expressions for $\frac{\partial w}{\partial r'}$, $\frac{\partial^2 w}{\partial r'^2}$, $\frac{\partial^2 w}{\partial \phi^2}$, $\frac{\partial w}{\partial \phi}$, and $\frac{\partial^2 w}{\partial r' \partial \phi}$ ... 87

APPENDIX B

Ber, Bei Functions and Their Derivatives 89

LIST OF TABLES

Table.		Page
1.	Numerical Results for Uniformly Loaded Clamped Eccentric Annular Plates	18
2.	Maximum Boundary Errors for Deflection and Normal Slope Along the Outer Edge for Uniformly Loaded Eccentric Annular Plates	23
3.	Comparison of Numerical Result of This Work With That of Georgian [6] for the case $\beta = 0$	24
4.	Comparison of Numerical Result of This Work With That of Yamanaka and Kakae [10] for Uniformly Loaded Clamped Eccentric Annular Plate for the Case $\alpha = 0.5$ and $\beta = 0.391$	25
5.	Numerical Result for Uniformly Loaded Clamped Regular Polygonal Plates Having a Concentric Circular Hole	40
6.	Numerical Values of Boundary Errors for Deflection and Normal Slope Along the Outer Edge for Uniformly Loaded Clamped Regular Polygonal Plate With a Concentric Circular Hole	42
7.	Percentage of Boundary Errors for Deflection and Normal Slope Along the Outer Edge for Uniformly Loaded Clamped Regular Polygonal Plate With a Concentric Circular Hole	43
8.	Numerical Result for Uniformly Loaded Clamped Elliptic Plates With a Concentric Circular Hole	54

Table.		Page
9.	Numerical Result for Uniformly Loaded Clamped Elliptic Plate With a Concentric Circular Hole for the Case $\gamma = 1.0$	59
10.	Maximum Boundary Errors for Deflection and Normal Slope Along the Outer Edge for Uniformly Loaded Clamped Elliptic Plate With a Concentric Circular Hole	60
11.	Numerical Result for Uniformly Loaded Clamped Regular Polygonal Plate on Elastic Foundation	74

LIST OF FIGURES

Fig.		Page
1.	Coordinate system for a plate with circular internal hole and arbitrary external boundary symmetric about the axis $\phi = 0$.	9
2.	Coordinate system for an accentric annular plate	12
3.	Distribution of deflection along AB, CD and EF for uniformly loaded clamped eccentric annular plate for the case $\alpha = 0.5$ and $\beta = 0.5$	26
4.	Distribution of radial slope along AB, CD and EF for uniformly loaded clamped eccentric annular plate for the case $\alpha = 0.5$ and $\beta = 0.5$	27
5.	Distribution of radial moment along AB, CD and EF for uniformly loaded clamped eccentric annular plate for the case $\alpha = 0.5$ and $\beta = 0.5$	28
6.	Distribution of tangential moment along AB, CD and EF for uniformly loaded clamped eccentric annular plate for the case $\alpha = 0.5$ and $\beta = 0.5$	29
7.	Distribution of moments M_n, M_s along the outer edge for uniformly loaded clamped eccentric annular plate for the case $\alpha = 0.5$ and $\beta = 0.5$	30
8.	Distribution of moments M_r, M_t along the inner edge for uniformly loaded clamped eccentric annular plate for the case $\alpha = 0.5$ and $\beta = 0.5$	31
9.	Comparison of deflection curve along AB from this work with that of Yamanaka and Kakae for uniformly loaded clamped eccentric annular plate for the case $\alpha = 0.5$ and $\beta = 0.391$	32

Fig.		Page
10.	Comparison of radial moment curve along AB from this work with that of Yamanaka and Kakae for uniformly loaded clamped eccentric annular plate for the case $\alpha = 0.5$ and $\beta = 0.391$	33
11.	Comparison of tangential moment curve along AB from this work with that of Yamanaka and Kakae for uniformly loaded clamped eccentric annular plate for the case $\alpha = 0.5$ and $\beta = 0.391$	34
12.	Coordinate system for a regular polygonal plate with a concentric circular hole	35
13.	Distribution of deflection along AB and CD for uniformly loaded clamped regular polygonal plate having a concentric circular hole for the case $\alpha = 0.5$ and $N = 4$	44
14.	Distribution of radial slope along AB and CD for uniformly loaded clamped regular polygonal plate having a concentric circular hole for the case $\alpha = 0.5$ and $N = 4$	45
15.	Distribution of radial moment along AB and CD for uniformly loaded clamped regular polygonal plate having a concentric circular hole for the case $\alpha = 0.5$ and $N = 4$	46
16.	Distribution of tangential moment along AB and CD for uniformly loaded clamped regular polygonal plate having a concentric circular hole for the case $\alpha = 0.5$ and $N = 4$	47

Fig.		Page
17.	Distribution of moments M_n and M_s along the outer edge for uniformly loaded clamped regular polygonal plate having a concentric circular hole for the case $\alpha = 0.5$ and $N = 4$	48
18.	Distribution of moments M_r and M_t along the inner edge for uniformly loaded clamped regular polygonal plate having a concentric circular hole for the case $\alpha = 0.5$ and $N = 4$	49
19.	Coordinate system for elliptic plate with a concentric circular hole	50
20.	Distribution of deflection along AB and CD for uniformly loaded clamped elliptic plate having a concentric circular hole for the case $\alpha = 0.5$ and $\gamma = 1.5$	61
21.	Distribution of radial slope along AB and CD for uniformly loaded clamped elliptic plate having a concentric circular hole for the case $\alpha = 0.5$ and $\gamma = 1.5$	62
22.	Distribution of radial moment along AB and CD for uniformly loaded clamped elliptic plate having a concentric circular hole for the case $\alpha = 0.5$ and $\gamma = 1.5$	63
23.	Distribution of tangential moment along AB and CD for uniformly loaded clamped elliptic plate having a concentric circular hole for the case $\alpha = 0.5$ and $\gamma = 1.5$	64

Fig.		Page
24.	Distribution of moments M_n and M_s along the outer edge for uniformly loaded clamped elliptic plate having a concentric circular hole for the case $\alpha = 0.5$ and $\gamma = 1.5$	65
25.	Distribution of moments M_r and M_t along the inner edge for uniformly loaded clamped elliptic plate having a concentric circular hole for the case $\alpha = 0.5$ and $\gamma = 1.5$	66
26.	Coordinate system for a regular polygonal plate	67
27.	Distribution of deflection along OB and OD for uniformly loaded clamped regular polygonal plate on elastic foundation for the case N = 4	75
28.	Distribution of radial slope along OB and OD for uniformly loaded clamped regular polygonal plate on elastic foundation for the case N = 4	76
29.	Distribution of radial moment along OB and OD for uniformly loaded clamped regular polygonal plate on elastic foundation for the case N = 4	77
30.	Distribution of tangential moment along OB and OD for uniformly loaded clamped regular polygonal plate on elastic foundation for the case N = 4	78
31.	Distribution of moments M_n and M_s along the edge for uniformly loaded regular polygonal plate on elastic foundation for the case N = 4	79

NOMENCLATURE

A_j, B_j, C_j, D_j Coefficients of the general solution of biharmonic equation in polar coordinates.

a Non-dimensional radius for external circle, a'/a_1 .

a_1 Reference length for a configuration.

a_2 Length of semi-major axis of the ellipse.

a' Radius of the external circle.

Ber, Bei, Ber', Bei', Ber", Bei" Kelvin functions and their derivatives with respect to the argument.

b Non-dimensional radius of the circular hole, b'/a_1 .

b' Radius of the circular hole.

D Flexural rigidity of a plate.

e eccentricity (distance between centres).

k Modulus of elastic foundation.

M_r, M_t, M_n, M_s Bending moments per unit length of sections of a plate perpendicular to r, t, n and s directions, respectively.

M_{rt} Twisting moment per unit length of section of the plate.

N Number of sides of regular polygon.

n Normal to the boundary or order of the Kelvin function.

Q_n, R_n Coefficients of the infinite series.

q Intensity of loading.

r' Radial coordinate.

r Dimensionless radial coordinate, r'/a_1 .

w Deflection of the plate.

x Argument of the Kelvin functions.

α Radius ratio of the circular hole to the reference length.

β Eccentricity ratio, $e/(a'-b')$.

γ Aspect ratio of the ellipse, a_2/a_1 .

∇^4 Biharmonic operator.

∇_ρ^2 Dimensionless Laplacian operator, $\frac{\partial^2}{\partial \rho^2} + (\frac{1}{\rho}) \frac{\partial}{\partial \rho} + (\frac{1}{\rho^2}) \frac{\partial^2}{\partial \phi^2}$.

ε Eccentricity ratio of the ellipse, $1 - (a_2^2/a_1^2)$.

ϕ Angular coordinate.

ψ Angle defined in Fig. 1.

ν Poisson's ratio.

λ Stiffness parameter, $\sqrt[4]{k/D}$.

ρ Dimensionless radial coordinate, $\lambda r'$.

Subscript

j	Subscript for infinite series.
m	Maximum value.
n	Normal direction for moments or order of the Kelvin functions.
r	Radial direction.
s	Perpendicular to normal direction.
t	Tangential direction.

Superscript

'	First derivative of the function.
"	Second derivative to the function.

CHAPTER I

INTRODUCTION

Bending of annular plates, with various combinations of boundary conditions at the inner and outer edges subjected to different types of loading, has been studied extensively by many investigators in the past. The coefficients for the maximum stress and deflection were given by Wahl and Lobo [1] which were also tabulated in references [2,3] for axially symmetric loading under eight different types of loading and edge conditions. The edge conditions considered by Wahl and Lobo may be superimposed to obtain the maximum stress and deflection for clamped and simply supported edges. Numerical and graphical results were presented by Trumpler [4] and Labrow [5] for deflection and stress for annular plates under various axially symmetric loads. However, the results presented in the tables given in references [1, 4, 5] provided the design data for annular plates with various types of loading but with a significant point that these solutions leave one of the edges free to deflect. The cases where both edges are either simply supported or clamped have not been considered by these authors. The numerical and graphical results for uniformly loaded annular plates with both edges either clamped or simply supported were provided by Georgian [6]. Recently, Heap [7] presented the numerical design data for the maximum deflections and moments of annular plates subjected to a line loading on a concentric circle for various combinations of simply supported and

clamped edge conditions. It may also be of interest to note that the solution for a clamped or simply supported elliptic plate, with or without an elliptic hole, subjected to a concentrated load at an arbitrary point was solved by Saito, Kimura and Shimazaki [8].

In contrast to numerous results for various problems related to annular plates, only a few solutions can be found in the literature for the case of eccentric annular plates. The exact solution in bi-polar coordinates for uniformly loaded, clamped, eccentric annular plates was given by Woinowsky-Krieger [9] without numerical results. Yamanaka and Kakae [10] used the infinite series in bipolar coordinates to analyse the stress distribution of boiler flat-end eccentric annular plates, which is essentially the same problem solved by Woinowsky-Krieger [9]. Good agreement for the deflections and stress distributions was obtained between the above exact solution using five terms of the infinite series and the simplified analysis previously done by Yamanaka for the case where the radius ratio $\alpha = 0.5$ and the eccentricity ratio $\beta = 0.391$. In view of the difficulty in performing calculations using bi-polar coordinates, the numerical results were not given for any other eccentricity and radius ratios except for the above mentioned case. In this study, the problem considered by Woinowsky-Krieger [9] and Yamanaka and Kakae [10] will be approached by the point matching technique using the exact solution in polar coordinates. It will be shown the point matching method readily yields the numerical results. The numerical and graphical results given by Yamanaka and Kakae will

be compared with the results of the present analysis.

In recent years, the point matching technique has been used for solving the boundary value problems where the boundary conditions are satisfied only at discrete points. For examples, the series solution of the biharmonic differential equation in polar coordinates was successfully used by Lo and Leissa [11], Leissa and Niedenfuhr [12], Hulbert and Niedenfuhr [13], Conway [14] and many others to solve the boundary value problem on bending of plates. In addition it may be of interest to note that Saito [15] obtained a solution for eccentric annular plate subjected to a concentrated load at an arbitrary point in the form of infinite series using bi-polar coordinates. Recently, the problem of laminar forced convection with heat sources in eccentric annular ducts was solved by Cheng and Hwang [16] using the point matching technique. A class of doubly connected plate problems, characterized by an inner circular hole, can be approached readily by using the exact solution of the biharmonic equation in polar coordinates. For example, Lo and Leissa [11] presented the solution for uniformly loaded, simply supported or clamped square plate with a concentric free circular hole of various sizes. The above geometrical shape treated by Lo and Leissa [11] can be generalized to a regular polygonal plate with a concentric circular hole of various sizes.

The main purpose of this study is to explore further the possibility of solving a class of doubly connected plate problems

characterized by an inner circular hole. The clamped boundary conditions at the inner edge can be satisfied exactly and the boundary conditions at the outer edge may be satisfied by the point matching method. It is possible to develop a solution for the deflection of a plate with an arbitrary external boundary, satisfying the boundary conditions exactly at the inner circular hole. However, it is not suggested that any arbitrary external boundary can be dealt with using the point matching method. In this study the following two examples are further considered in addition to the uniformly loaded clamped eccentric annular plates.

1. Uniformly loaded clamped regular polygonal plate with a concentric circular hole.
2. Uniformly loaded clamped elliptic plate with a concentric circular hole.

Numerical and typical graphical results for deflection, slope and moments are presented for the above cases.

The point matching technique is also applied to uniformly loaded regular polygonal plates resting on elastic foundation. Circular plates on elastic foundation subjected to transverse loading were discussed by Timoshenko and Woinowsky-Krieger [3]. Saito [17] presented the solutions for bending of clamped circular plates on an elastic foundation subjected to a line loading either along a radius or concentric circular arc. Saito [18] also provided the solutions and distributions of moments for circular plates loaded over a concentric

or eccentric circular domain. The unknown coefficients are determined by satisfying the boundary conditions and the conditions of continuity for deflection and its derivatives at the boundary of loading. Reismann [19] developed a general solution under general boundary conditions for deflections, moments, shears and stresses of a circular or ring-shaped plate resting on an elastic foundation and subjected to arbitrary specified transverse loads acting on the edges and surfaces of the plate. In this study, an analysis of uniformly loaded, clamped regular polygonal plates on elastic foundations is made using the general solution in terms of Kelvin functions [17, 18, 19]. The unknown coefficients of the series are determined by satisfying the clamped edge boundary conditions in the least squares sense. A detailed mathematical treatment on least squares technique of solving the boundary value problems was given by Lo [20]. Numerical results for deflection and moments are given for regular polygonal plates with $N = 4$, 6 and 8 only.

CHAPTER II

THEORETICAL ANALYSIS

2.1 Analysis of Uniformly Loaded Clamped Doubly Connected Plates with a Circular Internal Boundary and Arbitrary External Boundary.

The given problem is to develop a deflection function $w(r,\phi)$ for a plate of doubly connected shape. The plate will have a circular internal boundary and an arbitrary shaped external contour with both internal and external edges clamped. The governing differential equation for bending of thin plates is

$$\nabla^4 w = \frac{q}{D} \tag{1}$$

where ∇^4 is the biharmonic operator, q is the intensity of loading and D is the flexural rigidity.

Since, only the clamped edges will be considered, the corresponding boundary conditions are

$$\begin{aligned} w &= 0 \\ \frac{\partial w}{\partial n} &= 0 \end{aligned} \tag{2}$$

where n is the outward normal to the boundary.

The general solution of the plate equation (1) was given by Timoshenko and Woinowsky-Krieger [3]. It will be shown that this

general solution in polar coordinates yields solutions to a class of doubly connected plates characterized by an internal circular hole. To non-dimensionalize the governing equation, a reference length a_1 was selected on the basis of the geometrical shape of the external boundary. As we are concerned with plates having an internal circular hole, the origin of the coordinate system is conveniently located at the centre of the circular hole as shown in Fig. 1.

Since we are concerned only with the plates having symmetry about the lines $\phi = 0$ and π (see Fig. 1) the general solution [3] can be simplified as follows by using a_1 ,

$$w = \frac{qa_1^4}{D}\left[\frac{r^4}{64} + A_o + B_o r^2 + c_o \log r + D_o r^2 \log r \right.$$
$$+ (A_1 r + B_1 r^{-1} + C_1 r^3 + D_1 r \log r) \cos \phi \qquad (3)$$
$$\left. + \sum_{j=2}^{\infty} (A_j r^j + B_j r^{-j} + C_j r^{j+2} + D_j r^{-j+2}) \cos j\phi\right] .$$

By satisfying the clamped edge boundary conditions exactly along the inner circular edge $r' = b'$, the coefficients A_j and C_j can be expressed in terms of B_j and D_j as follows

$$A_o = \frac{b^4}{64}(4 \log b - 1) + B_o b^2 (2 \log b - 1) + 2D_o b^2 (\log b)^2$$

$$C_o = -\frac{b^4}{64} - 2B_o b^2 - D_o (b^2 + 2b^2 \log b)$$

$$A_1 = -\frac{2B_1}{b^2} - D_1 (\log b - \tfrac{1}{2}) \qquad (4)$$

$$C_1 = \frac{B_1}{b^4} - \frac{D_1}{2b^2}$$

$$A_j = -\frac{(1+j)B_j}{b^{2j}} - \frac{j\,D_j}{b^{2j-2}} \qquad (4)$$

$$C_j = \frac{j\,B_j}{b^{2j+2}} + \frac{(j-1)D_j}{b^{2j}}$$

$$j = 2, 3, \ldots, \infty \quad .$$

The final expression for the deflection is

$$\begin{aligned} w = \frac{qa_1^4}{D}\Big[&\frac{r^4}{64} - \frac{b^4}{64}\left(4\log\frac{r}{b} + 1\right) \\ &+ B_o\left(r^2 - b^2 - 2b^2\log\frac{r}{b}\right) \\ &- D_o\left(2b^2\log b\log\frac{r}{b} - (r^2-b^2)\log r\right) \\ &+ B_1\left(\frac{1}{r} - \frac{2r}{b^2} + \frac{r^3}{b^4}\right)\cos\phi \qquad (5) \\ &+ D_1\left(\frac{r}{2} - \frac{r^3}{2b^2} + r\log\frac{r}{b}\right)\cos\phi \\ &+ \sum_{j=2}^{\infty} B_j\left(\frac{1}{r^j} - \frac{(1+j)r^j}{b^{2j}} + \frac{j\,r^{j+2}}{b^{2j+2}}\right)\cos j\phi \\ &+ \sum_{j=2}^{\infty} D_j\left(\frac{1}{r^{j-2}} - \frac{j\,r^j}{b^{2j-2}} + \frac{(j-1)r^{j+2}}{b^{2j}}\right)\cos j\phi\Big] \quad . \end{aligned}$$

The slope in the normal direction n along the external boundary can be obtained from the slopes in the radial and tangential directions by using the following equation.

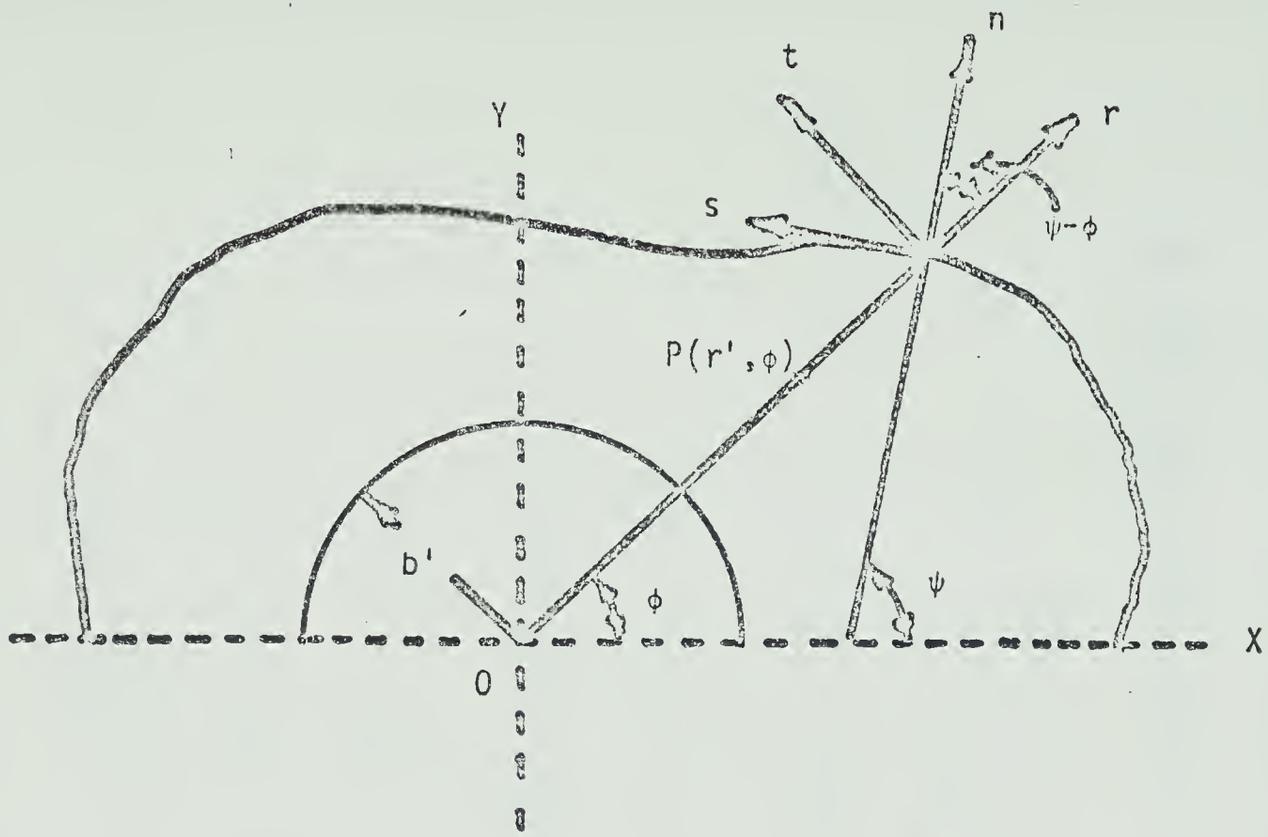

Fig. 1. Coordinate system for a plate with circular internal hole and arbitrary external boundary symmetric about the axis $\phi = 0$.

$$\frac{\partial w}{\partial n} = \frac{\sin(\psi-\phi)}{r'} \frac{\partial w}{\partial \phi} + \cos(\psi-\phi) \frac{\partial w}{\partial r'} \quad . \tag{6}$$

Substituting the appropriate expressions into equation (6) yields,

$$\begin{aligned}
\frac{\partial w}{\partial n} = \frac{qa_1^3}{D} \Big[& \left(-\frac{b^4}{16r} + \frac{r^3}{16}\right) \cos(\psi-\phi) \\
& + B_0 \left(-\frac{2b^2}{r} + 2r\right) \cos(\psi-\phi) \\
& - D_0 \left(-2r \log r + \frac{2b^2}{r} \log b + \frac{b^2-r^2}{r}\right) \cos(\psi-\phi) \\
& + B_1 \left\{\left(-\frac{1}{r^2} - \frac{2}{b^2} + \frac{3r^2}{b^4}\right) \cos(\psi-\phi) \cos\phi \right. \\
& \left. - \left(\frac{1}{r^2} - \frac{2}{b^2} + \frac{r^2}{b^4}\right) \sin(\psi-\phi) \sin\phi \right\} \qquad (7) \\
& + D_1 \left\{\left(\log\frac{r}{b} + \frac{3}{2} - \frac{3r^2}{2b^2}\right) \cos(\psi-\phi) \cos\phi \right. \\
& \left. - \left(\log\frac{r}{b} + \frac{1}{2} - \frac{r^2}{2b^2}\right) \sin(\psi-\phi) \sin\phi \right\} \\
& + \sum_{j=2}^{\infty} B_j \left\{\left(-\frac{j}{r^{j+1}} - \frac{j(j+1)r^{j-1}}{b^{2j}} + \frac{j(j+2)r^{j+1}}{b^{2j+2}}\right) \cos(\psi-\phi) \cos j\phi \right. \\
& \left. - \left(\frac{j}{r^{j+1}} - \frac{j(j+1)r^{j-1}}{b^{2j}} + \frac{j^2 r^{j+1}}{b^{2j+2}}\right) \sin(\psi-\phi) \sin\phi \right\} \\
& + \sum_{j=2}^{\infty} D_j \left\{\left(-\frac{(j-2)}{r^{j-1}} - \frac{j^2 r^{j-1}}{b^{2j-2}} + \frac{(j-1)(j-2)r^{j+1}}{b^{2j}}\right) \cos(\psi-\phi) \cos j\phi \right. \\
& \left. - \left(\frac{j}{r^{j-1}} - \frac{j^2 r^{j-1}}{b^{2j-2}} + \frac{j(j-1)r^{j+1}}{b^{2j}}\right) \sin(\psi-\phi) \sin j\phi \right\} \Big]
\end{aligned}$$

The unknown coefficients B_j and D_j can be determined by satisfying the boundary conditions (2) along the external contour at discrete points. The convergence of the solution can be checked by gradually increasing the number of points to be matched. Furthermore, the maximum boundary errors can be compared with the maximum deflection and slope inside the plate.

The expressions for $\frac{\partial w}{\partial r'}$, $\frac{\partial^2 w}{\partial r'^2}$, $\frac{\partial w}{\partial \phi}$, $\frac{\partial^2 w}{\partial \phi^2}$, and $\frac{\partial^2 w}{\partial r' \partial \phi}$ are given in Appendix A. These derivatives are used to compute the radial, tangential and twisting moments, where

$$M_r = -D \left\{\frac{\partial^2 w}{\partial r'^2} + \nu \left(\frac{1}{r'} \frac{\partial w}{\partial r'} + \frac{1}{r'^2} \frac{\partial^2 w}{\partial \phi^2}\right)\right\}$$

$$M_t = -D \left(\nu \frac{\partial^2 w}{\partial r'^2} + \frac{1}{r'} \frac{\partial w}{\partial r'} + \frac{1}{r'^2} \frac{\partial^2 w}{\partial \phi^2}\right) \qquad (8)$$

and

$$M_{rt} = -D (1-\nu)\left(\frac{1}{r'} \frac{\partial^2 w}{\partial r' \partial \phi} - \frac{1}{r'^2} \frac{\partial w}{\partial \phi}\right) .$$

Moments along a given general contour in the directions n and s (see Fig. 1) are given by

$$M_n = \left(\frac{M_r+M_t}{2}\right) + \left(\frac{M_r-M_t}{2}\right) \cos 2(\psi-\phi) + M_{rt} \sin 2(\psi-\phi)$$

$$M_s = \left(\frac{M_r+M_t}{2}\right) - \left(\frac{M_r-M_t}{2}\right) \cos 2(\psi-\phi) - M_{rt} \sin 2(\psi-\phi) \quad . \qquad (9)$$

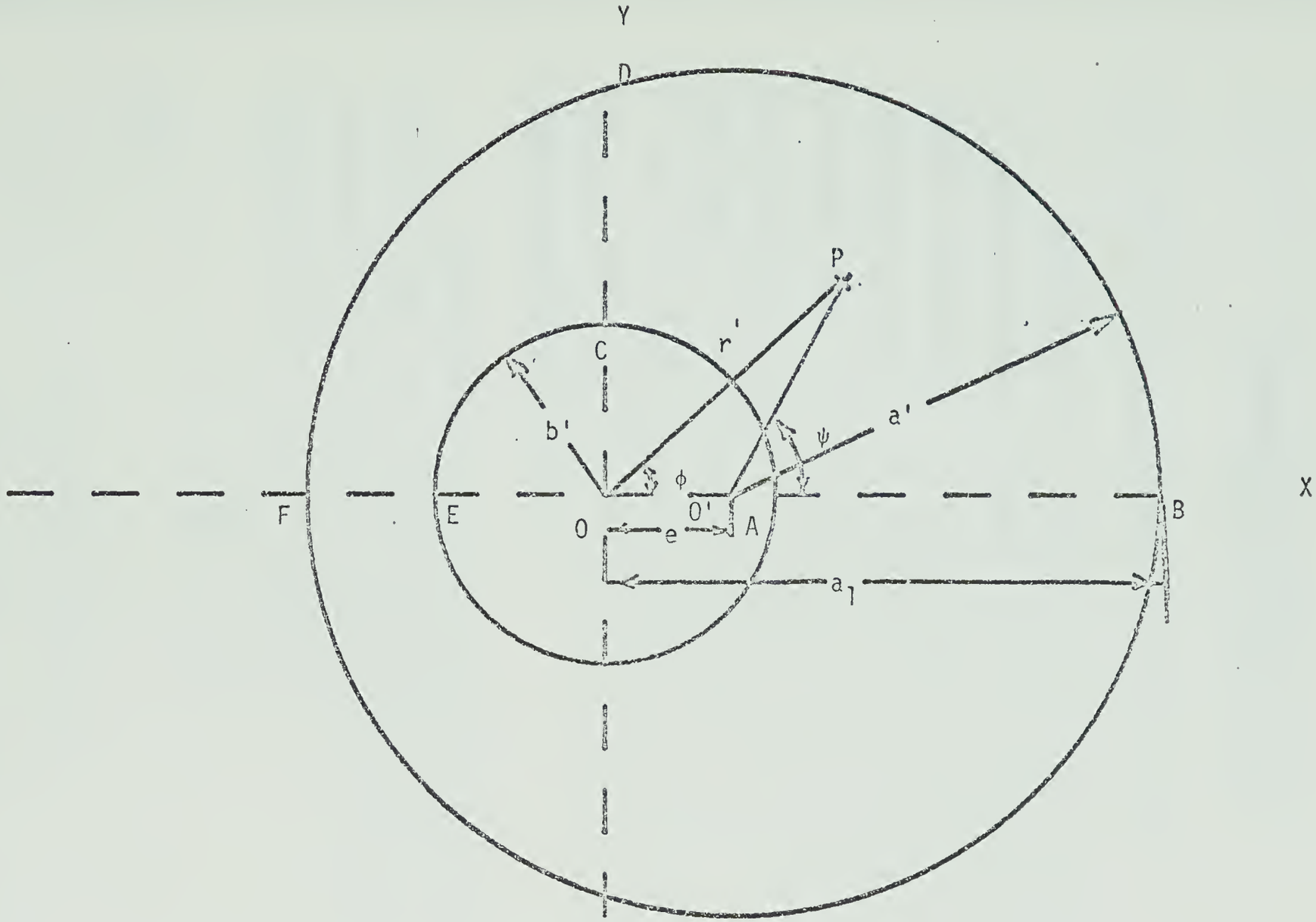

Fig. 2. Coordinate system for an eccentric annular plate

CHAPTER III

APPLICATIONS AND NUMERICAL RESULTS

3.1 Uniformly Loaded Clamped Eccentric Annular Plate.

As stated earlier, the exact solutions in bi-polar coordinates for the present problem were given by both Woinowsky-Krieger [9] and Yamanaka and Kakae [10]. Since the numerical calculation using bi-polar coordinates is tedious, these authors did not give numerical results for various radius ratios and eccentricity ratios. Yamanaka and Kakae gave the numerical and graphical results for only one case where the radius ratio $\alpha = 0.5$ and eccentricity ratio $\beta = 0.391$. In this work, the numerical results for maximum deflection and moments for various radius ratios and eccentricity ratios will be obtained using the equations developed in Chapter II.

The coordinate system for an eccentric annular plate is shown in Fig. 2. Length OB is taken as the reference length a_1. Considering a triangle OPO' with the point P on the boundary, the equation for the external contour in polar coordinates is

$$r^2 = 1 - \frac{2ae}{a_1}\ (1 - \cos\psi) \qquad (10)$$

where

$$\psi = \phi + \sin^{-1}\ (\beta(1-\alpha)\ \sin\phi)$$

$$\alpha = \frac{b'}{a'}\ ;\quad \beta = \frac{e}{a'-b'}\ ;\quad r = \frac{r'}{a_1}\ ;\quad a = \frac{a'}{a_1}\ \text{ and }\ b = \frac{b'}{a_1}\ .$$

Cheng and Hwang [16] in solving the problem of laminar forced convection problem for eccentric annular ducts using the point matching method have shown that twenty-one equally spaced points along the outer boundary BDF (see Fig. 2) are sufficient to obtain accurate solutions. It is also found that 21 equally spaced points are adequate for the present problem. The resulting 42 linear equations with 42 unknowns obtained by satisfying the boundary conditions at 21 equally spaced points are solved by the Gauss-Jordan method. In general, the numerical values of the coefficients decrease rapidly indicating the convergence of the solution. Equation (8) and (9) are used to calculate the moments along AB, CD, EF (see Fig. 2) and along the inner and outer edges.

The convergence of the solution may be ascertained by computing the boundary errors and comparing their maximum magnitudes with the maximum deflection and slope inside the plate. Furthermore, one can study the convergence of the maximum deflection and moments by gradually increasing the number of points matched along the boundary. It is found that the numerical results using 21 equally spaced points are satisfactory. As can be expected, the maximum deflection is located along the line AB and the maximum moment along the inner edge occurs at A and along the outer edge at B (Fig. 2). For convenience in design, numerical values for the maximum deflection and its location and maximum moments along the outer and inner edges, respectively, are listed in Table 1 for radius-ratio α and eccentricity ratio β both

varying from 0.1 to 0.9 with an increment of 0.1, for the case of Poisson's ratio = 0.3.

A study of the behaviour of the maximum values with respect to the two parameters α and β yields the following observations. Qualitatively, the values of the maximum deflection and moments decrease as radius ratio α increases. But, as the eccentricity ratio β increases, the values of the maximum deflection and moments increase correspondingly. However, for the case $\alpha = 0.1$, the maximum deflection decreases as β increases and themoments M_n at B and M_r at A do not seem to follow the expected trend for some ranges of the eccentricity ratio β. One notes that the numerical results for $\alpha = 0.1$ and $\beta = 0.1$ are quite close to those of the annular plate with $\alpha = 0.1$ as expected. Also for the case $\alpha = 0.2$, the maximum deflection for the eccentricity ratio ranging from $\beta = 0.5$ to $\beta = 0.7$ seems to decrease in value and the moment M_n at B is less in value for the case $\beta = 0.4$ as compared with those for $\beta = 0.1$ to $\beta = 0.3$. The minor difficulty with M_n at B also exists for the case $\alpha = 0.3$ with $\beta = 0.5$ and 0.6. An attempt was made to improve the results in the above mentioned cases by increasing the number of points matched along the external boundary. The behaviour of the moment M_n at B improved somewhat in the range $\beta = 0.1$ to 0.4 for the cases $\alpha = 0.1$ and $\alpha = 0.2$ with a 25 point matching solution. It is not known why the numerical result can not be improved by increasing the number of points matched along the external boundary for the case $\alpha = 0.1$ and in the ranges of $\beta = 0.5$ to 0.7 for the case $\alpha = 0.2$. The erratic behaviour of the maximum deflection is found to exist for smaller radius ratios ($\alpha = 0.1$ and 0.2) only and may

be due to ill conditioned matrix. For a given value of eccentricity ratio β, the location of the maximum deflection moves towards the inner edge along AB as the size of the hole increases. It is of interest to note that the computing time required to obtain the numerical results for all the radius ratios and eccentricity ratios considered in this study was about 47 minutes by using the IBM 360/67.

To demonstrate the accuracy of the solution, the percentage of the maximum boundary errors for the deflection and slope with respect to the maximum values inside the plate are presented in Table 2 for the extreme cases with β= 0.1 and 0.9 and radius ratio α ranging from 0.1 to 0.9. The boundary errors are large for larger values of α and β but they never exceed 0.17% for deflection and 0.51% for slope. The numerical values for the dimensionless deflection and slope along the circular hole are of the order of 10^{-17} or less and thereby checking the algebraic manipulation for satisfying the clamped edge conditions. The validity of the numerical results can be further checked by considering the limiting case of zero eccentricity (β = 0). Since the solution for annular plates is available in the literature, the computed values for the maximum deflection and maximum moments along both edges for annular plates are compared against the values calculated from Georgian's analysis (see Table 3). It is seen that the agreement is very good. It is noted that the boundary errors for this case are absolutely negligible and the convergence of the solution is extremely rapid. The coefficients B_1, B_2,..., and D_1,D_2,..., in equations (5) and (7) are insignificant as compared with the leading terms B_o and D_o.

The deflection, slope and the bending moment curves along the lines AB, CD and EF are shown in Figs. 3 to 6 for the case of $\alpha = \beta = 0.5$. The deflection and slope along the line EF is considerably less than that along the lines AB and CD (see Figs. 3 and 4). For a given angular coordinate ϕ, the values of the moments M_r and M_t at the inner circular boundary are larger than at the outer edge (see Figs. 5 and 6). The moments M_n and M_s along the outer edge and M_r and M_t along the inner edge are shown in Figs. 7 and 8 for the above case. As expected, the clamped edge moments are negative. The maximum moments for the inner and outer edges occur at points A and B, respectively, and the numerical values of the moments decrease with increase of polar angle ϕ.

In order to further assess the accuracy of the present results, the numerical values given by Yamanaka and Kakae [10] for the case of $\alpha = 0.5$ and $\beta = 0.391$ are compared with the results from this analysis in Table 4. Yamanaka and Kakae in obtaining their results, used only five terms of the infinite series for the numerical calculations. It is seen that the agreement is generally good. In addition graphical results from this work are also compared against those of Yamanaka and Kakae in Figs. 9 to 11. The agreements for deflection and radial bending moments are good (see Figs. 9 and 10). Some discrepancy is noticed in the values of tangential moments along AB (see Fig. 11).

Table 1 Numerical Results for Uniformly Loaded Clamped Eccentric Annular Plates

Eccentricity Ratio	Maximum Value	Deflection Location	Maximum M_n at B	Moment M_r at A
β	$(w/\frac{qa_1^4}{D}) \times 10^2$	r	$(M_n/qa_1^2) \times 10$	$(M_r/qa_1^2) \times 10$
Radius Ratio $\alpha = 0.1$				
0.1	.1757	.5050	.5290	1.4965
0.2	.1734	.4966	.5138	1.5361
0.3	.1692	.4933	.4967	1.5537
0.4	.1636	.4904	.5668	1.5508
0.5	.1566	.4926	.8516	1.5281
0.6	.1487	.4904	1.2633	1.4860
0.7	.1385	.4790	1.3635	1.4216
0.8	.1132	.4349	1.4372	1.3157
0.9	.0992	.5276	1.5161	1.2457
Radius Ratio $\alpha = 0.2$				
0.1	.1143	.5600	.4428	.9105
0.2	.1179	.5500	.4407	.9492
0.3	.1200	.5470	.4353	.9785
0.4	.1208	.5418	.4281	.9986
0.5	.1203	.5371	.6057	1.0097
0.6	.1188	.5330	.6804	1.0116
0.7	.1163	.5293	.8516	1.0244
0.8	.1560	.5609	.9932	1.0936
0.9	.1693	.4695	.9835	1.1697

Eccentricity Ratio	Maximum Value	Deflection Location	Maximum M_n at B	Moment M_r at A
β	$(w/\frac{qa_1^4}{D}) \times 10^3$	r	$(M_n/qa_1^2) \times 10$	$(M_r/qa_1^2) \times 10$
Radius Ratio $\alpha = 0.3$				
0.1	.6966	.6186	.3577	.6112
0.2	.7498	.6095	.3646	.6480
0.3	.7943	.5976	.3685	.6799
0.4	.8302	.5904	.3698	.7069
0.5	.8577	.5830	.3687	.7290
0.6	.8772	.5780	.3660	.7460
0.7	.8891	.5687	.3650	.7582
0.8	.8929	.5638	.3672	.7652
0.9	.9012	.5920	.3683	.7677
Radius Ratio $\alpha = 0.4$				
0.1	.3909	.6731	.2765	.4150
0.2	.4381	.6625	.2885	.4472
0.3	.4821	.6529	.2981	.4769
0.4	.5224	.6410	.3055	.5039
0.5	.5586	.6331	.3109	.5283
0.6	.5906	.6260	.3146	.5499
0.7	.6181	.6193	.3168	.5688
0.8	.6414	.6096	.3181	.5849
0.9	.6601	.6040	.3203	.5982

Eccentricity Ratio	Maximum Value	Deflection Location	Maximum M_n at B	Moment M_r at A
β	$(w/\frac{qa_1^4}{D}) \times 10^3$	r	$(M_n/qa_1^2) \times 10$	$(M_r/qa_1^2) \times 10$
Radius Ratio $\alpha = 0.5$				
0.1	.1959	.7276	.2017	.2739
0.2	.2284	.7164	.2152	.2999
0.3	.2608	.7060	.2271	.3247
0.4	.2927	.6938	.2376	.3483
0.5	.3236	.6850	.2467	.3706
0.6	.3532	.6760	.2545	.3916
0.7	.3813	.6696	.2610	.4111
0.8	.4776	.6625	.2663	.4292
0.9	.4320	.6520	.2705	.4458
Radius Ratio $\alpha = 0.6$				
0.1	.0834	.7821	.1353	.1695
0.2	.1011	.7711	.1456	.1885
0.3	.1197	.7609	.1591	.2073
0.4	.1390	.7513	.1699	.2256
0.5	.1589	.7400	.1798	.2434
0.6	.1790	.7316	.1890	.2608
0.7	.1999	.7238	.1974	.2775
0.8	.2194	.7163	.2050	.2937
0.9	.2392	.7094	.2120	.3092

Eccentricity Ratio	Maximum Value	Deflection Location	Maximum M_n at B	Moment M_r at A
β	$(w/\frac{qa_1^4}{D}) \times 10^4$	r	$(M_n/qa_1^2) \times 10$	$(M_r/qa_1^2) \times 10$
Radius Ratio $\alpha = 0.7$				
0.1	.2743	.8366	.0797	.0932
0.2	.3456	.8267	.0888	.1054
0.3	.4245	.8175	.0978	.1176
0.4	.5107	.8088	.1065	1299
0.5	.6033	.7985	.1150	.1422
0.6	.7018	.7905	.1231	.1544
0.7	.8055	.7829	.1310	.1666
0.8	.9137	.7757	.1385	.1786
0.9	1.0256	.7689	.1457	.1904
Radius Ratio $\alpha = 0.8$				
0.1	.0564	.8910	.3702	.4084
0.2	.0738	.8835	.4217	.4694
0.3	.0941	.8761	.4741	.5324
0.4	.1173	.8678	.5271	.5971
0.5	.1434	.8609	.5803	.6632
0.6	.1725	.8430	.6336	.7305
0.7	.2044	8479	.6857	.7988
0.8	.2392	.8417	.7396	.8679
0.9	.2768	.8357	.7920	.9375

Eccentricity Ratio	Maximum Value	Deflection Location	Maximum M_n at B	Moment M_r at A
β	$(w/\frac{qa_1^4}{D}) \times 10^5$	r	$(M_n/qa_1^2) \times 10^2$	$(M_r/qa_1^2) \times 10^2$
Radius Ratio $\alpha = 0.9$				
0.1	.0367	.9450	.0966	.1012
0.2	.0499	.9406	.1125	.1184
0.3	.0661	.9363	.1292	.1365
0.4	.0855	.9320	.1467	.1556
0.5	.1083	.9278	.1648	.1756
0.6	.1349	.9237	.1836	.1964
0.7	.1656	.9197	.2029	.2180
0.8	.2005	.9058	.2279	.2403
0.9	.2397	.9172	.2431	.2634

Table 2 Maximum Boundary Errors for Deflection and Normal Slope Along the Outer Edge for Uniformly Loaded Clamped Eccentric Annular Plates.

Radius Ratio	Eccentricity Ratio	Maximum Boundary Errors				Maximum Values Inside the Plate	
		Deflection		Slope		Deflection	Slope
α	β	$(w/\frac{qa_1^4}{D})$	%	$(\frac{\partial w}{\partial n})/(\frac{qa_1^3}{D})$	%	$(w/\frac{qa_1^4}{D})$	$(\frac{\partial w}{\partial n})/(\frac{qa_1^3}{D})$
0.1	0.1	$.91 \times 10^{-10}$	$.52 \times 10^{-5}$	$.20 \times 10^{-8}$	$.30 \times 10^{-4}$	$.1757 \times 10^{-2}$	$.6644 \times 10^{-2}$
	0.9	$.17 \times 10^{-8}$	$.17 \times 10^{-3}$	$.31 \times 10^{-8}$	$.30 \times 10^{-3}$	$.9992 \times 10^{-3}$	$.1035 \times 10^{-2}$
0.2	0.1	$.73 \times 10^{-8}$	$.70 \times 10^{-3}$	$.51 \times 10^{-7}$	$.11 \times 10^{-2}$	$.1143 \times 10^{-2}$	$.4696 \times 10^{-2}$
	0.9	$.70 \times 10^{-7}$	$.64 \times 10^{-2}$	$.21 \times 10^{-6}$	$.10 \times 10^{-1}$	$.1693 \times 10^{-2}$	$.1942 \times 10^{-2}$
0.3	0.1	$.25 \times 10^{-8}$	$.36 \times 10^{-3}$	$.68 \times 10^{-7}$	$.21 \times 10^{-2}$	$.6966 \times 10^{-3}$	$.3171 \times 10^{-2}$
	0.9	$.94 \times 10^{-7}$	$.10 \times 10^{-1}$	$.11 \times 10^{-6}$	$.87 \times 10^{-2}$	$.9012 \times 10^{-3}$	$.1195 \times 10^{-2}$
0.4	0.1	$.41 \times 10^{-8}$	$.11 \times 10^{-2}$	$.46 \times 10^{-7}$	$.23 \times 10^{-2}$	$.3909 \times 10^{-3}$	$.2037 \times 10^{-2}$
	0.9	$.55 \times 10^{-6}$	$.83 \times 10^{-1}$	$.57 \times 10^{-6}$	$.20 \times 10^{-1}$	$.6601 \times 10^{-3}$	$.2947 \times 10^{-2}$
0.5	0.1	$.36 \times 10^{-8}$	$.18 \times 10^{-2}$	$.51 \times 10^{-7}$	$.42 \times 10^{-2}$	$.1959 \times 10^{-3}$	$.1202 \times 10^{-2}$
	0.9	$.95 \times 10^{-7}$	$.22 \times 10^{-1}$	$.60 \times 10^{-6}$	$.20 \times 10^{-1}$	$.4320 \times 10^{-3}$	$.2843 \times 10^{-2}$
0.6	0.1	$.39 \times 10^{-8}$	$.47 \times 10^{-2}$	$.51 \times 10^{-7}$	$.81 \times 10^{-2}$	$.8340 \times 10^{-4}$	$.6269 \times 10^{-3}$
	0.9	$.11 \times 10^{-7}$	$.46 \times 10^{-2}$	$.19 \times 10^{-6}$	$.14 \times 10^{-1}$	$.2392 \times 10^{-3}$	$.1386 \times 10^{-2}$
0.7	0.1	$.42 \times 10^{-9}$	$.15 \times 10^{-2}$	$.24 \times 10^{-7}$	$.88 \times 10^{-2}$	$.2743 \times 10^{-4}$	$.2697 \times 10^{-3}$
	0.9	$.12 \times 10^{-7}$	$.12 \times 10^{-1}$	$.31 \times 10^{-6}$	$.43 \times 10^{-1}$	$.1026 \times 10^{-3}$	$.7307 \times 10^{-3}$
0.8	0.1	$.51 \times 10^{-9}$	$.90 \times 10^{-2}$	$.42 \times 10^{-8}$	$.51 \times 10^{-2}$	$.5640 \times 10^{-5}$	$.8156 \times 10^{-4}$
	0.9	$.28 \times 10^{-8}$	$.10 \times 10^{-1}$	$.53 \times 10^{-7}$	$.20 \times 10^{-1}$	$.2768 \times 10^{-4}$	$.2712 \times 10^{-3}$
0.9	0.1	$.32 \times 10^{-9}$	$.87 \times 10^{-1}$	$.54 \times 10^{-8}$	$.70 \times 10^{-1}$	$.3670 \times 10^{-6}$	$.7808 \times 10^{-5}$
	0.9	$.42 \times 10^{-8}$	.17	$.83 \times 10^{-8}$	.51	$.2397 \times 10^{-5}$	$.1632 \times 10^{-5}$

Table 3 Comparison of Numerical Result of This Work With That of Georgian [6] for the case $\beta = 0$.

Radius Ratio α	Maximum Deflection Value $(w/\frac{qa_1^4}{D})$	Location r	M_n Along Outer Edge (M_n/qa_1^2)	M_r Along Inner Edge (M_r/qa_1^2)
0.1	$.1757 \times 10^{-2}$	.5095	$.5402 \times 10^{-1}$	.1433
	* $.1757 \times 10^{-2}$	.5095	$.5402 \times 10^{-1}$	.1433
0.2	$.1090 \times 10^{-2}$	.5720	$.4409 \times 10^{-1}$	$.8624 \times 10^{-1}$
	$.1090 \times 10^{-2}$	.5720	$.4409 \times 10^{-1}$	$.8625 \times 10^{-1}$
0.3	$.6347 \times 10^{-3}$	.6290	$.3470 \times 10^{-1}$	$.5697 \times 10^{-1}$
	$.6347 \times 10^{-3}$	.6290	$.3474 \times 10^{-1}$	$.5697 \times 10^{-1}$
0.4	$.3408 \times 10^{-3}$	.6880	$.2625 \times 10^{-1}$	$.3804 \times 10^{-1}$
	$.3408 \times 10^{-3}$	.6880	$.2620 \times 10^{-1}$	$.3804 \times 10^{-1}$
0.5	$.1637 \times 10^{-3}$	.7425	$.1863 \times 10^{-1}$	$.2469 \times 10^{-1}$
	$.1637 \times 10^{-3}$	.7425	$.1866 \times 10^{-1}$	$.2469 \times 10^{-1}$
0.6	$.6693 \times 10^{-4}$	.7960	$.1248 \times 10^{-1}$	$.1502 \times 10^{-1}$
	$.6689 \times 10^{-4}$	.7940	$.1223 \times 10^{-1}$	$.1502 \times 10^{-1}$
0.7	$.2110 \times 10^{-4}$	.8470	$.7038 \times 10^{-2}$	$.8121 \times 10^{-2}$
	$.2113 \times 10^{-4}$	.8470	$.7038 \times 10^{-2}$	$.8121 \times 10^{-2}$
0.8	$.4092 \times 10^{-5}$	.8990	$.3038 \times 10^{-2}$	$.3512 \times 10^{-2}$
	$.4169 \times 10^{-5}$	.8990	$.3196 \times 10^{-2}$	$.3496 \times 10^{-2}$
0.9	$.2620 \times 10^{-6}$	.9500	$.8247 \times 10^{-3}$	$.8543 \times 10^{-3}$
	$.2604 \times 10^{-6}$	.9495	$.8165 \times 10^{-3}$	$.8517 \times 10^{-3}$

* The second value represents numerical result calculated from Georgian's analysis.

Table 4 Comparison of Result From This Work With That of Yamanaka and Kakae [10] for Uniformly Loaded Clamped Eccentric Annular Plate for the Case $\alpha = 0.5$ and $\beta = 0.391$.

	$(w/\frac{qa_1^4}{D})$	M_r/qa_1^2		M_t/qa_1^2		
	$r = r_m$	at A	$r = r_m$ at B	at A	$r = r_m$	at B
Yamanaka and Kakae	0.2791×10^{-3}	-0.3435×10^{-1}	$+0.1321\times10^{-1}$	-0.2218×10^{-1}	-0.1031×10^{-1}	$+0.0462\times10^{-1}$	-0.0681×10^{-1}
This Work	0.2818×10^{-3}	-0.3412×10^{-1}	$+0.1353\times10^{-1}$	-0.2345×10^{-1}	-0.1024×10^{-1}	$+0.0504\times10^{-1}$	-0.0703×10^{-1}
% Error	0.96%	0.68%	2.36%	5.41%	0.68%	8.33%	3.12%

1. r_m represents the location of the maximum value for deflection and positive moments along AB

2. Percentage error is based on this work.

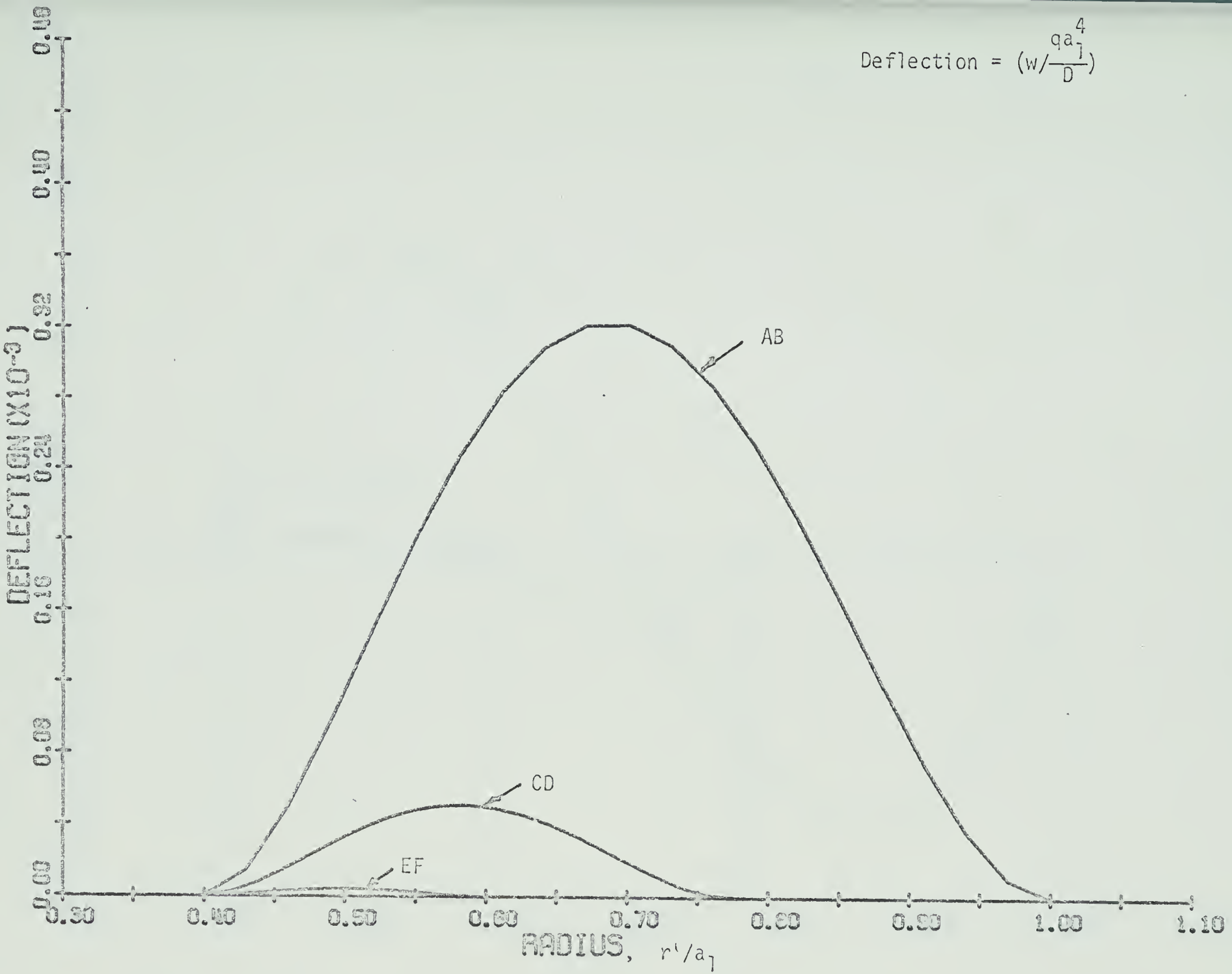

Fig. 3. Distribution of deflection along the lines AB, CD and EF for uniformly loaded clamped eccentric annular plate for the case $\alpha = 0.5$ and $\beta = 0.5$

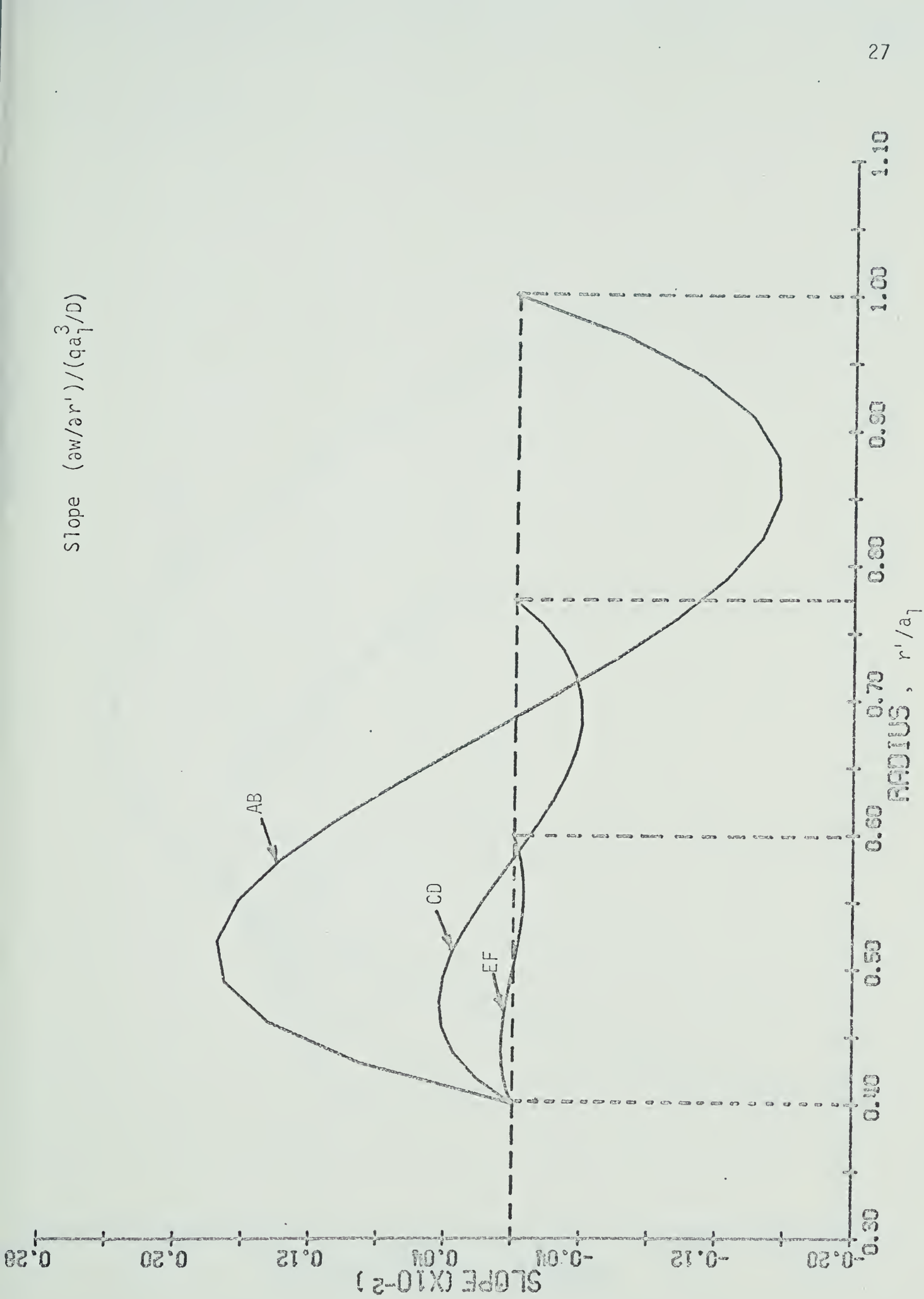

Fig. 4. Distribution of radial slope along the lines AB, CD and EF for uniformly loaded clamped eccentric annular plate for the case $\alpha = 0.5$ and $\beta = 0.5$

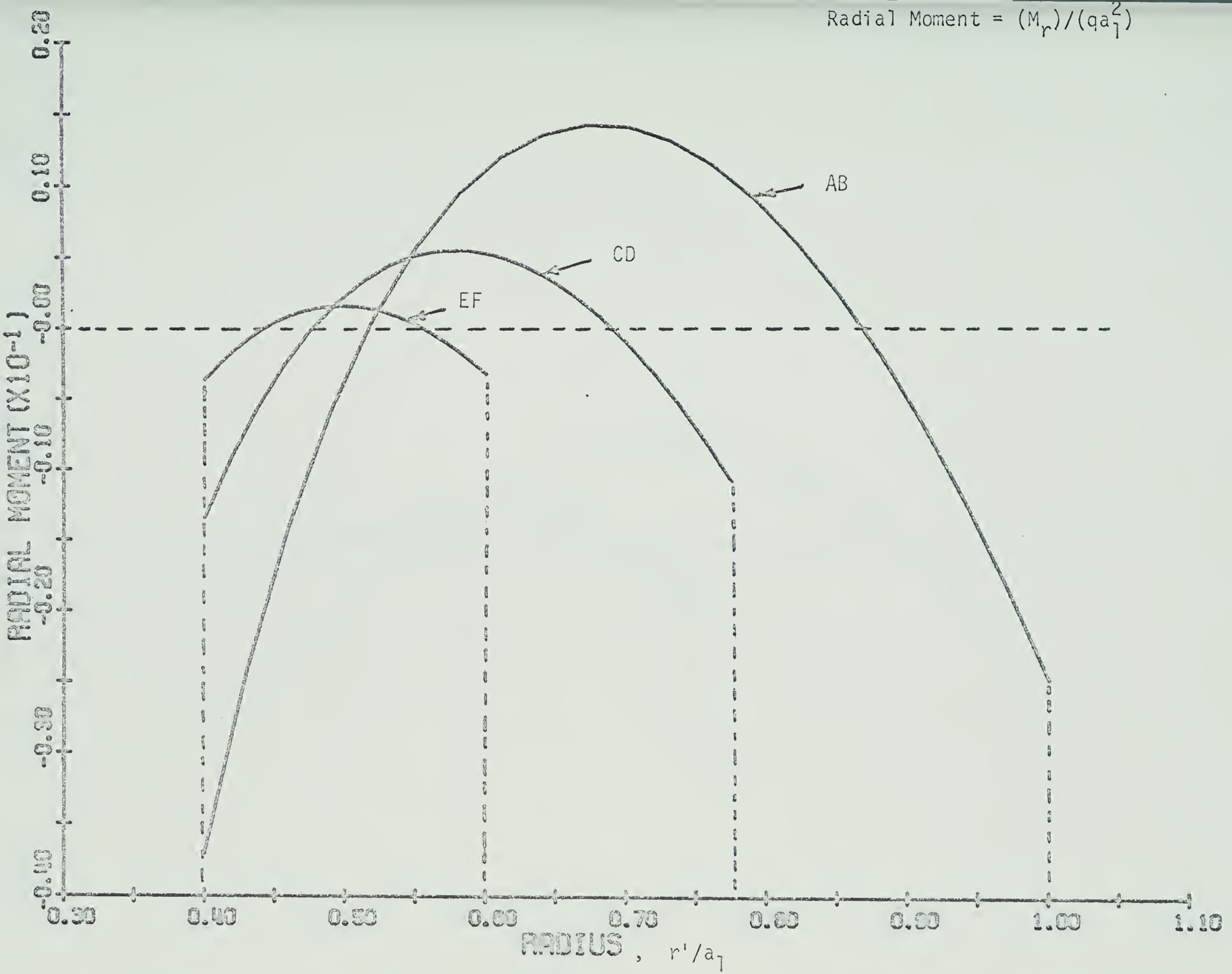

Fig. 5. Distribution of radial moment along the lines AB, CD, and EF for uniformly loaded clamped eccentric annular plate for the case $\alpha = 0.5$ and $\beta = 0.5$

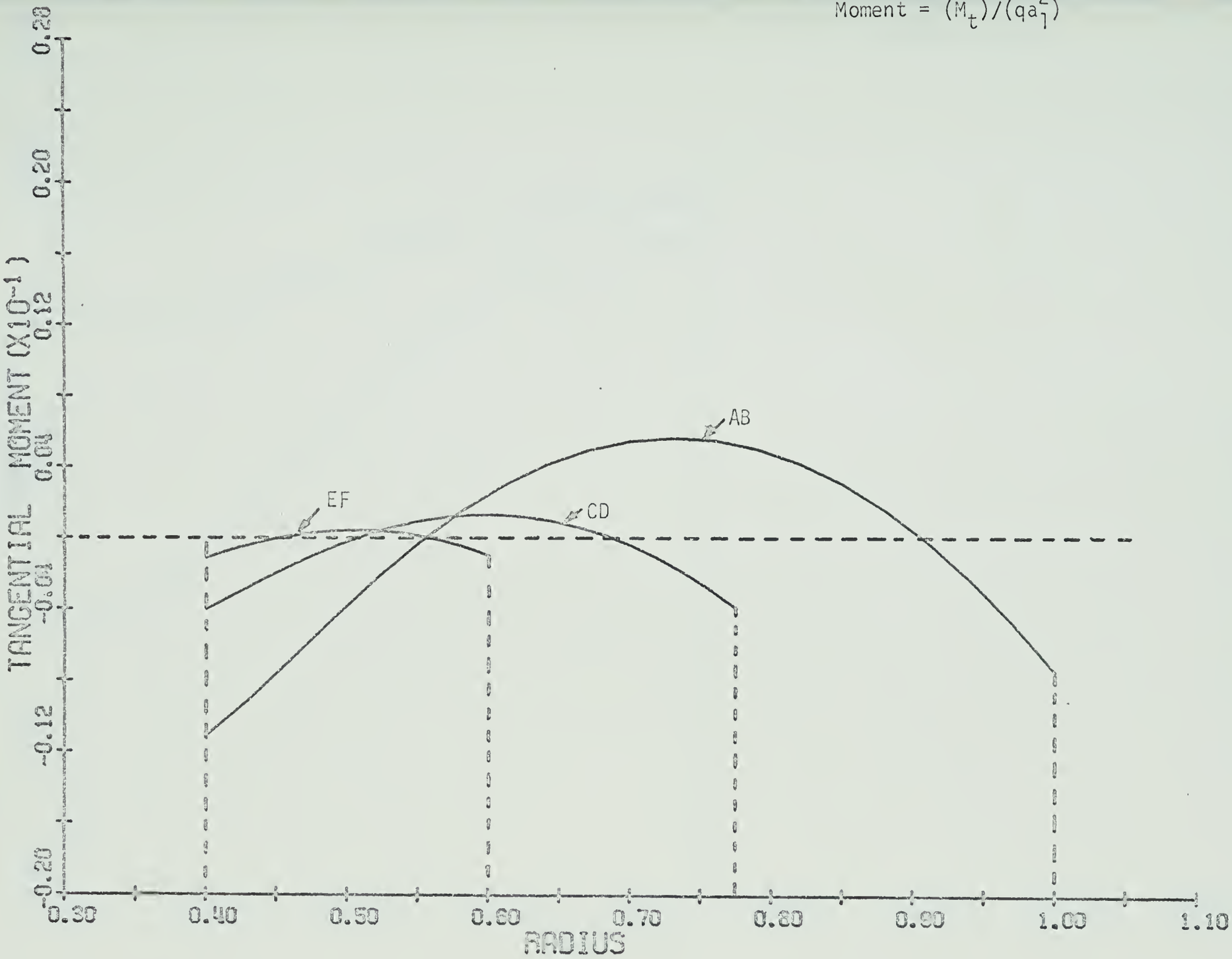

Fig. 6. Distribution of tangential moment along the lines AB, CD and EF for uniformly loaded clamped eccentric annular plate for th case $\alpha = 0.5$ and $\beta = 0.5$

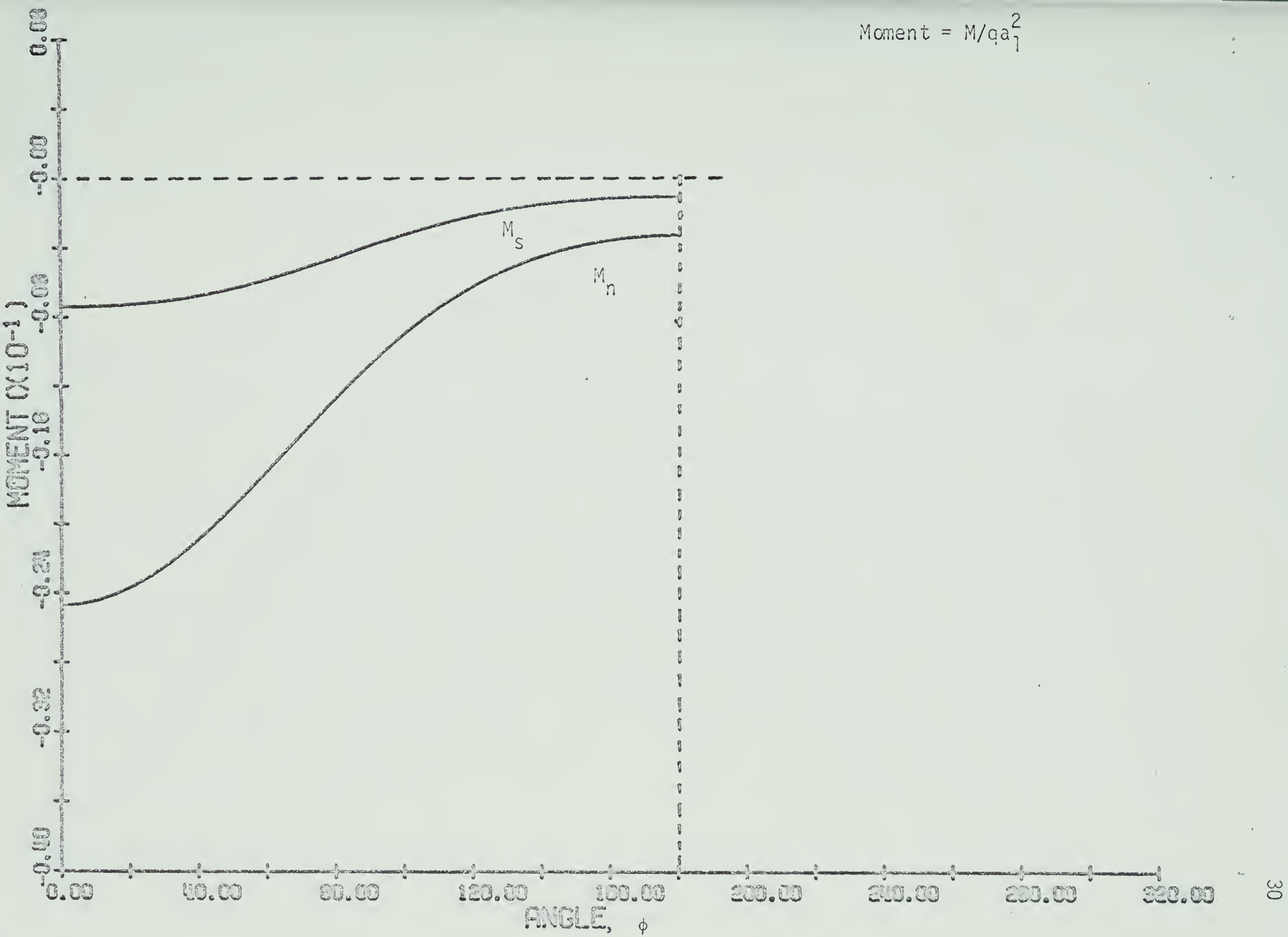

Fig. 7. Distribution of moments M_n, M_s along the outer edge for uniformly loaded clamped eccentric annular plate for the case $\alpha = 0.5$ and $\beta = 0.5$

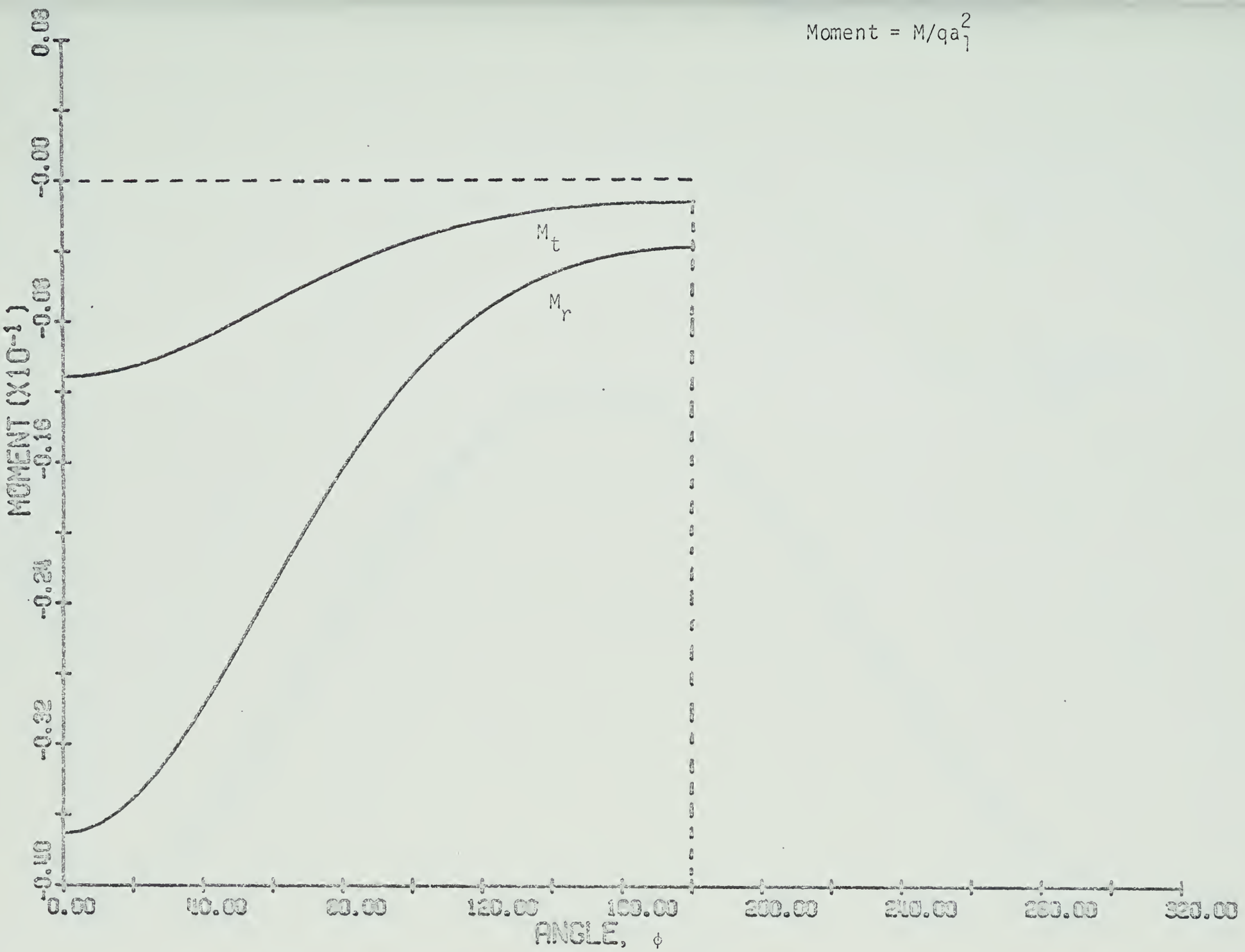

Fig. 8. Distribution of moments M_r, M_t along the inner edge for uniformly loaded clamped eccentric annular plate for the case $\alpha = 0.5$ and $\beta = 0.5$

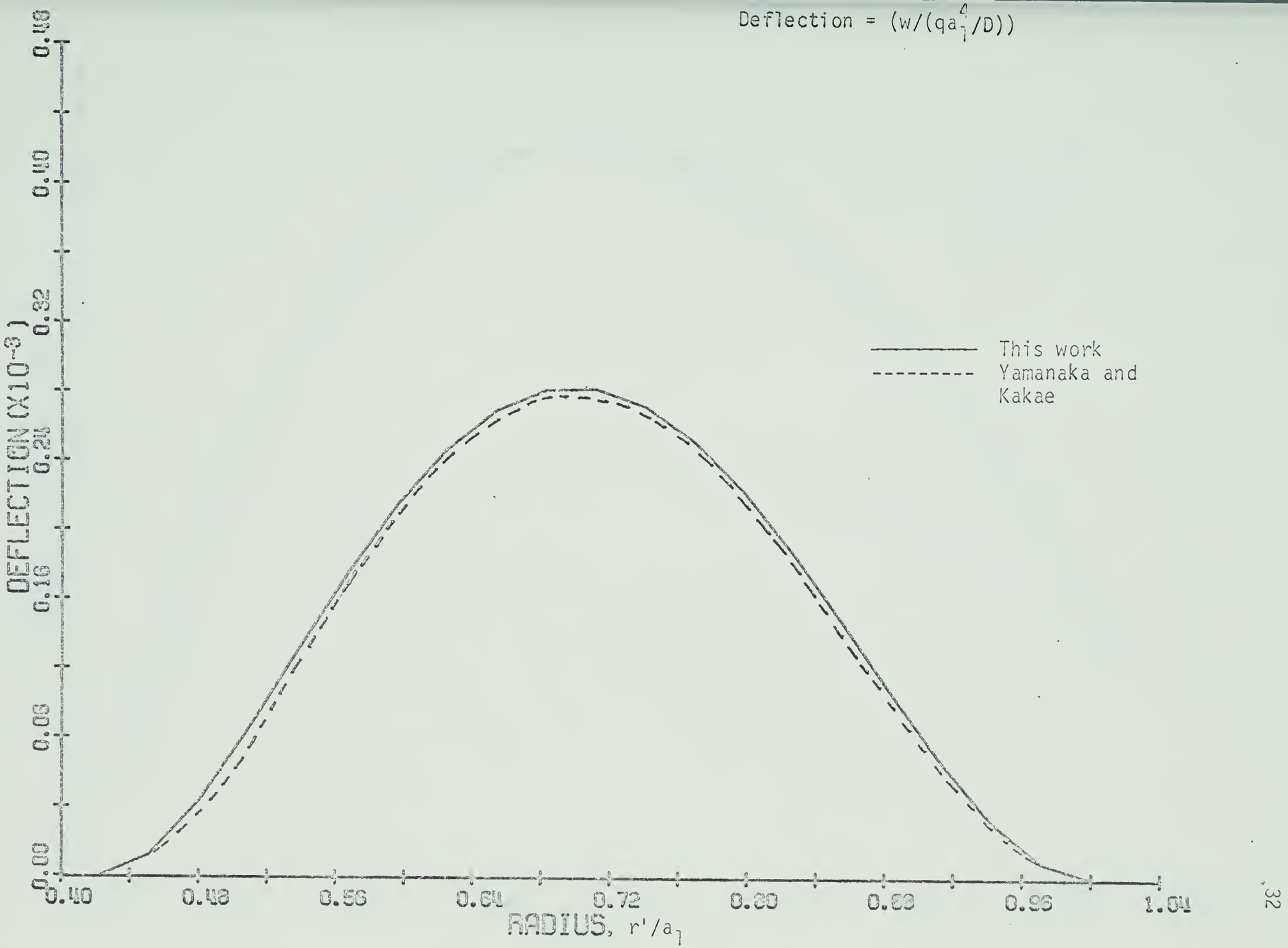

Fig. 9. Comparison of deflection curve along AB from this work with that of Yamanaka and Kakae for uniformly loaded clamped eccentric annular plate for the case $\alpha = 0.5$ and $\beta = 0.391$

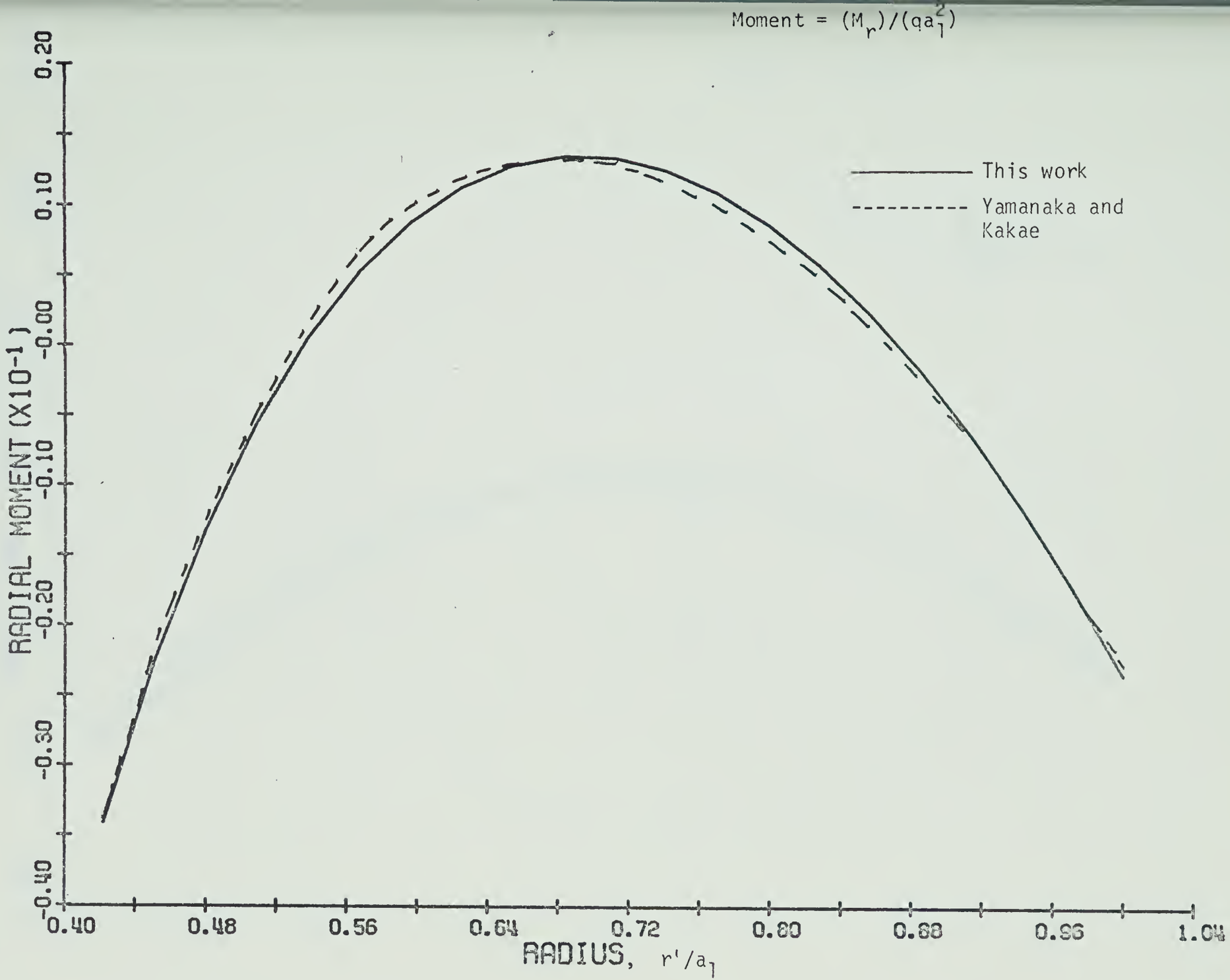

Fig. 10. Comparison of radial moment distribution along AB from this work with that of Yamanaka and Kakae for uniformly loaded clamped eccentric annular plate for the case $\alpha = 0.5$ and $\beta = 0.391$

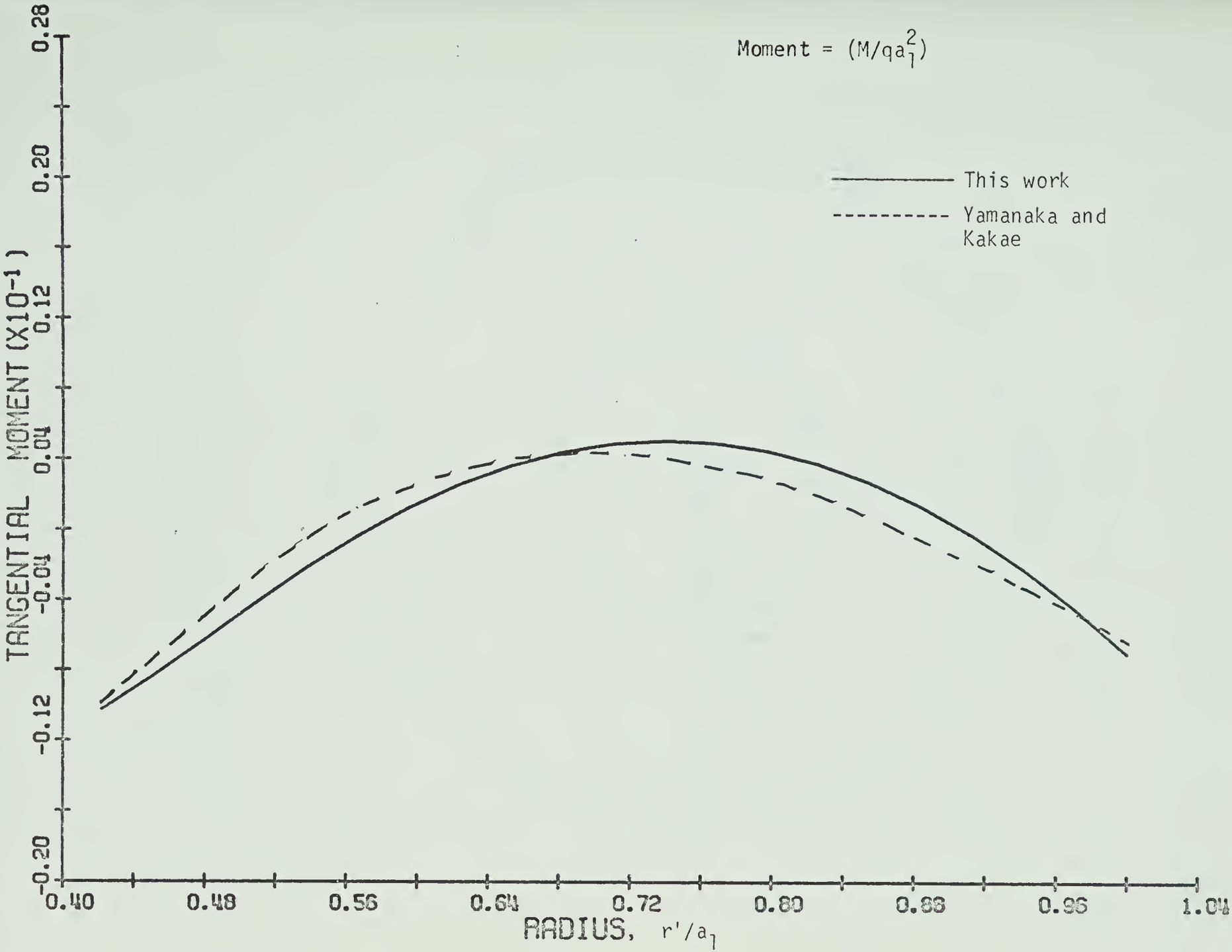

Fig. 11. Comparison of tangential moment distribution along AB from this work with that of Yamanaka and Kakae for uniformly loaded clamped eccentric annular plate for the case $\alpha = 0.5$ and $\beta = 0.391$

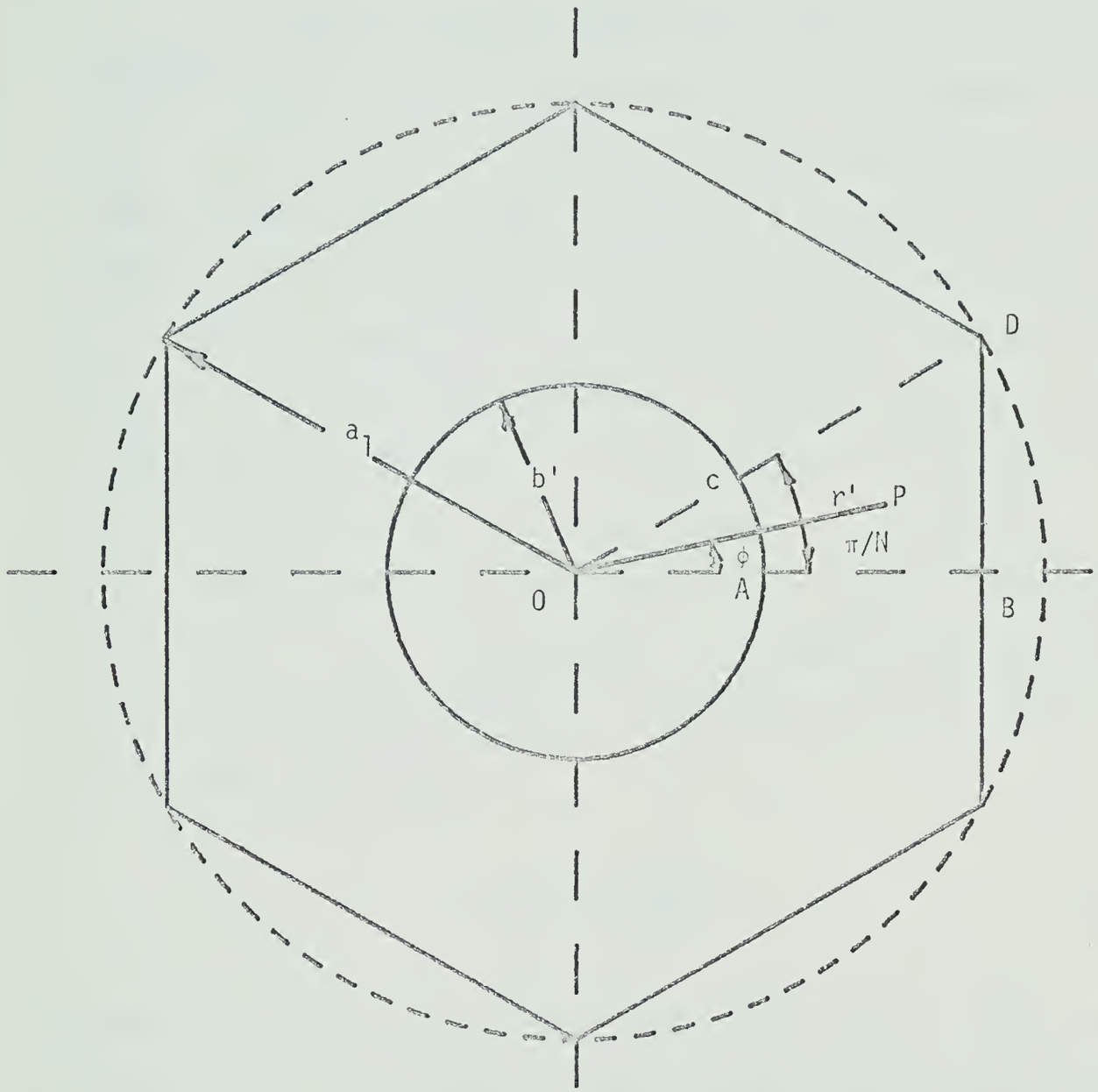

Fig. 12. Coordinate system for regular polygonal plate with a concentric circular hole

3.2 Uniformly Loaded Clamped Regular Polygonal Plate Having a Concentric Circular Hole.

Lo and Leissa [11] presented the solution for uniformly loaded clamped or simply supported square plate with a free concentric circular hole. In this work, it is proposed to extend this problem to uniformly loaded clamped regular polygonal plate with a concentric circular hole. Because of the N-fold symmetry of the problem under consideration (see Fig. 12), it is required to consider only the region OBD for the analysis. Furthermore, the subscript j for the coefficients of the infinite series in equation (3) is now multiple of the number of sides (N) of the polygon viz., $j = 0, N, 2N, 3N, \ldots$ as against 1 to ∞ in the case of eccentric annular plate. Hence, only the coefficients $B_0, B_N, B_{2N}, \ldots$ and $D_0, D_N, D_{2N}, \ldots$ are needed in equations (5) and (7) for the present analysis. The equation for the polygonal edge BD in polar coordinates is

$$r = \frac{r'}{a_1} = \frac{\cos \frac{\pi}{N}}{\cos \phi} \tag{11}$$

where a_1 is the radius of the circumscribed circle for regular polygon (Fig. 12). It is found that six equally spaced points chosen along the external boundary give sufficiently accurate results. A system of twelve equations with twelve unknown results after satisfying the boundary conditions at the six points along BD . By solving them simultaneously, the unknown coefficients are obtained. Equation (8) or (9) is then used to calculate the moments along the edge BD and the lines AB and CD .

Table 5 lists the numerical values for the maximum deflection and its location and the maximum moments along the inner and outer edges corresponding to the six-point matching solution for polygons of sides N = 3, 4 and 6 and for different radius ratios $\alpha = \frac{b'}{a_1 (\cos \pi/N)}$ varying from 0.1 to 0.9 at intervals of 0.1. The maximum deflection is located along CD and the maximum moment along the outer edge occurs near B and along the inner edge at C (Fig. 12). The maximum deflection and maximum moments are found to increase as the number of sides is increased from N = 3 to 6 and α ranging from 0.1 to 0.6. The distribution of deflection, radial slope and moments along the lines AB and CD are presented in Figs. 13 to 16 for α = 0.5 and N = 4. It is seen that the deflections and slopes along the line AB are smaller than those along the line CD. For a given angular coordinate ϕ, the moments M_r and M_t along the circular hole are larger than those at the outer edge. Cases of positive moments are clearly shown in the region very close to the corner. This small region of positive moments is attributed to the difficulty of the method of solution and also the boundary errors which will be discussed later. One notes that the normal to the external boundary is discontinuous at the corner. The distribution of moments along both edges are shown in Figs. 17 and 18, respectively. Variation of moments along the circular edge is smaller than that observed along the polygonal edge. One notes that the maximum bending moment along the outer edge occurs at around 16^o relative to the line AB, for the case α = 0.5 and N = 4.

It is found that a six-point matching solution gives results of sufficient accuracy and the convergence of the coefficients of the

series is rapid. The accuracy of the solution can also be checked by comparing the magnitude of the maximum boundary errors for deflection and slope with the maximum deflection and slope inside the plate. The maximum boundary errors for the worst case ($N = 3$) are of the magnitude 13.2% for deflection and 33.9% for slope. It is noted that the boundary errors are large in the region $40^\circ < \phi < 45^\circ$ for the case $\alpha = 0.5$ and $N = 4$. However, the errors decrease rapidly to less than .003% for both deflection and slope in the range $0 < \phi < 40^\circ$. This clearly shows that the solution is valid only for the region away from the corners. Hence, it may be of interest to indicate the average amplitude of the errors excluding the large errors in the region close to the corners, for example, $40 < \phi < 45^\circ$ for the case where $\alpha = 0.5$ and $N = 4$. Table 6 shows the average and maximum values of boundary errors for deflection and slope along the edge for extreme cases with $\alpha = 0.1$ and 0.9. It is noted that the maximum boundary error decreases as N is increased from 3 to 6 (see Table 6). This may be due to the fact that the corners become smoother as the number of sides is increased. On the other hand, the average value of the boundary errors along the edge increases as the number of sides of the polygon is increased (see Table 6). Table 7 lists the percentage of errors based on the maximum deflection and slope inside the plate. The average error never seems to exceed 1.2% for deflection and 1.8% for slope with range $0 < \phi < 25^\circ$, for example, for the case $\alpha = 0.9$ and $N = 6$. The numerical results are checked with the results of 9-point matching solution. They agree up to 3 significant

digits for all the cases where α ranges from 0.1 to 0.9 and $N = 3, 4$ and 6 . Unreasonable results are obtained when N is increased beyond six. The difficulty seems to arise from the fact that the values r^j , r^{j+2}, etc., in equations (5) and (7) reduce the terms B_N and D_N $(N > 40)$ to negligibly small values since the subscript j for the coefficients of the infinite series is a multiple of the number of sides N . This in turn leads to an ill conditioned coefficient matrix which could not be solved by the computer. It is of interest to note that the computing time involved in collecting all the data was about eight minutes.

Table 5 Numerical Result for Uniformly Loaded Clamped Regular Polygonal Plates with a Concentric Circular Hole.

Radius Ratio	Maximum Value	Deflection Location[1]	Maximum M_n near B	Moment M_r at C
α	$(w/\frac{qa_1^4}{D}) \times 10^3$	r	(M_n/qa_1^2)	$(M_r/qa_1^2) \times 10$
N = 3				
0.1	.2682	.3445	$.2027 \times 10^{-1}$	.5355
0.2	.2135	.3835	$.1549 \times 10^{-1}$	.3740
0.3	.1682	.4220	$.1128 \times 10^{-1}$	.2928
0.4	.1303	.4560	$.7881 \times 10^{-3}$	.2376
0.5	.0997	.4900	$.5278 \times 10^{-3}$	.1954
0.6	.0751	.5205	$.3350 \times 10^{-3}$	.1614
0.7	.0547	.5603	$.1901 \times 10^{-3}$	.1338
0.8	.0436	.6130	$.8451 \times 10^{-4}$	.1124
0.9	.0341	.6645	$.2093 \times 10^{-4}$	.0949
N = 4				
0.1	.6615	.4099	$.3890 \times 10^{-1}$	.8715
0.2	.4630	.4634	$.3067 \times 10^{-1}$	.5550
0.3	.3189	.5115	$.2303 \times 10^{-1}$	.4009
0.4	.2148	.5590	$.1640 \times 10^{-1}$	.3024
0.5	.1398	.6024	$.1137 \times 10^{-1}$	.2300
0.6	.0867	.6459	$.6817 \times 10^{-2}$	.1732
0.7	.0509	.6919	$.3800 \times 10^{-2}$	.1280
0.8	.0278	.7324	$.1686 \times 10^{-2}$	.0919
0.9	.0132	.7782	$.4189 \times 10^{-3}$	.0620

1. Maximum deflection occurs along $\phi = \pi/N$

Radius Ratio	Maximum Value	Deflection Location[1]	Maximum M_n near B	Moment M_r at C
α	$(w/\frac{qa_1^4}{D}) \times 10^3$	r	(M_n/qa_1^2)	$(M_r/qa_1^2) \times 10$
N = 6				
0.1	1.1593	.4611	$.5410 \times 10^{-1}$	1.1734
0.2	.7452	.5163	$.4349 \times 10^{-1}$	.7147
0.3	.4579	.5707	$.3353 \times 10^{-1}$	.4825
0.4	.2680	.6242	$.2455 \times 10^{-1}$	.3359
0.5	.1476	.6768	$.1678 \times 10^{-1}$	.2341
0.6	.0746	.7262	$.1047 \times 10^{-1}$	.1591
0.7	.0331	.7755	$.5753 \times 10^{-2}$	.1023
0.8	.0120	.8264	$.2533 \times 10^{-2}$	.0599
0.9	$.3096 \times 10^{-2}$	.8754	$.9788 \times 10^{-3}$	.0300

1. Maximum deflection occurs along $\phi = \pi/N$

Table 6 Numerical Values for Boundary Errors for Deflection and Normal Slope Along the Edge for Uniformly Loaded Clamped Regular Polygonal Plate With a Concentric Circular Hole.

Number Sides N	Radius Ratio	Boundary Errors: Deflection Average[1] $w/(\frac{qa_1^4}{D})$	Boundary Errors: Deflection Maximum[2] $w/(\frac{qa_1^4}{D})$	Boundary Errors: Slope Average[1] $(\partial w/\partial n)/(qa_1^3/D)$	Boundary Errors: Slope Maximum[2] $(\partial w/\partial n)/(qa_1^3/D)$	Maximum Values: Deflection $w/(\frac{qa_1^4}{D})$	Maximum Values: Slope $(\partial w/\partial n)/(qa_1^3/D)$
3	0.1	$.82 \times 10^{-8}$	$.74 \times 10^{-5}$	$.61 \times 10^{-6}$	$.62 \times 10^{-4}$	$.2682 \times 10^{-3}$	$.1176 \times 10^{-2}$
	0.9	$.28 \times 10^{-7}$	$.45 \times 10^{-5}$	$.73 \times 10^{-6}$	$.11 \times 10^{-3}$	$.3410 \times 10^{-4}$	$.3236 \times 10^{-3}$
4	0.1	$.21 \times 10^{-7}$	$.12 \times 10^{-5}$	$.37 \times 10^{-6}$	$.41 \times 10^{-4}$	$.6615 \times 10^{-3}$	$.3040 \times 10^{-2}$
	0.9	$.27 \times 10^{-8}$	$.48 \times 10^{-6}$	$.23 \times 10^{-6}$	$.21 \times 10^{-4}$	$.1315 \times 10^{-4}$	$.1457 \times 10^{-3}$
6	0.1	$.78 \times 10^{-7}$	$.71 \times 10^{-6}$	$.21 \times 10^{-5}$	$.49 \times 10^{-4}$	$.1159 \times 10^{-2}$	$.4852 \times 10^{-2}$
	0.9	$.39 \times 10^{-7}$	$.33 \times 10^{-6}$	$.90 \times 10^{-6}$	$.13 \times 10^{-4}$	$.3096 \times 10^{-5}$	$.4984 \times 10^{-4}$

1. Average value is computed neglecting the region with larger errors close to the corners.

2. Maximum value occurs near the corner region.

Table 7 Percentage of Boundary Errors for Deflection and Normal Slope Along the Outer Edge for Uniformly Loaded Clamped Regular Polygonal Plate With a Concentric Circular Hole

Number of Sides	Radius Ratio	Errors in %			
		Deflection		Slope	
		Average	Maximum	Average	Maximum
3	0.1	.00031	2.75	.0052	5.27
	0.9	.012	13.2	.0225	33.9
4.	0.1	.0032	.18	.0012	1.35
	0.9	.00203	3.65	.016	14.4
6	0.1	.00067	.0061	.043	.1001
	0.9	1.2	10.07	1.8	26.1

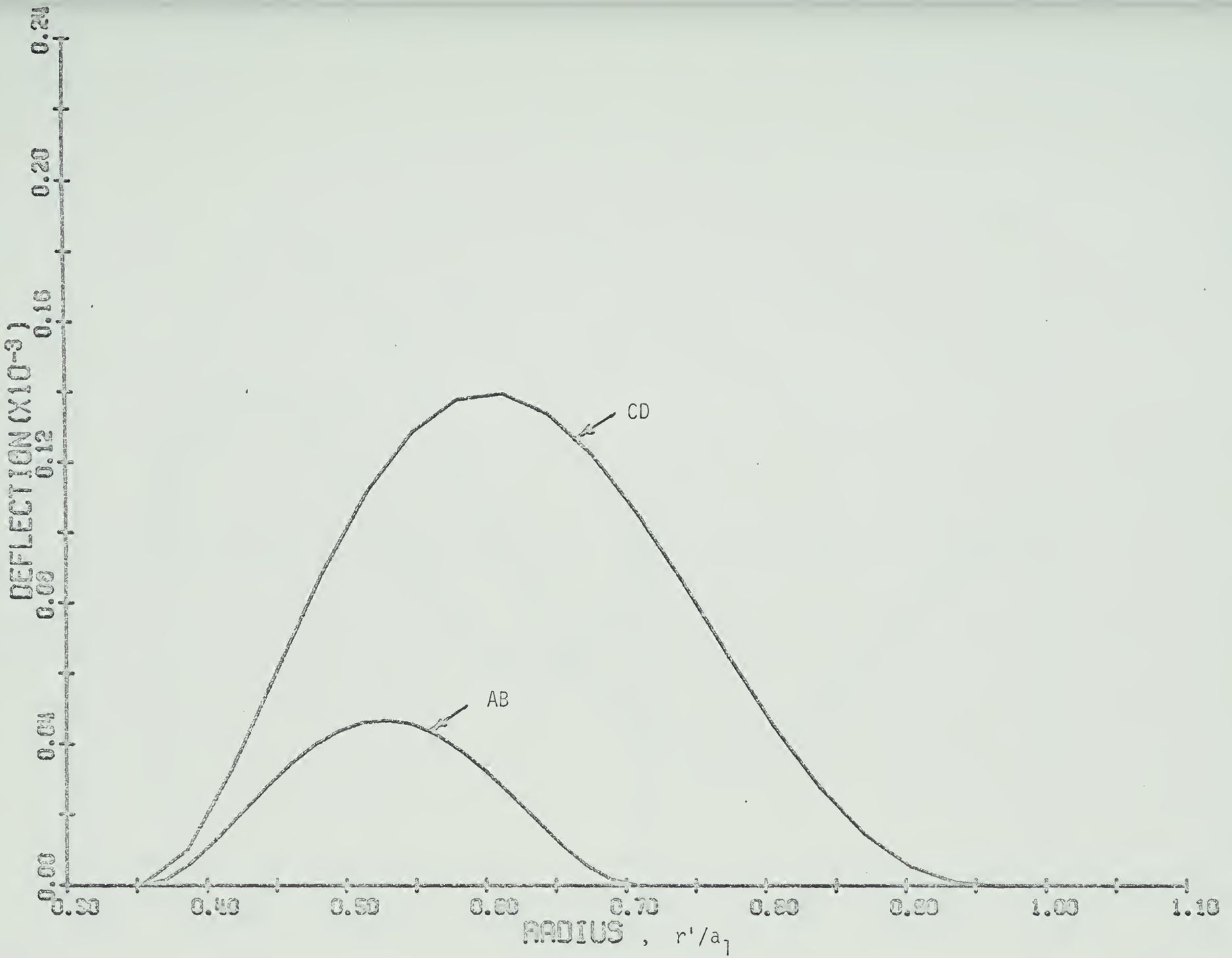

Fig. 13. Distributions of deflection along the lines AB and CD for uniformly loaded clamped regular polygonal plate having a concentric circular hole for the case $\alpha = 0.5$ and $N = 4$

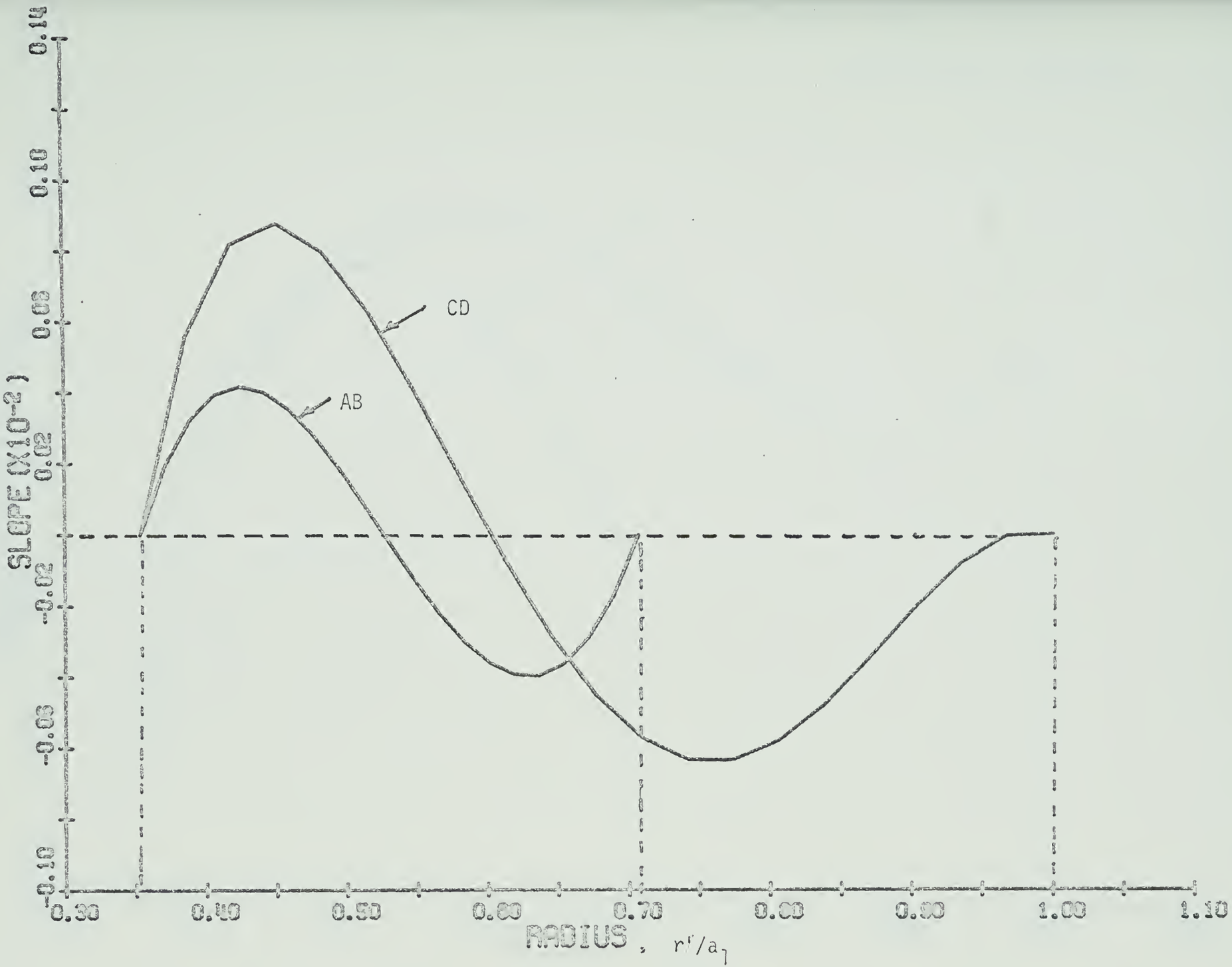

Fig. 14. Distributions of radial slope along the lines AB and CD for uniformly loaded clamped regular polygonal plate having a concentric circular hole for the case $\alpha = 0.5$ and $N = 4$

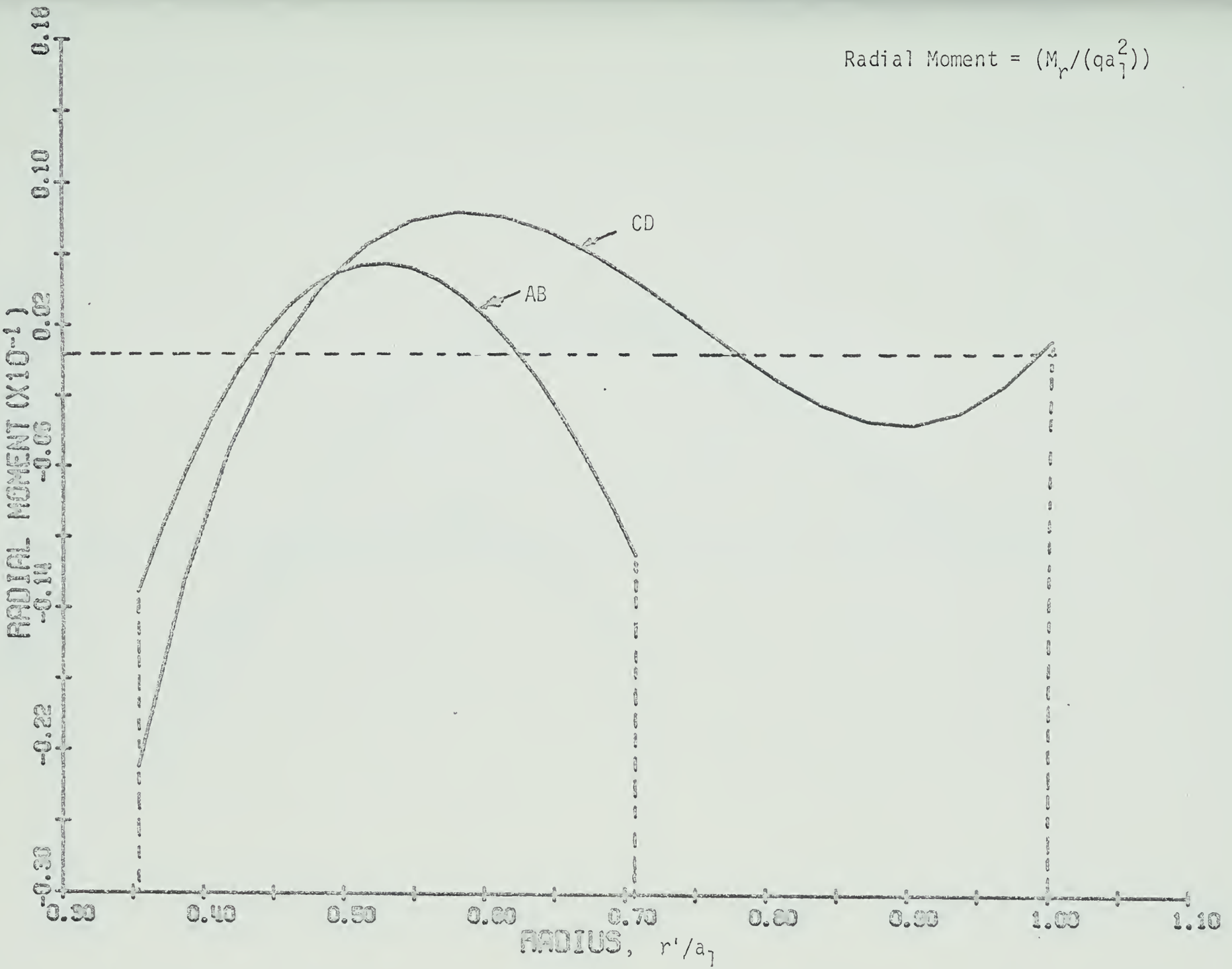

Fig. 15. Distributions of radial moments along the lines AB and CD for uniformly loaded clamped regular polygonal plate having a concentric circular hole for the case $\alpha = 0.5$ and $N = 4$

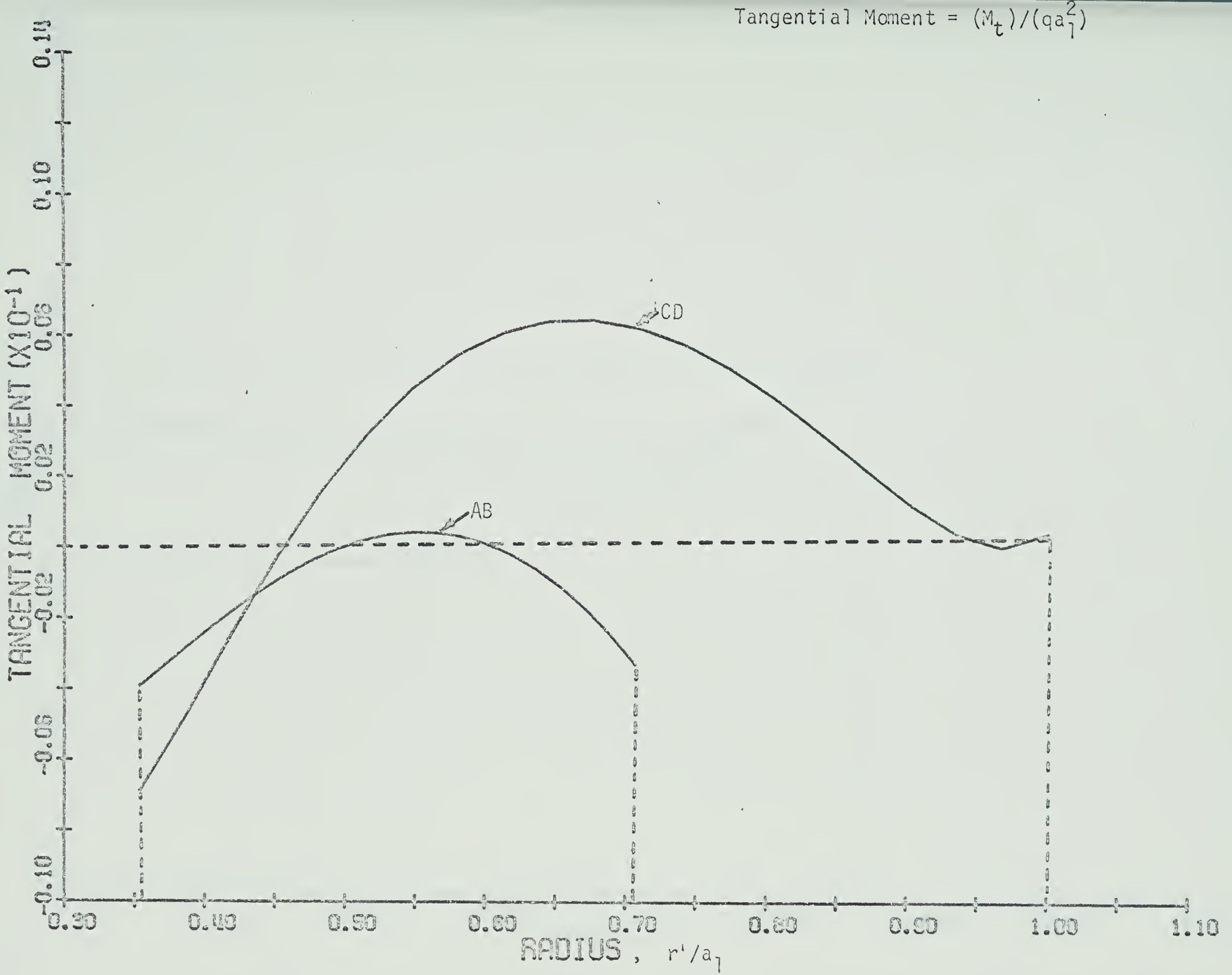

Fig. 16. Distributions of tangential moments along the lines AB and CD for uniformly loaded clamped regular polygonal plate having a concentric hole for the case $\alpha = 0.5$ and $N = 4$

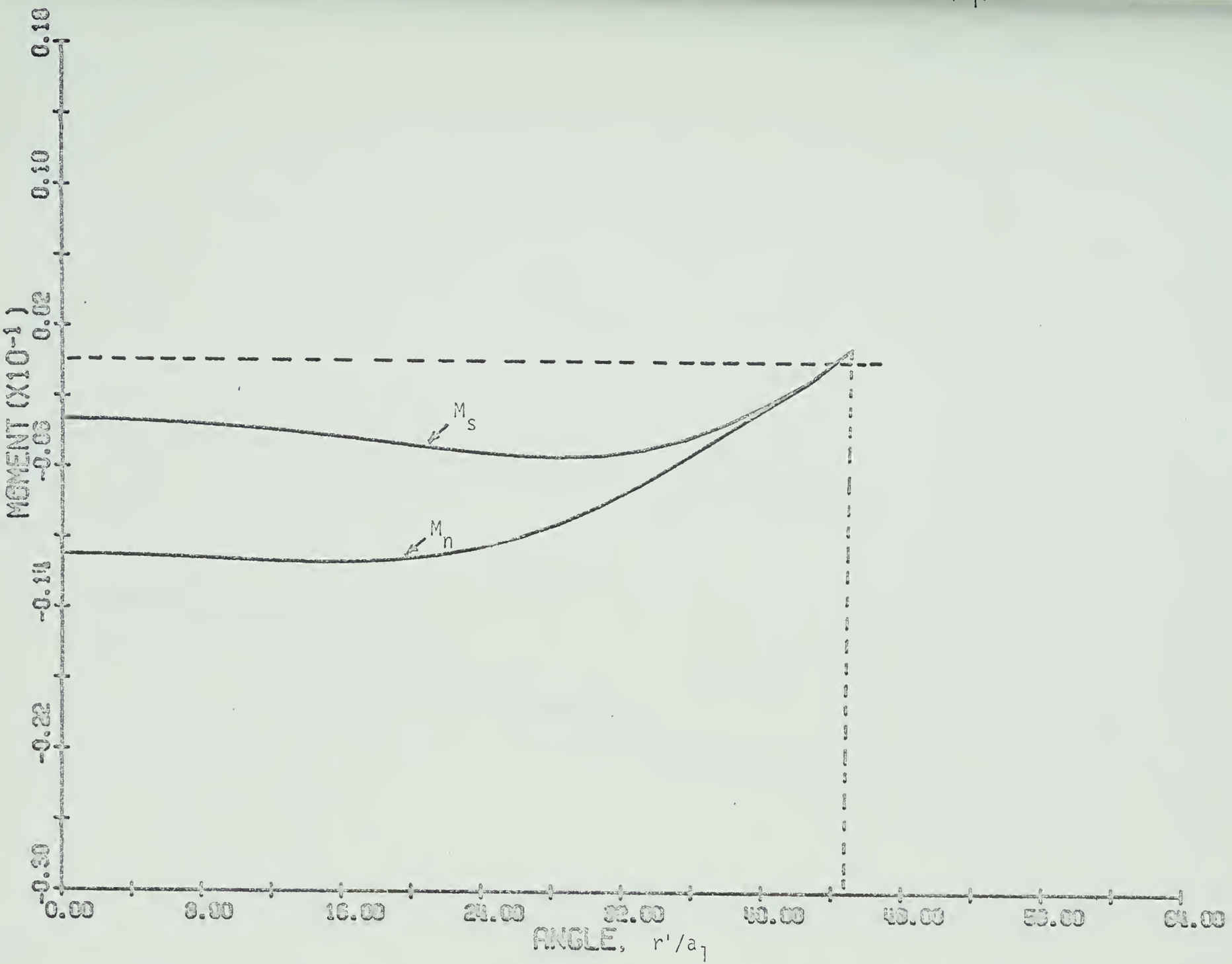

Fig. 17. Distribution of moments M_n and M_s along the outer edge for uniformly loaded clamped regular polygonal plate having a concentric circular hole for the case $\alpha = 0.5$ and $N = 4$

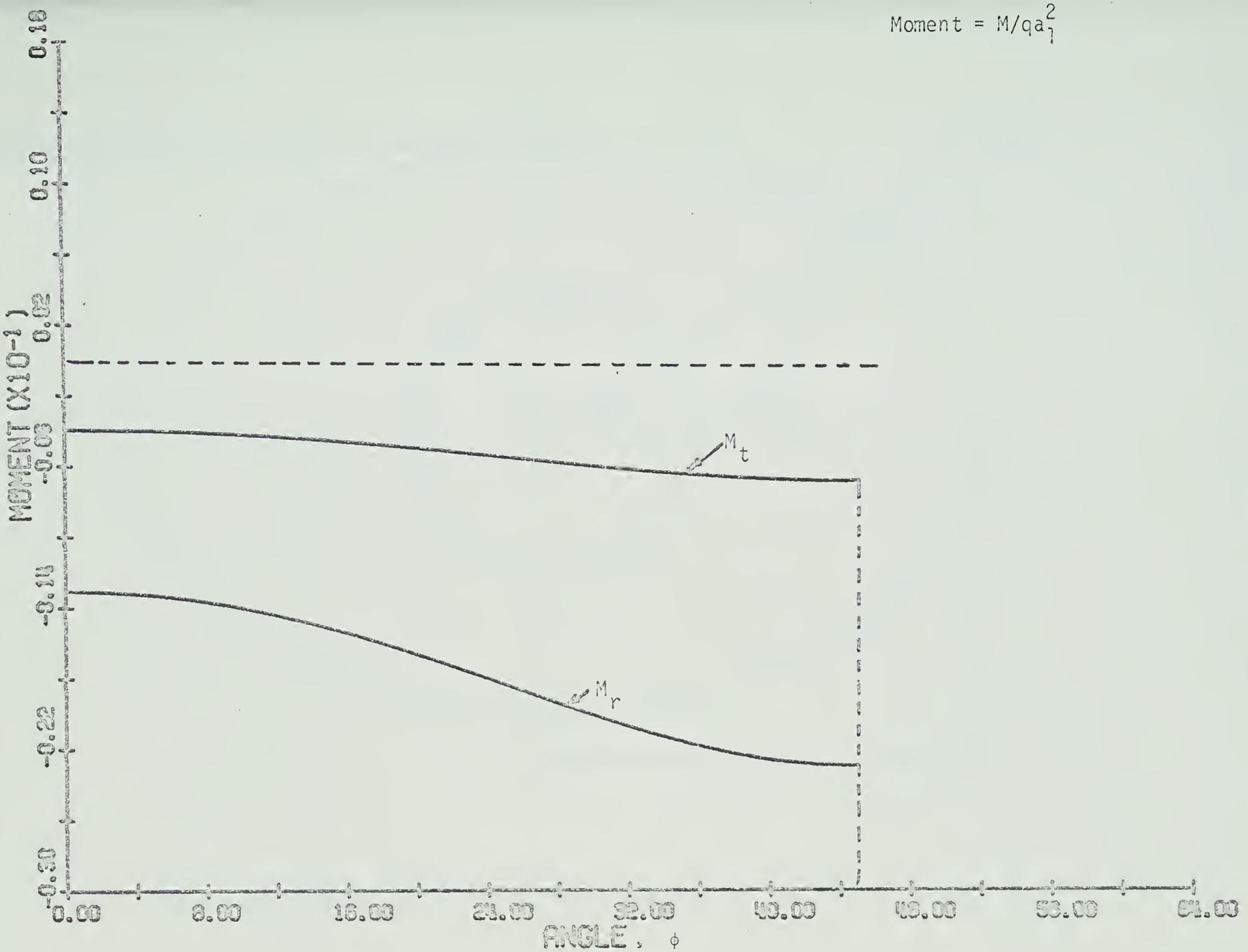

Fig. 18. Distribution of moments M_r and M_t along the inner edge for uniformly loaded clamped regular polygonal plate having a concentric circular hole for the case $\alpha = 0.5$ and $N = 4$

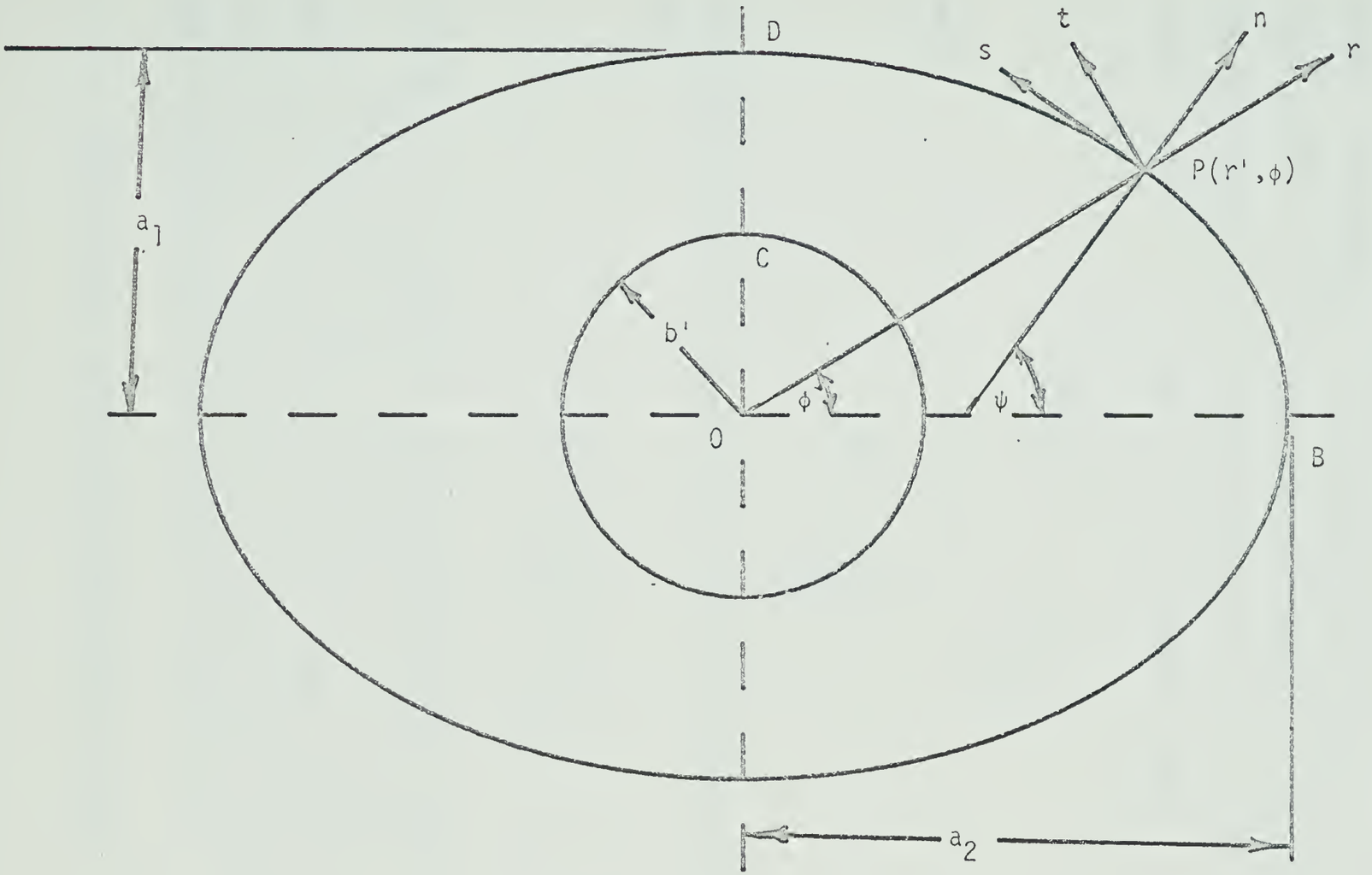

Fig. 19. Coordinate system for elliptic plate with a concentric circular hole

3.3 Uniformly Loaded Clamped Elliptic Plate Having a Concentric Circular Hole.

The coordinate system for this case is shown in Fig. 19. The length of the semi-minor axis OD $(= a_1)$ is taken as the reference length. For symmetry, it is only necessary to consider the region ABDC shown in Fig. 19. Also from two-fold symmetry, the subscript j for the coefficients of the infinite series (3) will now take only even integer numbers. The equation for the elliptic boundary BD is

$$r^2 = \left(\frac{r'}{a_1}\right)^2 = \frac{1}{1 - \varepsilon^2 \cos \phi} \qquad (12)$$

where

$$\varepsilon^2 = 1 - \frac{a_1^2}{a_2^2} \quad .$$

The angle subtended by the normal to the elliptic edge and the line AB is

$$\psi = \tan^{-1}\left(\frac{a_2^2}{a_1^2} \tan \phi\right) \quad . \qquad (13)$$

The angle ψ is required in calculating the normal slope and the moments in n and s directions, respectively, to the outer edge. A six-point matching solution is tried at first and it seems to yield reasonably accurate results. The mathematical procedure used is similar to the case of polygonal plate with a concentric circular hole.

The numerical results for various radius ratios $\alpha \left(= \frac{b'}{a_1}\right)$

ranging from 0.1 to 0.9 in increments of 0.1 and aspect ratios γ $(= \frac{a_2}{a_1})$ ranging from 1.1 to 2.0 in increments of 0.1 are tabulated in Table 8. The maximum deflection is located along AB . The maximum bending moment is found to occur very near B along the elliptic edge and the point A along the circular hole (see Fig. 19). For a given size of the hole with a radius ratio α, the location of the maximum deflection oves outwards along AB as the aspect ratio γ increases from 1.1 to 2.0 . It is noted that the values of the maximum deflection and moments increase with the increase of aspect ratio.

In general it is noted tha the values of the coefficnets for the infinite series converge rapidly for all aspect ratios ranging from 1.1 to 2.0 and radius ratios ranging from 0.1 to 0.9 . The values converge very rapidiy for smaller radius ratios. A nine-point matching solution was also tried and it was found that the results of both six-point and nine-point matching solutions agree up to three significant figures. The accuracy of the numerical results can also be ascertained by considering the limiting case $\gamma = 1.0$, namely, annular plate. The corresponding numerical results are provided in Table 9 and they check very well with the results in Table 3 for uniformly loaded clamped annular plate up to three significant figures. Furthermore, the percentages of maximum boundary errors for deflection and slope based on the maximum values inside the plate are listed in Table 10. The percentages of maximum boundary errors are less t 1.84% for deflection and 3.31% for slope for the aspect r s up to $\gamma = 1.5$.

When γ is increased beyond 1.5 , these values increase as high as 6.87% for deflection and 14.56% for slope for the case $\gamma = 1.7$ and $\alpha = 0.9$. However, for smaller radius ratios such as $\alpha = 0.1$ and $\gamma = 2.0$, the maximum boundary errors are 3.61% for deflection and 12.73% for slope. Unreasonable numerical results were obtained for the values of γ greater than 2 . This may be due to the fact that the values of the terms involving B_N and D_N $(N \geq 10)$ in equations (5) and (7) decrease considerably as compared with those of the leading terms B_o and D_o . The values of the terms involving B_N and D_N $(N \geq 10)$ tend toward zero for aspect ratios greater than 2.0 and may lead to an ill-conditioned matrix.

The graphical distributions for deflection, slope and moments along the lines AB and CD are shown for the case $\alpha = 0.5$ and $\gamma = 1.5$ in Figs. 20 to 23. The deflection and slope are considerably smaller in values along the line CD than along the line AB (see Figs. 20 and 21). For a given angular coordinate ϕ , the moments M_r and M_t are larger at the inner boundary than at the outer edge (see Figs. 22 and 23). The distributions of the moments along both edges are similar to the case of the eccentric annular plate except for the behaviour of normal moments M_n along the elliptic edge. The maximum moment for M_n is seen to occur at the point along the elliptic edge at about 30° from the line AB for the case $\alpha = 0.5$ and $\gamma = 1.5$ (see Figs. 24 and 25).

Table 8 Numerical Result for Uniformly Loaded Clamped Elliptic Plates with a Concentric Circular Hole

Radius Ratio	Maximum Value	Deflection Location[1]	Maximum M_n near B	Moment M_r at A
α	$(w/\frac{qa_1^4}{D})$	r	$(M_n/qa_1^2) \times 10$	$(M_r/qa_1^2) \times 10$
Aspect Ratio $\gamma = 1.1$				
0.1	$.2454 \times 10^{-2}$	.5550	.6063	1.7311
0.2	$.1629 \times 10^{-2}$	.6140	.5133	1.0835
0.3	$.1024 \times 10^{-2}$	.6760	.4217	.7447
0.4	$.6044 \times 10^{-3}$	.7325	.3347	.5211
0.5	$.3283 \times 10^{-3}$	.7880	.2543	.3592
0.6	$.1593 \times 10^{-3}$	.8500	.1832	.2378
0.7	$.6558 \times 10^{-4}$	.9000	.1202	.1466
0.8	$.2085 \times 10^{-4}$	.9470	.0695	.0800
0.9	$.4137 \times 10^{-5}$	.9990	.0317	.0347
Aspect Ratio $\gamma = 1.2$				
0.1	$.3268 \times 10^{-2}$	.5950	.6713	2.0259
0.2	$.2290 \times 10^{-2}$	.6600	.5763	1.3098
0.3	$.1534 \times 10^{-2}$	.7185	.4890	.9303
0.4	$.9736 \times 10^{-3}$	.7760	.4043	.6760
0.5	$.5801 \times 10^{-3}$	.8325	.3231	.4883
0.6	$.3178 \times 10^{-3}$	.9000	.2471	.3435
0.7	$.1554 \times 10^{-3}$	.9500	.1782	.2307
0.8	$.6442 \times 10^{-4}$	.9960	.1182	.1437
0.9	$.2060 \times 10^{-4}$	1.0470	.6872	.0790

1. Maximum delfection occurs along $\phi = 0$

Radius Ratio	Maximum Value	Deflection Location	Maximum M_n near B	Moment M_r at A
α	$(w/\frac{qa_1^4}{D})$	r	$(M_n/qa_1^2) \times 10$	$(M_r/qa_1^2) \times 10$
Aspect Ratio $\gamma = 1.3$				
0.1	$.4186 \times 10^{-2}$	.6400	.6970	2.3109
0.2	$.3067 \times 10^{-2}$	.7005	.6239	1.5352
0.3	$.2158 \times 10^{-2}$	.7600	.5461	1.1206
0.4	$.1455 \times 10^{-2}$	.8185	.4670	.8401
0.5	$.9320 \times 10^{-2}$	.8760	.3885	.6298
0.6	$.5596 \times 10^{-3}$	.9500	.3123	.4642
0.7	$.3088 \times 10^{-3}$	1.0000	.2403	.3313
0.8	$.1520 \times 10^{-3}$	1.0430	.1743	.2248
0.9	$.6337 \times 10^{-4}$	1.0960	.1162	.1412
Aspect Ratio $\gamma = 1.4$				
0.1	$.5189 \times 10^{-2}$	.6785	.7209	2.5813
0.2	$.3945 \times 10^{-2}$	.7400	.6590	1.7543
0.3	$.2895 \times 10^{-2}$	.8060	.5909	1.3104
0.4	$.2049 \times 10^{-2}$	.8650	.5917	1.0082
0.5	$.1391 \times 10^{-2}$	.9230	.4468	.7792
0.6	$.8967 \times 10^{-3}$	.9600	.3739	.5959
0.7	$.5418 \times 10^{-3}$	1.0500	.3023	.4455
0.8	$.3008 \times 10^{-3}$	1.0880	.2338	.3214
0.9	$.1489 \times 10^{-3}$	1.1425	.1705	.2199

Radius Ratio	Maximum Value	Deflection Location	Maximum M_n near B	Moment M_r at A
α	$(w/\frac{qa_1^4}{D}) \times 10^2$	r	$(M_n/qa_1^2) \times 10$	$(M_r/qa_1^2) \times 10$
Aspect Ratio γ = 1.5				
0.1	.6255	.7160	.8718	2.8337
0.2	.4906	.7850	.7681	1.9634
0.3	.3728	.8460	.6676	1.4953
0.4	.2748	.9060	.5793	1.1758
0.5	.1956	.9650	.5021	.9320
0.6	.1332	1.0050	.4285	.7345
0.7	.0863	1.0600	.3604	.5696
0.8	.0526	1.1325	.2927	.4304
0.9	.0294	1.1880	.2275	.3131
Aspect Ratio γ = 1.6				
0.1	.7363	.7600	.9344	3.0664
0.2	.5929	.8230	.8297	2.1595
0.3	.4641	.8850	.7248	1.6722
0.4	.3539	.9460	.6291	1.3393
0.5	.2620	1.0060	.5564	1.0843
0.6	.1873	1.0500	.4787	.8759
0.7	.1284	1.1050	.4116	.6999
0.8	.0839	1.1800	.3472	.5485
0.9	.0512	1.2325	.2829	.4177

Radius Ratio	Maximum Value	Deflection Location	Maximum M_n near B	Moment M_r at A
α	$(w/\frac{qa_1^4}{D}) \times 10^2$	r	$(M_n/qa_1^2) \times 10$	$(M_r/qa_1^2) \times 10$
Aspect Ratio γ = 1.7				
0.1	.8495	.7960	.9927	3.2788
0.2	.6995	.8600	.8884	2.3415
0.3	.5616	.9230	.7823	1.8378
0.4	.4407	.9850	.6767	1.4959
0.5	.3373	1.0460	.6095	1.2327
0.6	.2509	1.0950	.5291	1.0167
0.7	.1804	1.1500	.4554	.8327
0.8	.1247	1.2230	.3951	.6722
0.9	.0814	1.2800	.3336	.5307
Aspect Ratio γ = 1.8				
0.1	.9633	.8310	1.0462	3.4711
0.2	.8086	.8960	.9449	2.5084
0.3	.6632	.9600	.8354	1.9934
0.4	.5331	1.0230	.7306	1.6434
0.5	.4196	1.0850	.6664	1.3748
0.6	.3228	1.1400	.5765	1.1154
0.7	.2417	1.1950	.5118	.9649
0.8	.1749	1.2650	.4380	.7985
0.9	.1208	1.3230	.3768	.6490

Radius Ratio	Maximum Value	Deflection Location	Maximum M_n near B	Moment M_r at A
α	$(w/\frac{qa_1^4}{D}) \times 10^2$	r	$(M_n/qa_1^2) \times 10$	$(M_r/qa_1^2) \times 10$
Aspect Ratio γ = 1.9				
0.1	1.0765	.8650	1.3676	3.6445
0.2	.9184	.9310	1.2656	2.6604
0.3	.7670	.9960	1.1481	2.1359
0.4	.6291	1.0600	1.0179	1.7860
0.5	.5070	1.1230	.8761	1.5087
0.6	.4015	1.1850	.7737	1.2853
0.7	.3114	1.2400	.7215	1.0940
0.8	.2346	1.3060	.6276	.9246
0.9	.1695	1.3650	.5185	.7699
Aspect Ratio γ = 2.0				
0.1	1.1880	.8980	1.1387	3.8003
0.2	1.0277	.9650	1.0448	2.7983
0.3	.8713	1.0310	.9382	2.2661
0.4	.7267	1.0960	.9673	1.9070
0.5	.5972	1.1600	.9083	1.6331
0.6	.4848	1.2300	.6974	1.4090
0.7	.3881	1.2850	.6402	1.2178
0.8	.3630	1.3520	.5837	1.0483
0.9	.2275	1.4060	.4816	.8912

Table 9 Numerical Result for Uniformly Loaded Clamped Elliptic Plates With a Concentric Circular Hole for the Case $\gamma = 1.0$

Radius Ratio α	Maximum Value $(w/\frac{qa_1^4}{D})$	Deflection Location r	Maximum M_n Along Outer Edge M_n/qa_1^2	Moment M_r Along Inner Edge M_r/qa_1^2
0.1	$.1757 \times 10^{-2}$	.0595	$.5402 \times 10^{-1}$	1.4332×10^{-1}
0.2	$.1090 \times 10^{-2}$	.5720	$.4410 \times 10^{-1}$	$.8624 \times 10^{-1}$
0.3	$.6347 \times 10^{-3}$	.6920	$.3474 \times 10^{-1}$	$.5697 \times 10^{-1}$
0.4	$.3408 \times 10^{-3}$	.6880	$.2620 \times 10^{-1}$	$.3804 \times 10^{-1}$
0.5	$.1637 \times 10^{-3}$	.7425	$.1866 \times 10^{-1}$	$.2469 \times 10^{-1}$
0.6	$.6693 \times 10^{-4}$	.7960	$.1222 \times 10^{-1}$	$.1502 \times 10^{-1}$
0.7	$.2112 \times 10^{-4}$	.8470	$.7038 \times 10^{-2}$	$.8121 \times 10^{-2}$
0.8	$.4169 \times 10^{-5}$	.8990	$.3198 \times 10^{-2}$	$.3497 \times 10^{-2}$
0.9	$.2604 \times 10^{-6}$	.9495	$.8165 \times 10^{-3}$	$.8517 \times 10^{-3}$

Table 10 Maximum Boundary Errors for Deflection and Normal Slope Along the Outer Edge for Uniformly Loaded Clamped Elliptic Plate With a Concentric Circular Hole

Aspect Ratio	Radius Ratio	Boundary Errors				Maximum Values	
		Deflection		Slope		Deflection	Slope
γ	α	$w/(\frac{qa_1^4}{D})$	%	$(\frac{\partial w}{\partial n})/(\frac{qa_1^3}{D})$	%	$w/(\frac{qa_1^4}{D})$	$(\frac{\partial w}{\partial n})/(\frac{qa_1^3}{D})$
1.0	0.1	$.13 \times 10^{-12}$	$.74 \times 10^{-8}$	$.13 \times 10^{-11}$	$.19 \times 10^{-7}$	$.1757 \times 10^{-2}$	$.6687 \times 10^{-2}$
	0.9	$.13 \times 10^{-12}$	$.50 \times 10^{-4}$	$.13 \times 10^{-11}$	$.16 \times 10^{-4}$	$.2604 \times 10^{-6}$	$.8057 \times 10^{-5}$
1.1	0.1	$.99 \times 10^{-10}$	$.40 \times 10^{-5}$	$.12 \times 10^{-8}$	$.14 \times 10^{-4}$	$.2454 \times 10^{-2}$	$.8439 \times 10^{-2}$
	0.9	$.20 \times 10^{-9}$	$.48 \times 10^{-2}$	$.26 \times 10^{-8}$	$.40 \times 10^{-2}$	$.4137 \times 10^{-5}$	$.6447 \times 10^{-4}$
1.2	0.1	$.78 \times 10^{-8}$	$.24 \times 10^{-3}$	$.90 \times 10^{-7}$	$.88 \times 10^{-3}$	$.3268 \times 10^{-2}$	$.1026 \times 10^{-1}$
	0.9	$.16 \times 10^{-7}$	$.78 \times 10^{-1}$	$.19 \times 10^{-6}$	$.88 \times 10^{-1}$	$.2060 \times 10^{-4}$	$.2157 \times 10^{-3}$
1.3	0.1	$.10 \times 10^{-6}$	$.24 \times 10^{-2}$	$.11 \times 10^{-5}$	$.93 \times 10^{-2}$	$.4186 \times 10^{-2}$	$.1211 \times 10^{-1}$
	0.9	$.20 \times 10^{-6}$	.32	$.24 \times 10^{-5}$	.47	$.6337 \times 10^{-4}$	$.5017 \times 10^{-3}$
1.4	0.1	$.63 \times 10^{-6}$	$.12 \times 10^{-1}$	$.66 \times 10^{-5}$	.47	$.5189 \times 10^{-2}$	$.1394 \times 10^{-1}$
	0.9	$.12 \times 10^{-5}$	.81	$.14 \times 10^{-4}$	1.43	$.1489 \times 10^{-3}$	$.9505 \times 10^{-3}$
1.5	0.1	$.28 \times 10^{-5}$	$.45 \times 10^{-1}$	$.26 \times 10^{-4}$	.20	$.6255 \times 10^{-2}$	$.1571 \times 10^{-1}$
	0.9	$.54 \times 10^{-5}$	1.84	$.52 \times 10^{-4}$	3.31	$.2935 \times 10^{-3}$	$.1575 \times 10^{-2}$
1.6	0.1	$.10 \times 10^{-4}$	.14	$.91 \times 10^{-4}$	.52	$.7363 \times 10^{-2}$	$.1739 \times 10^{-1}$
	0.9	$.19 \times 10^{-4}$	3.71	$.18 \times 10^{-3}$	7.39	$.5118 \times 10^{-3}$	$.2373 \times 10^{-2}$
1.7	0.1	$.31 \times 10^{-4}$	.37	$.26 \times 10^{-3}$	1.37	$.8495 \times 10^{-2}$	$.1897 \times 10^{-1}$
	0.9	$.56 \times 10^{-4}$	6.85	$.49 \times 10^{-3}$	14.56	$.8144 \times 10^{-3}$	$.3330 \times 10^{-2}$
1.8	0.1	$.81 \times 10^{-4}$	.84	$.63 \times 10^{-3}$	3.13	$.9633 \times 10^{-2}$	$.2043 \times 10^{-1}$
	0.9	$.14 \times 10^{-3}$	11.58	$.12 \times 10^{-2}$	26.11	$.1208 \times 10^{-2}$	$.4421 \times 10^{-2}$
1.9	0.1	$.19 \times 10^{-3}$	1.77	$.14 \times 10^{-2}$	6.46	$.1077 \times 10^{-1}$	$.2176 \times 10^{-1}$
	0.9	$.32 \times 10^{-3}$	18.88	$.25 \times 10^{-2}$	44.5	$.1695 \times 10^{-2}$	$.5619 \times 10^{-2}$
2.0	0.1	$.43 \times 10^{-3}$	3.62	$.29 \times 10^{-2}$	12.6	$.1188 \times 10^{-1}$	$.2299 \times 10^{-1}$
	0.9	$.69 \times 10^{-3}$	30.33	$.49 \times 10^{-2}$	70.94	$.2275 \times 10^{-3}$	$.6914 \times 10^{-2}$

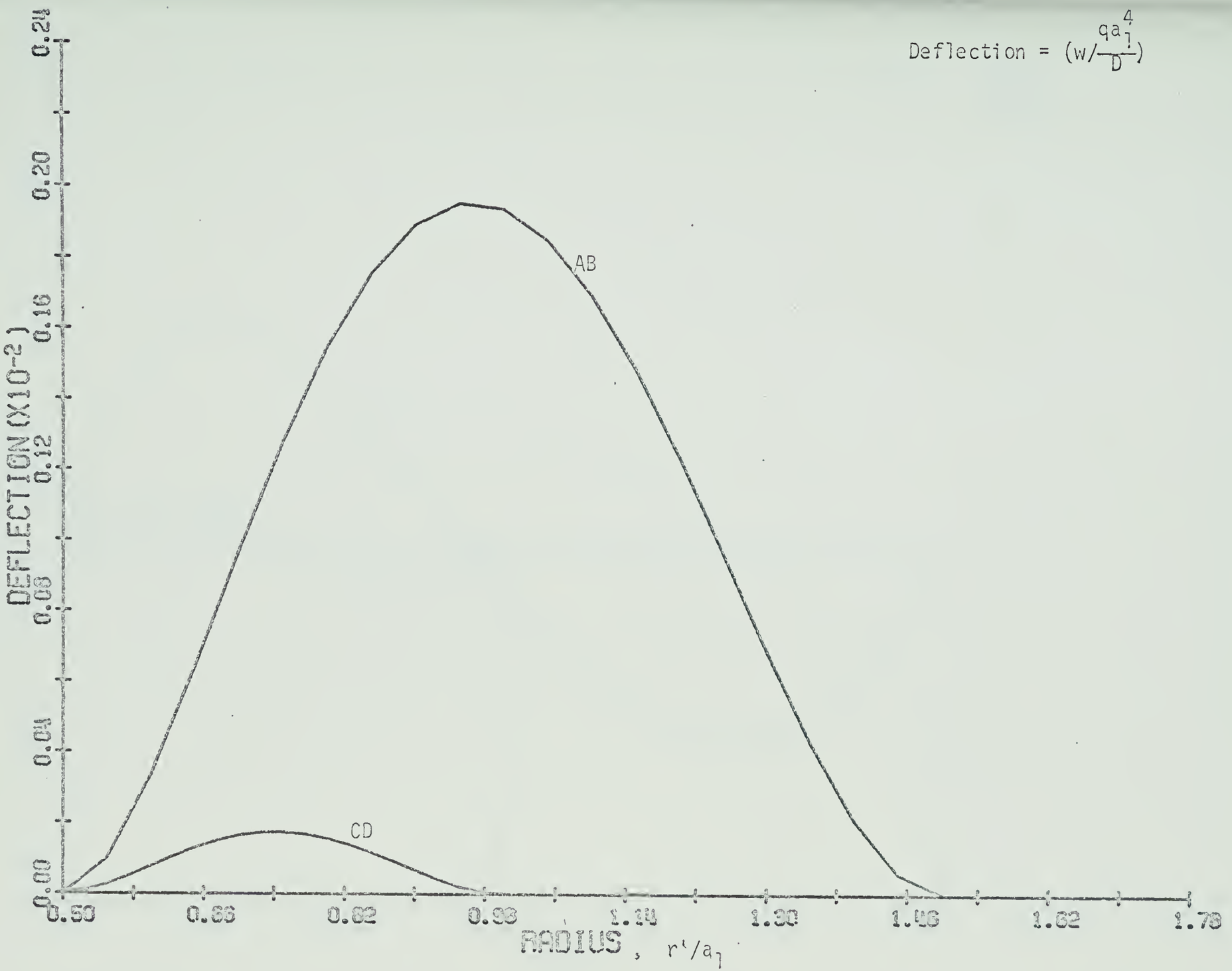

Fig. 20. Distribution of deflection along AB and CD for uniformly loaded clamped elliptic plate having a concentric circular hole for the case $\alpha = 0.5$ and $\gamma = 1.5$

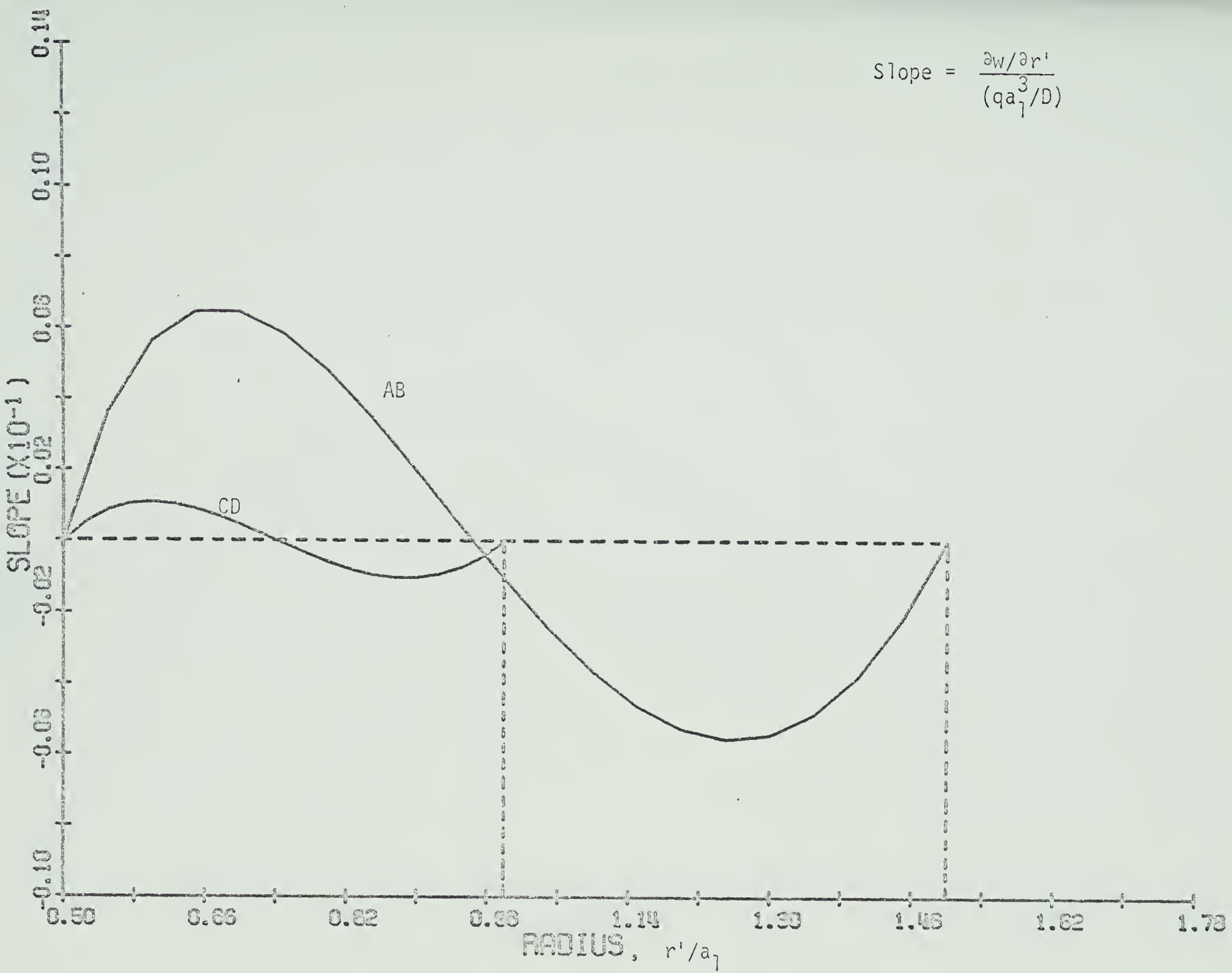

Fig. 21. Distribution of radial slope along AB and CD for uniformly loaded clamped elliptic plate having a concentric circular hole for the case $\alpha = 0.5$ and $\gamma = 1.5$

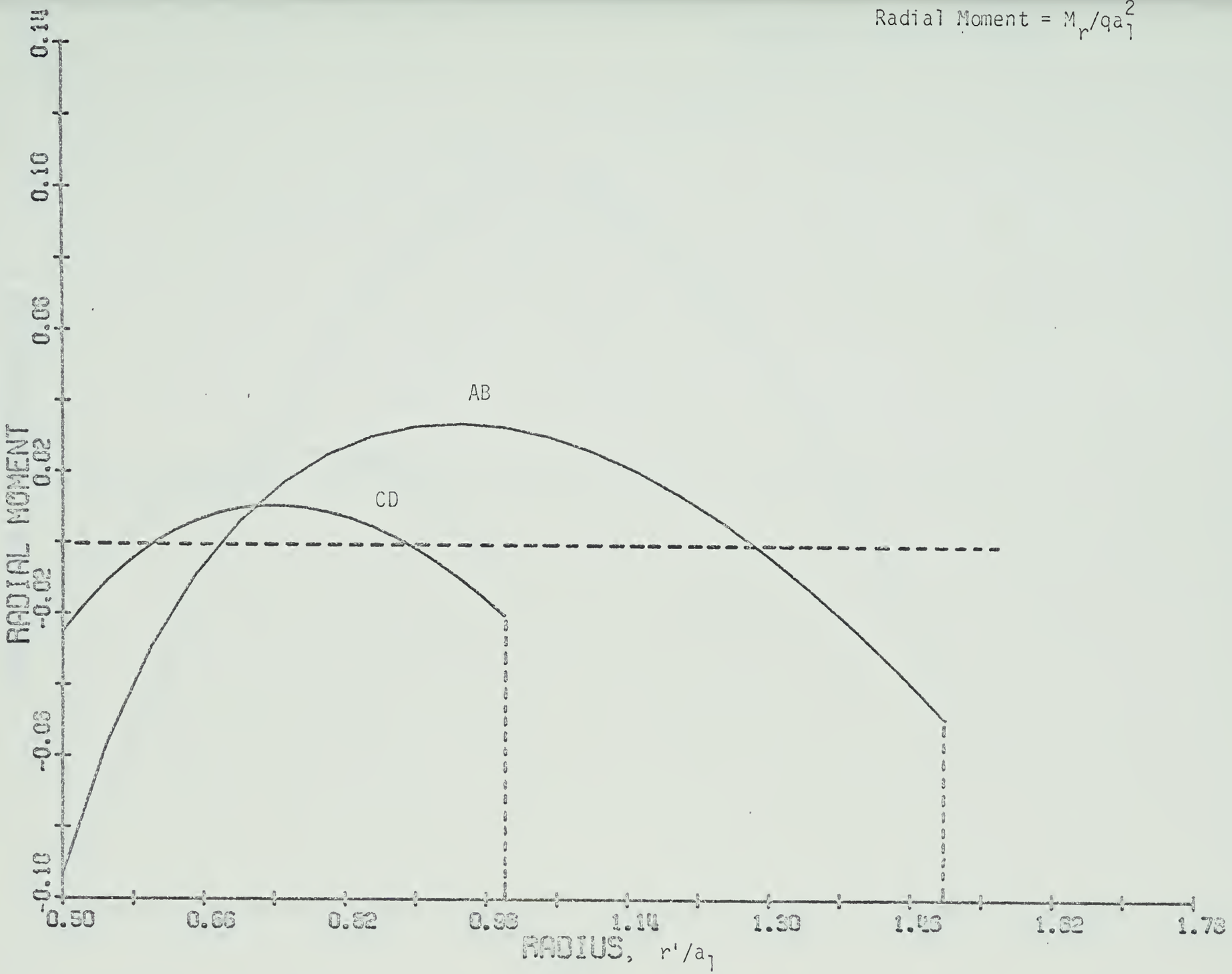

Fig. 22. Distribution of radial moment along AB and CD for uniformly loaded clamped elliptic plate having a concentric circular hole for the case $\alpha = 0.5$ and $\gamma = 1.5$

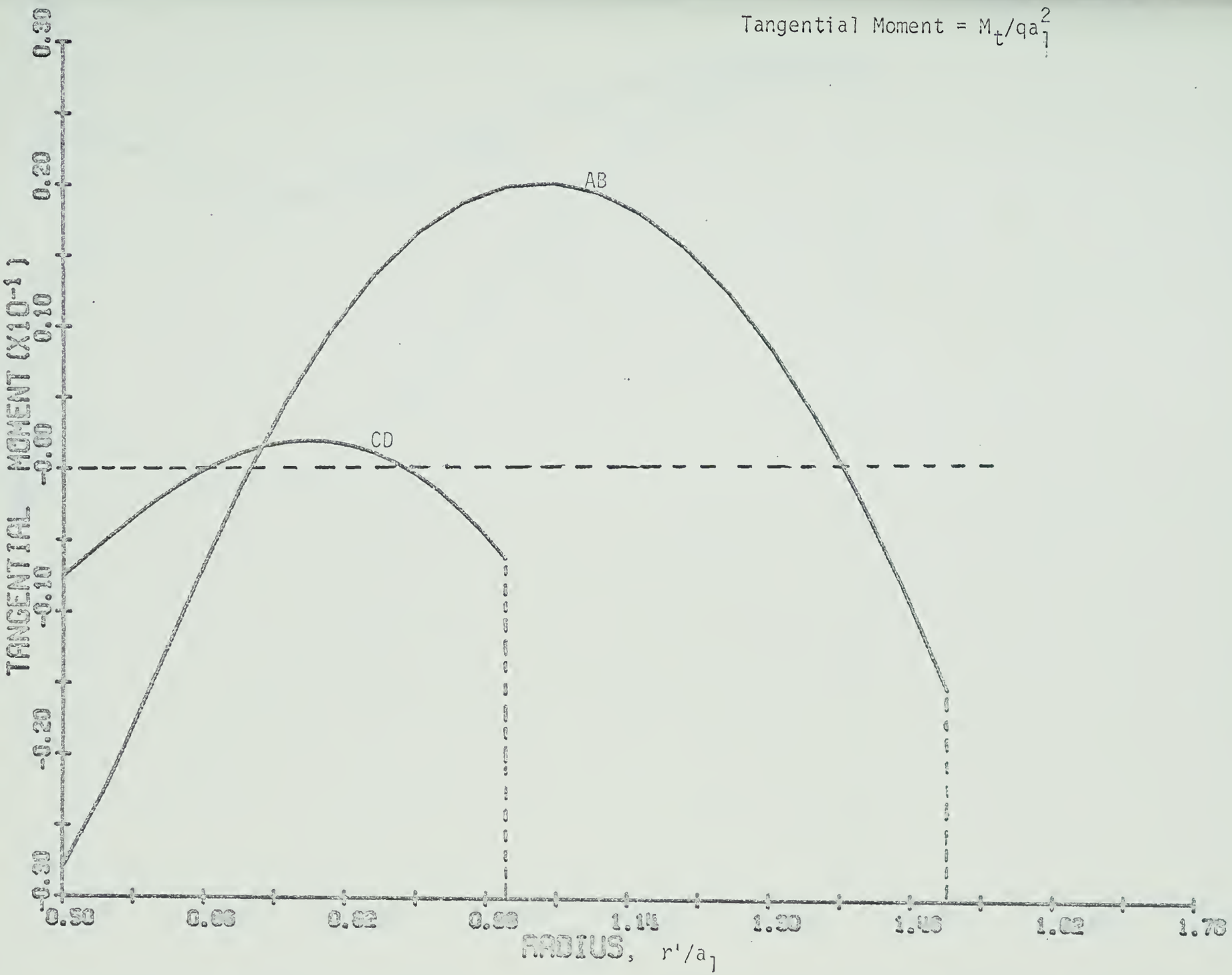

Fig. 23. Distributions of tangential moments along the lines AB and CD for uniformly loaded clamped elliptic plate having a concentric circular hole for the case $\alpha = 0.5$ and $\gamma = 1.5$

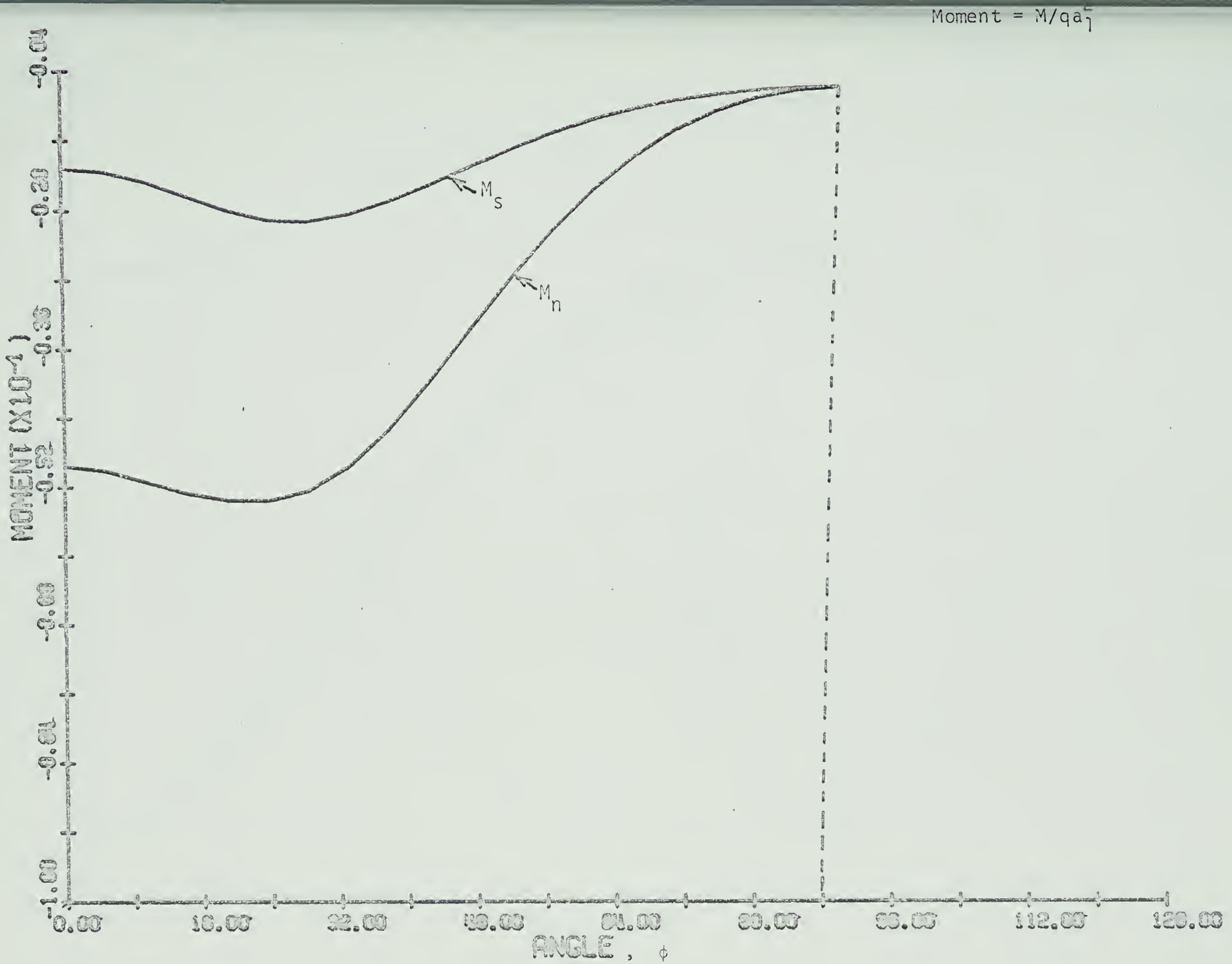

Fig. 24. Distribution of moments M_n and M_s along the outer edge for uniformly loaded clamped elliptic plate having a concentric circular hole for the case $\alpha = 0.5$ and $\gamma = 1.5$

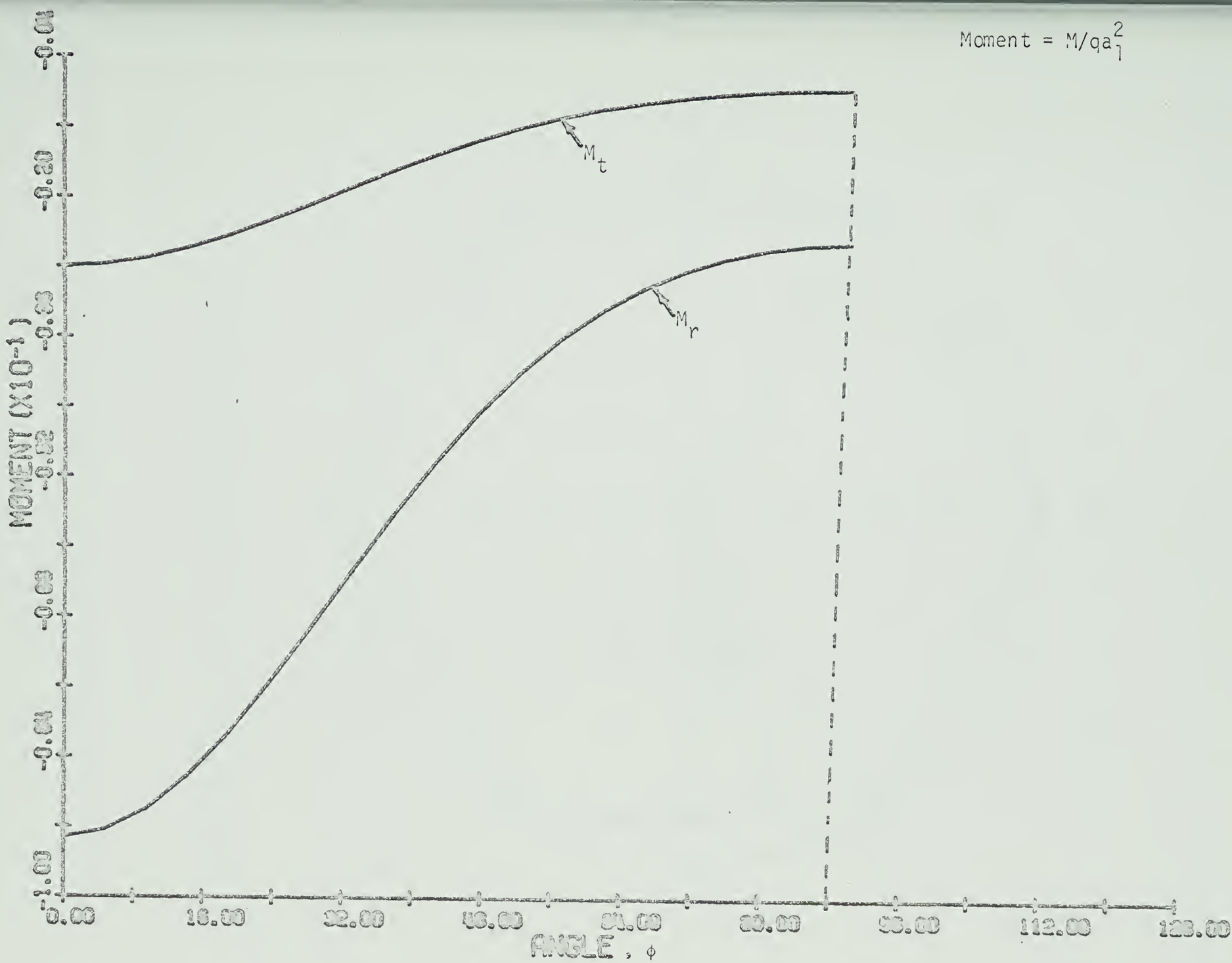

Fig. 25. Distribution of moments M_r and M_t along the inner edge for uniformly loaded clamped elliptic plate having a concentric circular hole for the case $\alpha = 0.5$ and $\gamma = 1.5$

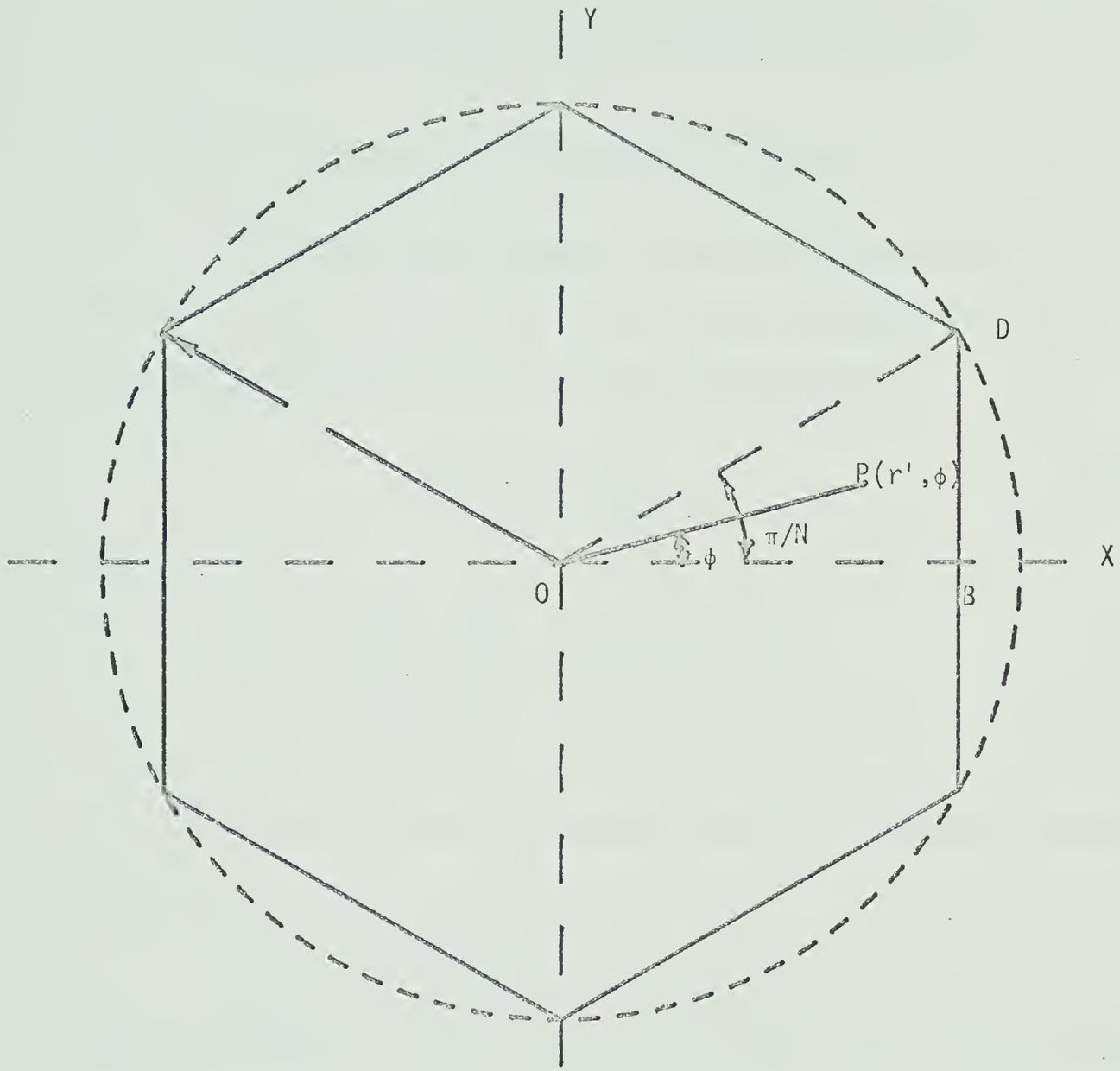

Fig. 26. Coordinate system for a regular polygonal plate

CHAPTER IV

REGULAR POLYGONAL PLATES ON ELASTIC FOUNDATION

4.1 Governing Equation and Its General Solution.

The differential equation characterizing the deflection w of middle plane of a thin plate on an elastic foundation was given, for example, by Reismann [19] in the following form,

$$\nabla_\rho^4 w + w = \frac{q}{\lambda^4 D} \tag{14}$$

where

$$\nabla_\rho^2 = \frac{\partial^2}{\partial \rho^2} + \frac{1}{\rho}\frac{\partial}{\partial \rho} + \frac{1}{\rho^2}\frac{\partial^2}{\partial \phi^2}$$

$$\lambda^4 = k/D \quad , \quad \rho = \lambda r'$$

k is the modulus of foundation and D is flexural rigidity of the plate.

The general solution of the equation (14), as obtained by Reismann, is given in terms of Kelvin functions in the following form

$$w = \frac{q}{\lambda^4 D} + \sum_{n=0}^{\infty} (R_n(\rho) \cos n\phi + Q_n(\rho) \sin n\phi) \tag{15}$$

where

$$R_n(\rho) = A_{1n}\, \mathrm{ber}_n \rho + B_{1n}\, \mathrm{bei}_n \rho + C_{1n}\, \mathrm{ker}_n \rho + D_{1n}\, \mathrm{kei}_n \rho$$

$$Q_n(\rho) = A_{2n}\, \mathrm{ber}_n \rho + B_{2n}\, \mathrm{bei}_n \rho + C_{2n}\, \mathrm{ker}_n \rho + D_{2n}\, \mathrm{kei}_n \rho$$

Equation (15) has also been successfully used by Saito [17, 18] for circular plates under two different types of loading. A detailed treatment of the Kelvin functions is given by Mclachlan [21]. However, the recurrence relations given by Oravas [22] were used for the second derivatives in the computation of moments using equations (8) or (9). The series expansion and the recurrence relations for the Kelvin functions are given in Appendix B .

4.2 Uniformly Loaded Clamped Regular Polygonal Plates on Elastic Foundation.

The general solution discussed in section 4.1 is applied to a uniformly loaded, clamped, regular polygonal plate resting on elastic foundation of modulus k . The coordinate system for the regular polygonal plate is shown in Fig. 26. The radius of the circle OD circumscribing the polygon is taken as the reference length a_1 to non-dimensionalize the equation. Since the deflection and slope are finite at the centre, $C_{1n} = C_{2n} = D_{1n} = D_{2n} = 0$, for all values of n . In addition the boundary conditions (2) for clamped polygonal edge must be satisfied. Equation (11), for the polygonal edge, is used to find the coordinates of the points to be matched. The expression for $\frac{\partial w}{\partial n}$ may be obtained from equation (6) by substituting $\psi = 0$. Due to symmetry of the problem, only region OBD need be considered. The general solution (15) can now be expressed in the following form

$$w(\rho,\phi) = \frac{q}{\lambda^4 D}\left[1 + R_o + 2 \sum_n R_n \cos n\phi\right] \qquad (16)$$

where $$R_n = A_n \, ber_n \rho + B_n \, bei_n \rho$$

$$n = 0, N, 2N, 3N, \ldots$$

and $$\rho = \lambda r' \quad .$$

Applying equation (2), the following relations are obtained

$$R_o + 2 \sum_{n=N,2N}^{\infty} R_n \cos n\phi = -1$$

$$R_o' \cos(\psi-\phi) + 2 \sum_{n=N,2N}^{\infty} \left(R_n' \cos n\phi \cos(\psi-\phi) + \frac{nR_n}{\rho} \sin n\phi \sin(\psi-\phi)\right) = 0 \quad . \tag{17}$$

As in the problem of uniformly loaded regular polygonal plate with a concentric circular hole, a six-point matching solution was used. As the direct point matching technique was not readily applicable, the developed equations (17) are solved in the least squares sense. As the best ratio of the number of points to be matched to the number of unknowns is 2 [20], the series in equation (15) is truncated at $n = 2N$ (6 unknowns). Using six-points, the twelve boundary condition equations with six unknowns can be represented in matrix form as

$$A\{A_n \; B_n\} = B \tag{18}$$

where A is the coefficient matrix, $\{A_n, B_n\}$ is the unknown vector and B is the right hand side column matrix of this set of linear equations. Premultiplying both sides of equation (18) by the transpose of A yields,

$$A^T A \{A_n \; B_n\} = A^T B \tag{19}$$

where $A^T A$ is a square matrix and $\{A_n, B_n\}$ can now readily be obtained by solving this set of equations. This process involves minimizing the integral of the error squared along the boundary. A detailed mathematical treatment is given by Lo [20]. Using equation (8), the equations for moments M_r, M_t and M_{rt} are

$$M_r = -\frac{q}{\lambda^2}\left[R_o'' + 2\sum_{n=N,2N}^{\infty} R_n'' \cos n\phi + \nu\left(\frac{1}{\rho} R_o' + \frac{2}{\rho}\sum_{n=N,2N}^{\infty} R_n' \cos n\phi - \frac{2}{\rho^2}\sum_{n=N,2N}^{\infty} n^2 R_n \cos n\phi\right)\right] . \tag{20}$$

$$M_t = -\frac{q}{\lambda^2}\left[\nu R_o'' + 2\nu\sum_{n=N,2N}^{\infty} R_n'' \cos n\phi + \frac{1}{\rho} R_o' + \frac{2}{\rho}\sum_{n=N,2N}^{\infty} R_n' \cos n\phi - \frac{2}{\rho^2}\sum_{n=N,2N}^{\infty} n^2 R_n \cos n\phi\right] . \tag{21}$$

$$M_{rt} = -\frac{q}{\lambda^2}\left[\frac{2}{\rho^2}\sum_{n=N,2N}^{\infty} n R_n \sin n\phi - \frac{2}{\rho}\sum_{n=N,2N}^{\infty} n_1 R_n' \sin n\phi\right](1-\nu) . \tag{22}$$

The expressions for M_n and M_s given in equation (9) are used to calculate moments along the edges.

After solving equation (17), the boundary errors for deflection and normal slope along the edge are calculated for polygons of sides $N = 3, 4, 6$ and 8. The percentages of maximum boundary errors based on the maximum deflection and slope are found to be of the order of 10% and 14.5% respectively for the case $N = 3$. Hence the numerical results are presented only for the cases $N = 4$, 6 and 8 in Table 11. Due to the significant boundary errors, the numerical results for moments must be regarded as tentative and Table 11 is presented only for reference purpose for future study. The errors are found to be maximum in the region close to corner in the range $40^{\circ} < \phi < 45^{\circ}$ for the case $N = 4$. The boundary errors decrease to negligibly small values as we proceed from the corner to the middle point. As can be expected, the maximum deflection occurs at the centre. The values of the maximum deflection and moments increase as N is increased from 4 to 8 (see Table 11).

In contrast to the problems treated so far, the coefficients for the infinite series in equation (15) seem to diverge for this case. When N is increased beyond 8, the matrix is found to be ill-conditioned. This may be due to the fact that the order of Kelvin function increases directly with N and the values of the terms R_n $(n > 48)$ are negligibly small as compared to the leading term R_o in equation (16) which may result in an ill-conditioned matrix. When checking the values of the deflection along the diagonal line OD, negative deflection is noticed in the region close to corners. It is found that the region of negative deflection reduces as the number of sides is increased from 4 to 8. The negative deflection may be due to

the fact that the solution is not valid in the region close to corner and also due to the large boundary errors in this region. The numerical results using six unknowns are also compared with those using ten unknowns in the series of the equation (16). The numerical results for the maximum deflection and moments agree with the results obtained from ten-point matching solution up to three significant digits.

The distribution for deflection, slope and moments M_r and M_t are shown along OB and OD for the case N = 4 in Figs. 27 to 30. The deflection is found to be positive in the circular region enclosed by the regular polygon (see Fig. 27). Negative deflection is found to occur in the fringe area between the circle with radius OB and the regular polygonal edges. The slope is found to be negative along OB and OD. Radial and tangential moments are positive at the centre and negative at points B and D. One notes that the moments M_n and M_s along the polygonal edge should decrease as the angle ϕ increases from $\phi = 0$ to $\phi = \frac{\pi}{N}$ and also the moments M_n and M_s should be related by the relation $M_s = \nu M_n$ along the polygonal edge. But it is seen from the Fig. 31 that the moments M_n and M_s do not behave in the above manner near the corner. The computational results show that the curvature in the S-direction is substantial along the polygonal edge. The above discrepancies are believed to be caused by large boundary errors near the corner (for example $32 < \phi < 45^o$ for the case N = 4). This unusual behaviour of moments and the negative deflection in the corner region indicate the difficulty in the method of the solution. One may note again that the difficulty may also be due to the fact that the normal to the boundary is discontinuous at the corner. However, the fact that the numerical results at $\rho = 0$ for six-point and ten-point matching solutions agree with each other may indicate that these large boundary errors are localized in the corner regions and they may not effect the numerical results at the center of the plate.

Table 11 Numerical Result for Uniformly Loaded Clamped Regular Polygonal Plates on Elastic Foundation

Number of Sides	Maximum Deflection	Moments at $\rho = 0$		Moments at B		Maximum Slope	Maximum Boundary Errors			
							Deflection		Slope	
N	$\left(\frac{w}{q/\lambda^4 D}\right)_{\rho=0}\times 10^2$	$\left(\frac{M_r}{q/\lambda^2}\right)\times 10$	$\left(\frac{M_t}{q/\lambda^2}\right)\times 10$	$\left(\frac{M_n}{q/\lambda^2}\right)\times 10$	$\left(\frac{M_s}{q/\lambda^2}\right)\times 10$	$\left(\frac{\frac{\partial w}{\partial n}}{q/\lambda^3 D}\right)\times 10^2$	$\left(\frac{w}{q/\lambda^4 D}\right)$	%	$\left(\frac{\frac{\partial w}{\partial n}}{q/\lambda^3 D}\right)$	%
4	.5704[1]	.4985	.4985	.3893	.1169	1.0169	$.2980\times 10^{-3}$	5.2	$.9386\times 10^{-3}$	9.3
	.5704[2]	.4985	.4985	.3893	.1169	1.0171				
6	1.0223	.6559	.6559	.9513	.2854	1.7413	$.8606\times 10^{-4}$	.85	$.1736\times 10^{-3}$	1.0
	1.0223	.6559	.6559	.9513	.2854	1.7412				
8	1.2449	.7225	.7225	.9599	.2880	2.0208	$.4605\times 10^{-4}$	.37	$.8825\times 10^{-4}$	.44
	1.2449	.7223	.7224	.9599	.2880	2.0209				

Note: [1] Solution using 6 coefficients.

[2] Solution using 10 coefficients.

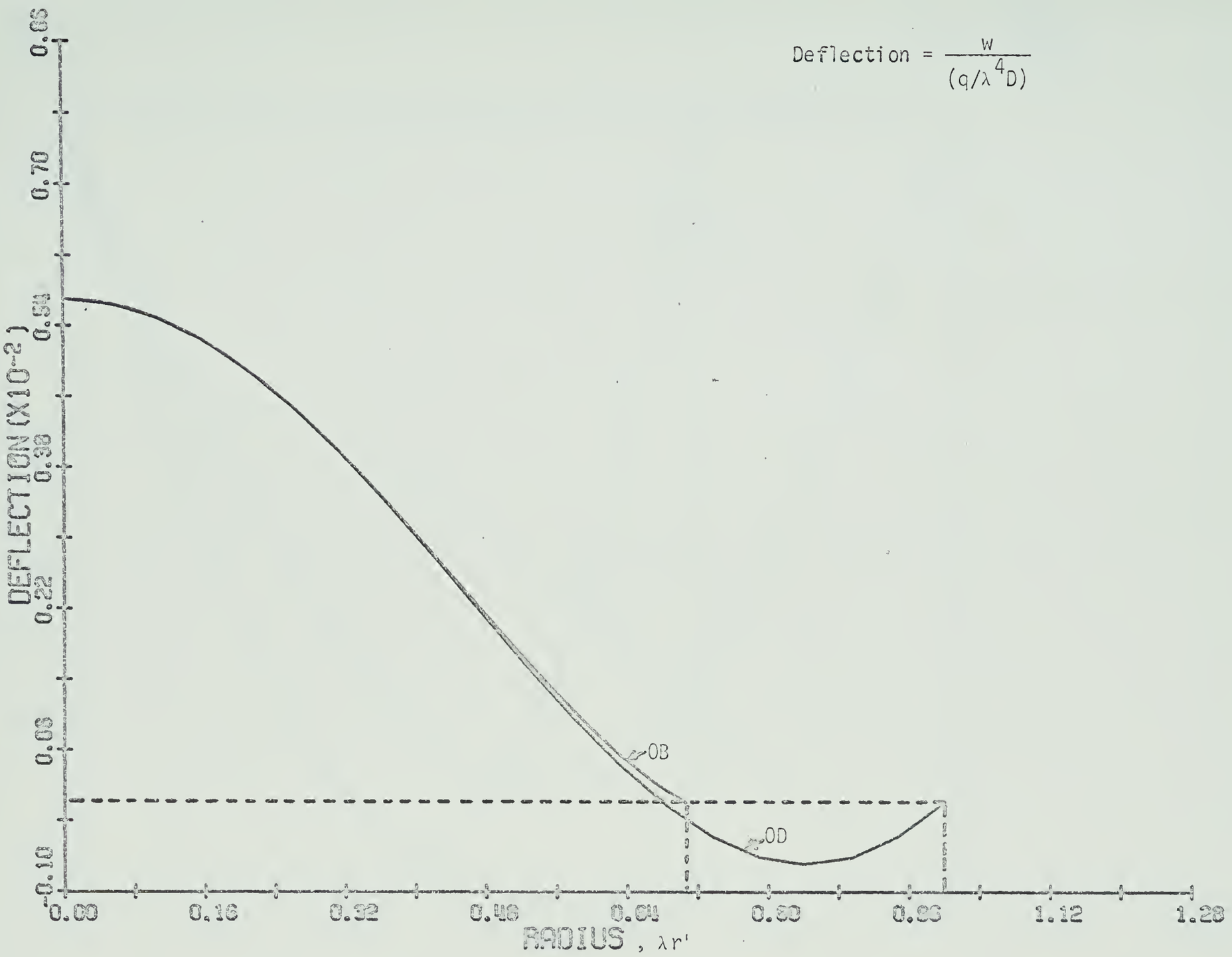

Fig. 27. Distribution of deflection along OB and OD for uniformly loaded clamped regular polygonal plate on elastic foundation for the case N = 4

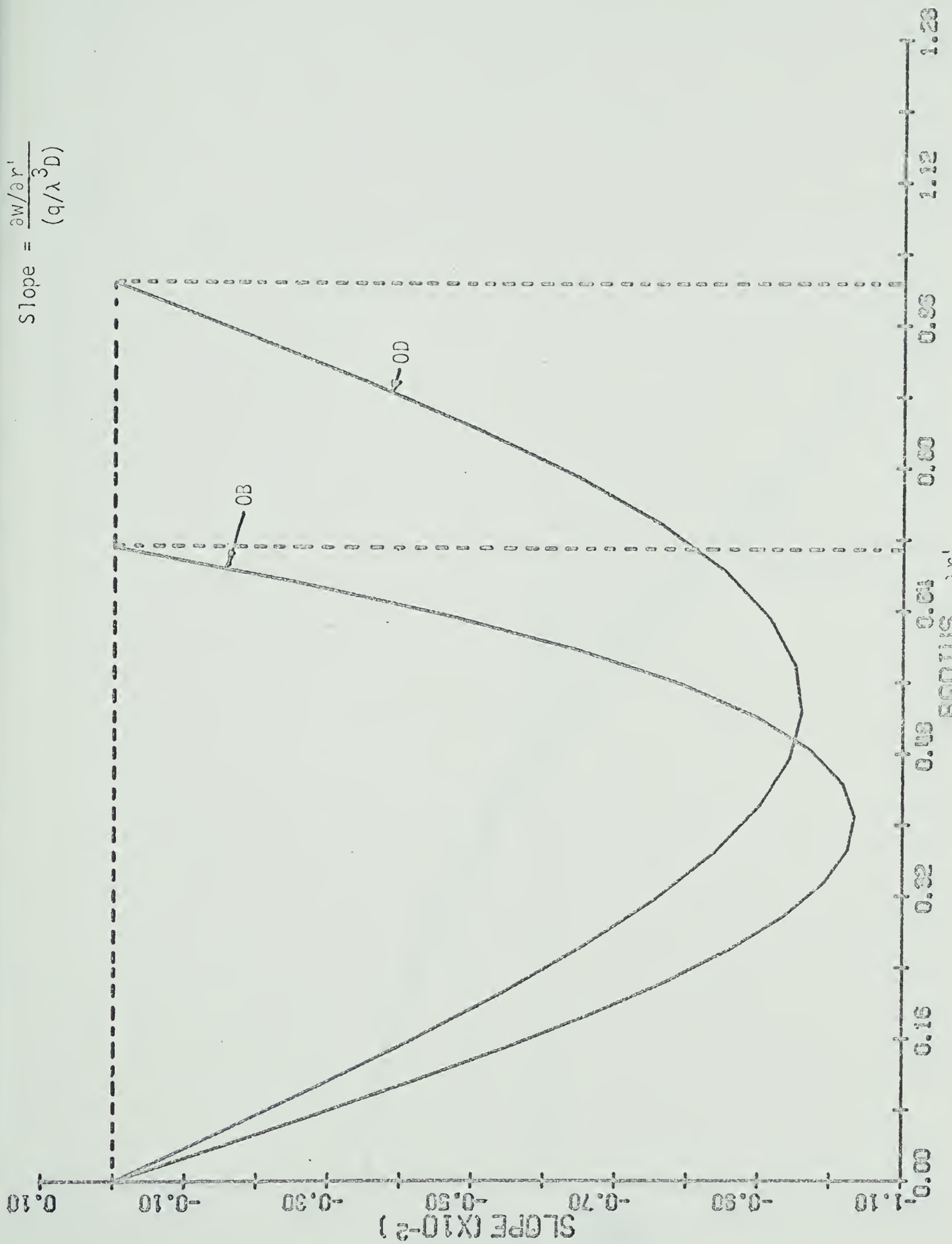

Fig. 28. Distributions of radial slope along OB and OD for uniformly loaded clamped regular polygonal plate on elastic foundation for the case N = 4

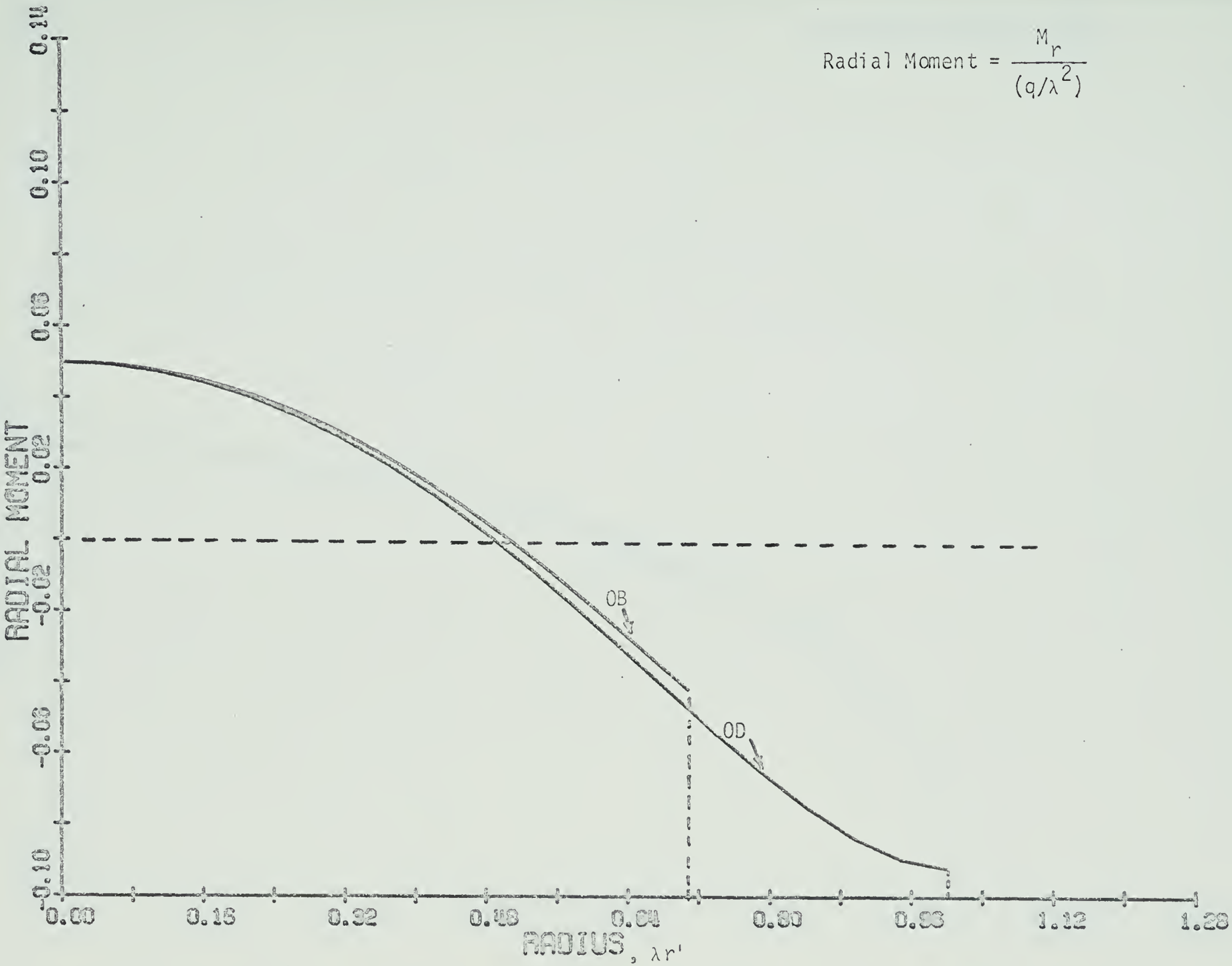

Fig. 29. Distribution of radial moment along OB and OD for uniformly loaded clamped regular polygonal plate on elastic foundation for the case $N = 4$

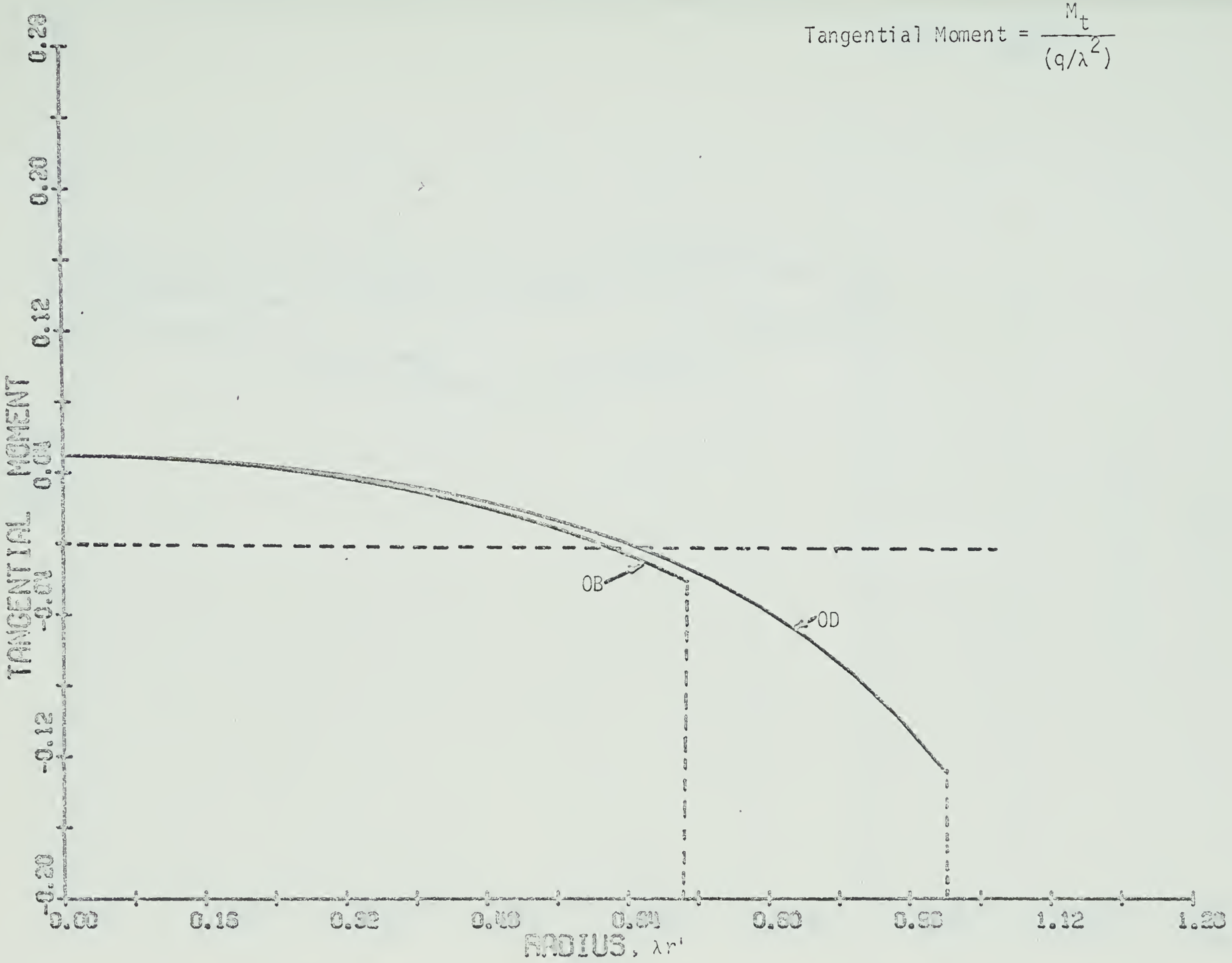

Fig. 30. Distribution of tangential moment along OB and OD for Uniformly loaded clamped regular polygonal plate on elastic foundation for the case N = 4.

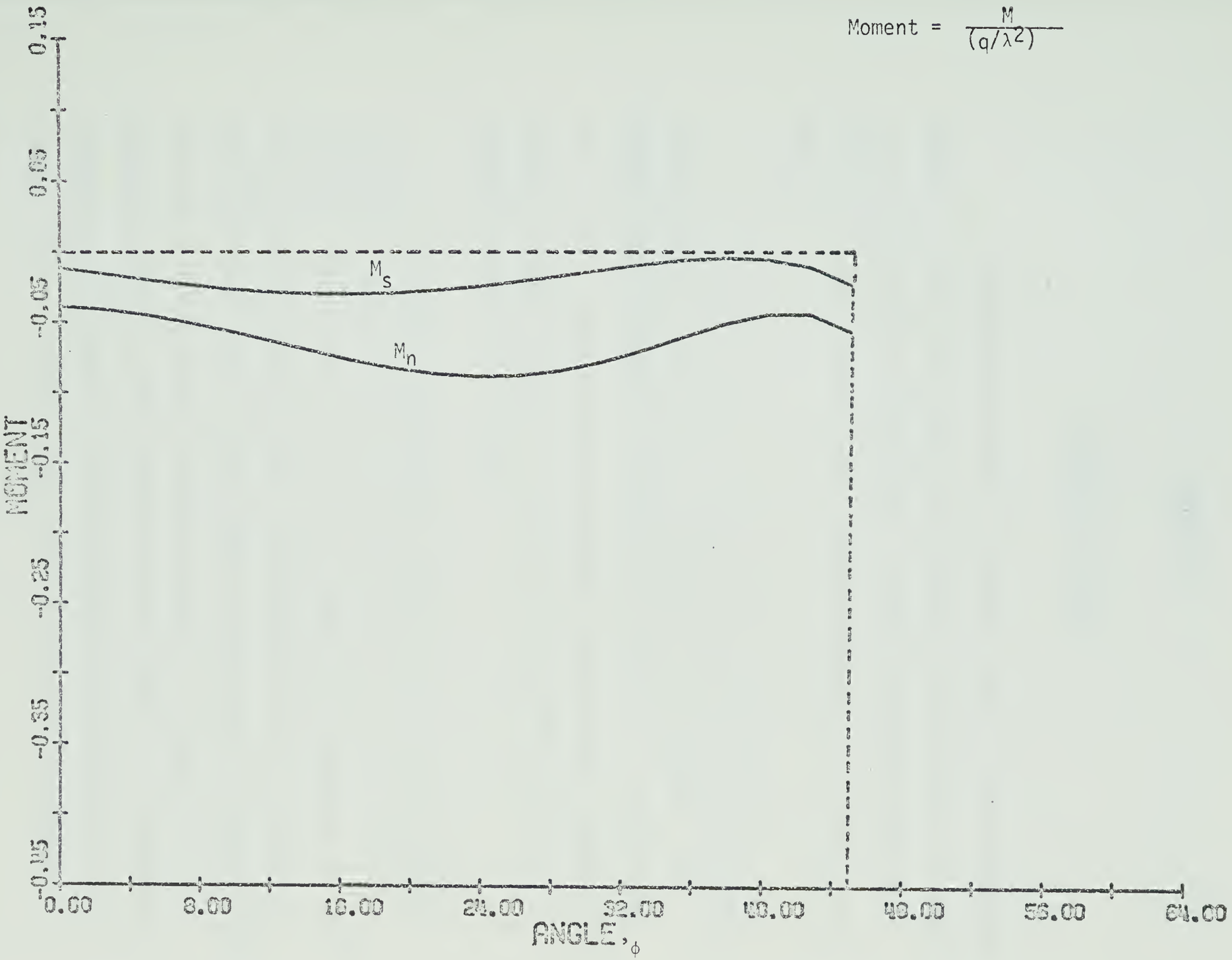

Fig. 31. Distribution of moments M_n and M_s along the edge for uniformly loaded regular polygonal plate on elastic foundation for the case N = 4.

CHAPTER V

CONCLUDING REMARKS

It has been shown that the general solution of the biharmonic equation in polar coordinates can be applied to the problem of bending of uniformly loaded clamped plates of doubly connected region. The following observations are noted from the examinations of the numerical results:

1. Numerical values of the coefficients for the infinite series decrease rapidly indicating the convergence of the solution. For example, the convergence is comparatively rapid for α ranging from 0.1 to 0.5 . For the case of uniformly loaded clamped regular polygonal plate on elastic foundation, the values of the coefficients behave differently and seem to diverge.

2. The clamped edge boundary conditions are satisfied exactly along the circular hole which are confirmed from the fact that the numerical values of the deflection and slope are of the order of 10^{-17} or less along the circular hole. The boundary errors for deflection and normal slope along the outer edge are quite small as compared with the maximum values inside the plate, except for the case of regular polygonal plate where the boundary errors are found to be considerably larger near the corners. As can be expected, the boundary errors for normal slope are slightly larger than the errors for the deflection.

3. As the size of the hole is increased, the maximum values of the deflection and moments decrease and the location of the maximum deflection moves towards the internal circular hole.

4. For the case of eccentric annular plate, the exact solution in polar coordinates using the point matching method yields the numerical results readily as compared with the solution using bi-polar coordinates given by Woinowsky-Krieger [9] and Yamanaka and Kakae [10]. This is considered to be the definite advantage of the method used. The numerical results from this analysis are checked with those of Georgian [6] for the limiting case $\beta = 0.0$ and Yamanaka and Kakae for the case $\alpha = 0.5$ and $\beta = 0.391$. In both cases, good agreement is observed between their analyses and the present work.

5. The numerical results are readily obtained for the case of regular polygonal or elliptic plate with a concentric hole with only minor changes in the analysis for eccentric annular plates. However, it was not possible to solve the problem for $N > 6$ in the case of regular polygonal plates and aspect ratio $\gamma > 2.0$ in the case of elliptic plates.

6. The boundary conditions are satisfied in the least squares sense for the case of uniformly loaded clamped regular polygonal plates on elastic foundation. The boundary errors for deflection and slope along the polygonal edge are small as compared with the respective maximum values inside the plate except for the region very close to corner. Negative deflection is observed in the small region close to

corners and contradicts with physical reasoning. The negative deflection represents the difficulty at the corner. In view of this difficulty, the numerical results presented in Table 11 must be regarded as tentative. The results are included for reference purpose. Nevertheless, it is believed that the numerical values at the center of the regular polygonal plate are reliable.

7. In the point matching technique, the boundary errors change sign alternatively at discrete points where the deflection and normal slope are zero. When the boundary errors are satisfied in the least squares sense as in the case of uniformly loaded clamped regular polygonal plates on elastic foundation, the erros do not change sign and the values of the errors decrease as one moves from the corner toward the mid-point of the edge.

8. The computed values of the Kelvin functions and the first derivatives for the case of regular polygonal plates on elastic foundation agree with the published values up to the four significant figures.

All the graphs presented in this work were plotted by Calcomp Plotter at the Data Center of the University of Alberta and the plotting time was about 0.9 hours.

The point matching technique was not readily applicable to the plates with the circular holes for other edge conditions such as free and simply supported. The method was also tried with external circular boundary and different internal boundaries such as regular polygon or ellipse and the coefficient matrix in each case is found to

be ill-conditioned. The problem of uniformly loaded clamped elliptic plates on elastic foundation was also tried and the coefficient matrix was found to be singular. In conclusion, it may be said that the point matching technique is applicable only to some special cases of geometry and boundary conditions.

REFERENCES

1. Wahl, A.M., and Lobo, G., Jr., "Stresses and Deflections in Flat Plates with Central Holes", Trans. ASME, Vol. 52, 1930, APM 52-3, pp. 29-43.

2. Flügge, W., "Handbook of Engineering Mechanics", First Ed., McGraw-Hill, New York, 1962.

3. Timoshenko, S., and Woinowsky-Krieger, S., "Theory of Plates and Shells", Second Ed., McGraw-Hill Book Co., Inc., New York, 1959.

4. Trumpler, W.E., Jr., "Design Data for Flat Circular Plates with Central Holes", Trans. ASME, Vol. 65, 1943, pp. A-173-175.

5. Labrow, S., "The Stresses in, and the Deflection of, Circular Flat Plates, with a Central Hole, under Normal Forces", Proceedings of the Institution of Mechanical Engineers, Vol. 145, 1941, pp. 115-125.

6. Georgian, J.C., "Uniformly Loaded Circular Plates with a Central Hole and Both Edges Supported", Trans. ASME, Vol. 24, No. 2, 1957, pp. 306-310.

7. Heap, J.C., "Bending of Annular Plates under Uniform Load on Cencentric Circle", Journal of Engineering for Industry, Trans. ASME, Vol. 90, 1968, pp. 279-294.

8. Saito, A., Kamura, S., and Shimazaki, T., "Bending of Elliptic Plates under Concentrated Load", JSME, Vol. 2, No. 6, 1959, pp. 299-305.

9. Woinowsky-Krieger, S., "Über die Verwendung von Bipolarkoordinaten zur Lösung einiger Problem der Plattenbiegung", Österreichisches Ingenieur-Archiv, XXIV. Band, 1956, pp. 47-52.

10. Yamanaka, H., and Kakae, H., "The Stress of Boiler Flat End Plate (Part 7)", JSME, Vol. 20, No. 92, Part 2, pp. 285-289.

11. Lo, C.C., and Leissa, A.W., "Bending of Plates with Circular Holes", Acta Mechanica, Vol. 4, 1966, pp. 64-78.

12. Leissa, A. H., and Niedenfuhr, F.W., "A Study of the Cantilevered Square Plate Subjected to Uniform Loading", Jnl. Aerospace Science, Vo. 29, 1962, pp. 162-169.

13. Hulber, L.E., and Niedenfuhr, F.W., "Accurate Calculation of Stress Distribution in Multiholed Plates", Trans. ASME, Vol. 87, 1965, pp. 331-334.

14. Conway, H.D., "The Approximate Analysis of Certain Boundary Value Problems", Jnl. Appl. Mech., Vol. 27, No. 2, 1960, pp. 275-277.

15. Saito, A., "Bending of Circular Plates with Eccentric Circular Hole Under Concentrated Load", Proc. 7th. Japan National Congress for Appl. Mech., 1957, pp. 99-103.

16. Cheng., K.C., and Hwang, G.J., "Laminar Forced Convection in Eccentric Annuli", A I Ch E Journal, Vol. 14, No. 3, 1968, pp. 510-512.

17. Saito, A., "Bending of Circular Plates on Elastic Foundation Loaded Over Concentric or Eccentric Circular Domain", Proc. 8th Japan National Congress for Applied Mechanics, 1958, pp. 99-102.

18. Saito, A., "Bending of Circular Plates on Elastic Foundation Loaded Along the Radius of the Circular Arc", Proc. 9th Japan National Congress for Applied Mechanics, 1959, pp. 55-60.

19. Reismann, H., "Bending of Circular or Ring Shaped Plates on Elastic Foundation", Jnl. Appl. Mech., Trans. ASME, Vol. 76, 1954, pp. 45-51.

20. Lo, C., "The Solutions of Plane Harmonic and Bi-Harmonic Boundary Value Problems in the Theory of Elasticity", Ph. D. Dissertation, Ohio State University, 1964.

21. Mclachlan, N.W., "Bessel Functions for Engineers" Oxford University Press, London, England, 1934, pp. 153-154.

22. Oravas, G.A., " Stress and Stain in Shallow Spherical Calotte Shells", Publ. Int. Ass. Bridge and Strc. Eng., Zurich, Vol. 17, 1957, pp. 139-160.

23. Lowell, H. H., "Tables of the Bessel-Kelvin Functions ber, bei, ker, kei and Their Derivatives for the Argument Range 0(0.01) 107.50", NASA Technical Report, R-32, 1959.

APPENDIX A

Expressions for $\frac{\partial w}{\partial r'}$, $\frac{\partial^2 w}{\partial r'^2}$, $\frac{\partial w}{\partial \phi}$, $\frac{\partial^2 w}{\partial \phi^2}$, and $\frac{\partial^2 w}{\partial r' \partial \phi}$.

$$\frac{\partial w}{\partial r'} = \frac{qa_1^3}{D}\left[\frac{r^3}{16} - \frac{b^4}{16r} + B_o\left(2r - \frac{2b^2}{r}\right)\right.$$

$$- D_o\left(\frac{2b^2 \log b}{r} - \frac{(r^2-b^2)}{r} - 2r \log r\right)$$

$$+ B_1\left(-\frac{1}{r^2} - \frac{2}{b^2} + \frac{3r^2}{b^4}\right)\cos\phi$$

$$+ D_1\left(\frac{3}{2} - \frac{3r^2}{2b^2} + \log\frac{r}{b}\right)\cos\phi \qquad (A.1)$$

$$+ \sum_{j=2}^{\infty} B_j\left(-\frac{j}{r^{j+1}} - \frac{j(1+j)r^{j-1}}{b^{2j}} + \frac{j(j+2)r^{j+1}}{b^{2j+2}}\right)\cos j\phi$$

$$\left. + \sum_{j=2}^{\infty} D_j\left(-\frac{j-2}{r^{j-1}} - \frac{j^2 r^{j-1}}{b^{2j-2}} + \frac{(j+2)(j-1)\, r^{j+1}}{b^{2j}}\right)\cos j\phi\right] .$$

$$\frac{\partial^2 w}{\partial r'^2} = \frac{qa_1^2}{D}\left[\frac{3r^2}{16} + \frac{b^4}{16r^2} + B_o\left(2 + \frac{2b^2}{r^2}\right)\right.$$

$$+ D_o\left(3 + \frac{b^2}{r^2} + 2\log r + \frac{2b^2}{r^2}\log b\right)$$

$$+ B_1\left(\frac{2}{r^3} + \frac{6r}{b^4}\right)\cos\phi + D_1\left(-\frac{3r}{b^2} + \frac{1}{r}\right)\cos\phi \qquad (A.2)$$

$$+ \sum_{j=2}^{\infty} B_j\left(\frac{j(j+1)}{r^{j+2}} - \frac{j(j+1)(j-1)\, r^{j-2}}{b^{2j}} + \frac{j(j+2)(j+1)\, r^{j}}{b^{2j+2}}\right)\cos j\phi$$

$$\left. + \sum_{j=2}^{\infty} D_j\left(\frac{(j-1)(j-2)}{r^{j}} - \frac{j^2(j-1)\, r^{j-2}}{b^{2j-2}} + \frac{(j-1)(j+2)(j+1)\, r^{j}}{b^{2j}}\right)\cos j\phi\right] .$$

$$\frac{\partial w}{\partial \phi} = \frac{qa_1^4}{D}\Big[- B_1 \left(\frac{1}{r} - \frac{2r}{b^2} + \frac{r^3}{b^4}\right) \sin\phi$$

$$- D_1 \left(\frac{r}{2} - \frac{r^3}{2b^2} + r \log \frac{r}{b}\right) \sin\phi$$

$$- \sum_{j=2}^{\infty} B_j \left(\frac{1}{r^j} - \frac{(1+j)r^j}{b^{2j}} + \frac{j\, r^{j+2}}{b^{2j+2}}\right) j \sin j\phi \qquad (A.3)$$

$$- \sum_{j=2}^{\infty} D_j \left(\frac{1}{r^{j-2}} - \frac{j\, r^j}{b^{2j-2}} + \frac{(j-1)\, r^{j+2}}{b^{2j}}\right) j \sin j\phi\Big]$$

$$\frac{\partial^2 w}{\partial \phi^2} = \frac{qa_1^4}{D}\Big[- B_1 \left(\frac{1}{r} - \frac{2r}{b^2} + \frac{r^3}{b^4}\right) \cos\phi$$

$$+ D_1 \left(\frac{r}{2} - \frac{r^3}{2b^2} + r \log \frac{r}{b}\right) \cos\phi$$

$$- \sum_{j=2}^{\infty} B_j \left(\frac{1}{r^j} - \frac{(1+j)\, r^j}{b^{2j}} + \frac{j\, r^{j+2}}{b^{2j+2}}\right) j^2 \cos j\phi \qquad (A.4)$$

$$- \sum_{j=2}^{\infty} D_j \left(\frac{1}{r^{j-2}} - \frac{j\, r^j}{b^{2j-2}} + \frac{(j-1)\, r^{j+2}}{b^{2j}}\right) j^2 \cos j\phi\Big] \ .$$

$$\frac{\partial^2 w}{\partial r\, \partial \phi} = \frac{qa_1^3}{D}\Big[B_1 \left(\frac{1}{r^2} + \frac{2}{b^2} - \frac{3r^2}{b^4}\right) \sin\phi$$

$$- D_1 \left(\frac{3}{2} - \frac{3r^2}{2b^2} + \log \frac{r}{b}\right) \sin\phi$$

$$+ \sum_{j=2}^{\infty} B_j \left(\frac{j}{r^{j+1}} + \frac{j(1-j)\, r^{j-1}}{b^{2j}} - \frac{j(j+2)\, r^{j+1}}{b^{2j+2}}\right) j \sin j\phi \qquad (A.5)$$

$$+ \sum_{j=2}^{\infty} D_j \left(\frac{(j-2)}{r^{j-1}} + \frac{j^2\, r^{j-1}}{b^{2j-2}} - \frac{(j+2)(j-1)\, r^{j+1}}{b^{2j}}\right) j \sin j\phi\Big] \ .$$

APPENDIX B

Ber, Bei Functions and Their Derivatives [21, 22] .

$$\mathrm{Ber}_n\, x = \sum_{p=0}^{\infty} \frac{(-1)^{n+p}\,(\frac{x}{2})^{n+2p}}{p!\;n+p!}\cos\left(\frac{(n+2p)\pi}{4}\right) \quad . \tag{B.1}$$

$$\mathrm{Bei}_n\, x = \sum_{p=0}^{\infty} \frac{(-1)^{n+p+1}\,(\frac{x}{2})^{n+2p}}{p!\;n+p!}\sin\left(\frac{(n+2p)\pi}{4}\right) \quad . \tag{B.2}$$

$$\mathrm{Ber}'_n\, x = \frac{n}{x}\,\mathrm{Ber}_n\, x + \frac{1}{\sqrt{2}}\,(\mathrm{Ber}_{n+1}\, x + \mathrm{Bei}_{n+1}\, x) \quad . \tag{B.3}$$

$$\mathrm{Bei}'_n\, x = \frac{n}{x}\,\mathrm{Bei}_n\, x - \frac{1}{\sqrt{2}}\,(\mathrm{Ber}_{n+1}\, x - \mathrm{Bei}_{n+1}\, x) \quad . \tag{B.4}$$

$$\mathrm{Ber}''_n\, x = -\frac{1}{x}\,\mathrm{Ber}'_n\, x + \left(\frac{n}{x}\right)^2 \mathrm{Ber}_n\, x - \mathrm{Bei}_n\, x \quad . \tag{B.5}$$

$$\mathrm{Ber}''_n\, x = -\frac{1}{x}\,\mathrm{Bei}'_n\, x + \left(\frac{n}{x}\right)^2 \mathrm{Bei}_n\, x - \mathrm{Ber}_n\, x \quad . \tag{B.6}$$

B29928